

**APPLICATION OF A METAL SOLUBILITY MODEL TO  
GEOCHEMICAL SURVEY DATA**

by

**Jessica Chloë Lenham**

Thesis submitted to the University of Nottingham  
for the degree of Doctor of Philosophy, September 2005

## TABLE OF CONTENTS

LIST OF FIGURES.....	vi
LIST OF TABLES.....	xii
ABBREVIATIONS.....	xiv
ABSTRACT.....	xv
ACKNOWLEDGEMENTS.....	xvii
 <b>1. INTRODUCTION.....</b>	 <b>1</b>
1.1 LAND CONTAMINATION.....	1
1.2 METAL SOLUBILITY.....	2
1.3 PREDICTING METAL SOLUBILITY.....	4
1.4 THE G-BASE SURVEY.....	6
1.5 MAPPING DATA.....	7
1.6 THESIS SUMMARY.....	10
 <b>2. METHODS.....</b>	 <b>12</b>
2.1 ANALYTICAL METHODS.....	12
2.1.1 pH.....	12
2.1.1.1 <i>Introduction.....</i>	12
2.1.1.2 <i>pH theory and measurement.....</i>	12
2.1.1.3 <i>Method used for measuring pH of archived G-BASE samples.....</i>	15
2.1.1.4 <i>Method of pH measurement for electrode selection.....</i>	15
2.1.1.5 <i>Method of pH measurement for short-range field study.....</i>	16
2.1.2 Loss on Ignition.....	16
2.1.3 Analysis of total soil metal content.....	17
2.1.4 Soil pore water extraction for large scale field study.....	17
2.1.5 Analysis of soil pore water.....	19
2.1.5.1 <i>Speciation of soil pore water using</i>	

WHAM-VI.....	20
2.1.6 Analysis of solid soil samples by XRF.....	21
2.2 GEOSTATISTICS.....	22
2.2.1 Introduction.....	22
2.2.2 Exploratory Data Analysis.....	23
2.2.3 Assessment of Trend.....	23
2.2.4 The Variogram.....	24
2.2.4.1 <i>Estimating the Variogram</i> .....	24
2.2.4.2 <i>Modelling the Variogram</i> .....	26
2.2.4.3 <i>Commonly used variogram models</i> .....	27
2.2.5 Kriging.....	29
2.2.6 Cross-Validation.....	31
2.2.7 Is kriging better than simple interpolation?.....	31
2.3 FIELD WORK.....	32
2.3.1 Large scale validation of the metal solubility algorithm.....	32
2.3.1.1 <i>Preliminary field work</i> .....	32
2.3.1.2 <i>Final large-scale study</i> .....	33
2.3.2 Relocating G-BASE sample sites .....	35
2.3.3 Short scale spatial variation of pH.....	37
2.3.3.1 <i>Sampling error estimation</i> .....	37
2.3.3.2 <i>Sample collection</i> .....	38
 <b>3. MAPPING METAL SOLUBILITY AND ANALYSIS OF SOLUBILITY ALGORITHM</b> .....	 43
3.1 INTRODUCTION.....	43
3.1.1 Introduction to the data.....	43
3.1.2 Metal solubility algorithm.....	46
3.2 SELECTION OF STUDY AREA.....	46
3.2.1 Introduction.....	46
3.2.1.1 <i>pH data</i> .....	48
3.2.1.2 <i>Concentration of zinc in solution</i> .....	49
3.3 MAPPING.....	52

3.3.1	Variograms.....	52
3.3.1.1	<i>Total zinc concentration.....</i>	52
3.3.1.2	<i>Total copper concentration.....</i>	54
3.3.1.3	<i>Total lead concentration.....</i>	55
3.3.1.4	<i>pH.....</i>	56
3.3.2	Kriging and Mapping.....	58
3.3.3	Estimation uncertainty.....	63
3.4	MAPPING METAL SOLUBILITY.....	68
3.4.1	Modelling the variograms.....	68
3.4.1.1	<i>Lead solubility.....</i>	68
3.4.1.2	<i>Zinc solubility.....</i>	69
3.4.1.3	<i>Copper solubility.....</i>	70
3.4.1.4	<i>Kriging and mapping of solubility.....</i>	71
3.4.2	Uncertainty analysis of metal solubility algorithm.....	77
3.4.2.2	<i>Results of Crystal Ball analysis.....</i>	82
3.5	CONCLUSIONS.....	83
3.6	INFLUENCE OF HISTORIC CONTAMINATION ON LEAD CONCENTRATION AND SUGGESTIONS FOR FURTHER WORK.....	85
<b>4.</b>	<b>LARGE SCALE FIELD WORK.....</b>	<b>87</b>
4.1	INTRODUCTION.....	87
4.1.1	Materials and Methods.....	87
4.2	RESULTS.....	88
4.2.1	Results of Preliminary Field work.....	88
4.2.2	Re-sampling of G-BASE survey sites.....	91
4.2.2.1	<i>Total soil concentrations.....</i>	91
4.2.2.2	<i>Prediction of zinc solubility.....</i>	95
4.3	CONCLUSIONS.....	104
<b>5.</b>	<b>SHORT-SCALE pH INVESTIGATION.....</b>	<b>106</b>
5.1	INTRODUCTION.....	106

5.1.1	Background.....	106
5.1.2	Causes of spatial variability of pH.....	107
5.1.2.1	<i>Urine Patches</i> .....	107
5.1.2.2	<i>Ammonium fertiliser application</i> .....	108
5.1.2.3	<i>Liming</i> .....	110
5.1.2.4	<i>Time</i> .....	111
5.1.2.5	<i>Drainage</i> .....	112
5.1.3	Influence of pH on metal solubility.....	113
5.1.5	Location of field study.....	115
5.2	RESULTS AND DISCUSSION.....	115
5.2.1	pH electrode selection.....	115
5.2.2	Results of field sampling.....	119
5.3	SAMPLING UNCERTAINTY AND IMPROVING THE VARIOGRAM.....	121
5.3.1	Measurement Uncertainty.....	121
5.3.2	Results of the Uncertainty Analysis.....	123
5.3.3	The Variogram.....	125
5.4	INTER-LABORATORY TRIAL.....	126
5.5	COMPARISON WITH OTHER FIELD STUDIES.....	129
5.6	SIMULATION EXPERIMENTS.....	132
5.6.1	Simulation of G-BASE sampling protocol.....	132
5.6.2	Simulation of wheat uptake of zinc and cadmium.....	134
5.6.3	Simulated metal solubility at Bunny.....	137
5.7	CHAPTER SUMMARY.....	140
<b>6.</b>	<b>CONCLUSIONS</b> .....	143
6.1	THESIS SUMMARY.....	143
6.2	THESIS CONCLUSIONS.....	145
6.3	SUGGESTIONS FOR FURTHER WORK.....	146
	BIBLIOGRAPHY.....	148
	APPENDICES.....	153

## LIST OF FIGURES

Figure 2.1	Centrifuge tubes for soil pore water separation, designed and manufactured by R&D Workshop. BGS, Keyworth...	19
Figure 2.2	Sample variogram with key features highlighted. Symbols (●) show the experimental variogram, and the solid black line is the model of the theoretical variogram, in this case a double spherical model.....	26
Figure 2.3	Variogram cloud for Pb across the Westphalian region. Points at the top of the graph represent local outliers.....	34
Figure 2.4	Location of the sample site for the pH survey. National grid reference SK 594 303. The field used is highlighted in yellow and bounded by Keyworth Lane and Wysall Road on two sides, a boundary with a neighbouring field on the west and a wall with woodland beyond on the southern side.....	39
Figure 2.5	Grid layout and numbering system for pH field sampling..	40
Figure 2.6	Location of random duplicate sites.....	41
Figure 3.1	Parent material map of the Humber-Trent region.....	44
Figure 3.2	Topsoil (0-15 cm depth) metal concentrations across the Humber-Trent region for a) Cu, b) Pb and c) Zn. Source: British Geological Survey, © NERC 2005.....	45
Figure 3.3	Relationship between NSI top-soil pH measurements and G-BASE sub-soil pH measurements kriged to NSI locations (n = 35).....	49
Figure 3.4	Sample locations in the Westphalian region chosen for further investigation overlying the parent material. Westphalian region is over the coal measures.....	52
Figure 3.5	Isotropic semivariances (symbols) of total Zn concentrations and a double-spherical model fitted through them (line).....	53
Figure 3.6	Isotropic semivariances (symbols) of total Cu concentrations and an exponential model fitted through	

	them (line). Data has been log transformed.....	54
Figure 3.7	Isotropic semivariances (symbols) of total Pb concentrations and an exponential model fitted through them (line). Data has had the trend removed.....	56
Figure 3.8	Isotropic semivariances (symbols) of soil pH values and an exponential model fitted through them (line). Parameters shown in Table 3.6.....	57
Figure 3.9	Map of kriged Cu concentration(log transformed mg kg <sup>-1</sup> ).....	59
Figure 3.10	Map of kriged Zn concentration (mg kg <sup>-1</sup> ).....	60
Figure 3.11	Map of kriged Pb concentration (mg kg <sup>-1</sup> ).....	61
Figure 3.12	Map of kriged soil pH.....	62
Figure 3.13	Kriging variances for soil pH.....	64
Figure 3.14	Kriging error as a percentage of the kriging estimate for a) Zn and b) pH.....	66
Figure 3.15	Cross Validation error as a percentage of the kriging estimate for a) Pb and b) Cu.....	67
Figure 3.16	Isotropic semivariances (symbols) of Pb solubility and a spherical model fitted through them (line).....	69
Figure 3.17	Isotropic semivariances (symbols) of Zn solubility and a linear model fitted through them (line). The model has a gradient of $3.85 \times 10^5$ and a nugget value of 1.913.....	70
Figure 3.18	Isotropic semivariances (symbols) of Cu solubility and a linear model fitted through them (line). The model has a gradient of $1.10 \times 10^{-4}$ and a nugget value of 4.2964.....	71
Figure 3.19	Graphs of error as a percentage of the kriging estimate as a result of cross validation for a) Zn solubility, b) Cu solubility and c) Pb solubility.....	73
Figure 3.20	Kriged predicted Zn solubility values (mmol l <sup>-1</sup> ).....	74
Figure 3.21	Kriged predicted Cu solubility values (mmol l <sup>-1</sup> ).....	75
Figure 3.22	Kriged predicted Pb solubility values (mmol l <sup>-1</sup> ).....	76
Figure 3.23	Percentage contribution to Variance for the metal solubility algorithm parameters for a) Cu, b) Zn and c)	

	Pb.....	82
Figure 3.24	Map of Pb concentration showing location of Pb rakes and the location of the Darley Dale smelter.....	84
Figure 4.1	Graphs of Pb, Zn and Cu concentrations at the four test survey sites showing G-BASE results and new sample results. 'GBASE <sub>XRF</sub> ' are the original GBASE values, 'GBASE <sup>2</sup> <sub>XRF</sub> ' are the archived G-BASE soils re-analysed by XRF, 'NEW <sub>AAS</sub> ' are the new soil samples measured by FAAS, and 'NEW <sub>XRF</sub> ' are the new soils measured by XRF.....	89
Figure 4.2	Graph showing the percentage change from G-BASE values (XRF) to new sample values (aqua regia digest and FAAS).....	92
Figure 4.3	Graph showing the percentage change from G-BASE values (XRF) to new sample values (aqua regia digest and FAAS) with sample 408982 removed in order to show the detail of the other sample sites.....	92
Figure 4.4	Scatter plots of soil metal concentrations (mg kg <sup>-1</sup> ) from the original G-BASE survey against equivalent values obtained in the new survey.....	94
Figure 4.5	Modelled free ion activity for Zn (pZn <sup>2+</sup> ) against measured values (chemical analysis plus WHAM speciation). Two versions of the solubility model have been used with either total Zn concentration or radio-labile Zn (assuming a lability of 48.7%) as a determinant of Zn <sup>2+</sup> solubility.....	97
Figure 4.6	Original data set used for the parameterisation of Model <sub>Tot</sub> with re-sampled G-BASE locations included.....	98
Figure 4.7	Original data set used for the parameterisation of Model <sub>Lab</sub> with re-sampled G-BASE locations included.....	100
Figure 4.8	Original data set used for the parameterisation of Model <sub>Lab</sub> with Zn <sup>2+</sup> predictions at re-sampled and original G-BASE locations included.....	102



Figure 4.9	Difference between measured and predicted $p(\text{Zn}^{2+})$ values using two sources of data for predictions.....	103
Figure 4.10	Surface plot of $p(\text{Zn}^{2+})$ with increasing Zn concentration and pH.....	104
Figure 5.1	Expected shift in soil pH from different applications of ammonium fertiliser on five soil textures, calculated using equation 5.1. Typical application of nitrogen fertiliser in 2000 was $149 \text{ kg ha}^{-1}$ (DEFRA, 2001).....	109
Figure 5.2	Difference in pH between a limed patch and a fertilised patch ( $(\text{NH}_4)_2\text{SO}_4$ ) on a medium textured soil for different initial soil pH values.....	111
Figure 5.3	Schematic change in soil pH over time when waterlogged, pH on the y-axis and time on the x-axis. Red lines show the equilibrium range.....	113
Figure 5.4	Chart-reader graphs for soil Q. Each electrode ('slow', 'medium' and 'fast') was tested twice, with the sub-samples labelled as 'a' and 'b'. Each of the above graphs shows the supernatant measurement and slurry measurement on a single sub-sample of soil (see §2.1.1.4).....	117
Figure 5.5	Chart reader results for soil U. Each electrode ('slow', 'medium' and 'fast') was tested twice, with the sub-samples labelled as 'a' and 'b'. Each of the above graphs shows the supernatant measurement and slurry measurement on a single sub-sample of soil (see §2.1.1.4).....	118
Figure 5.6	Histogram of 289 soil pH values at Bunny.....	120
Figure 5.7	Box-and-whisker diagram showing the variation in recorded pH for the whole dataset and for the control soil from the Bunny study site.....	120
Figure 5.8	Spatial distribution of soil pH values across the study field at Bunny.....	121
Figure 5.9	Balanced design for duplicate sampling, including	

	example sample labels.....	122
Figure 5.10	Orientation of sample and duplicate sample for sampling uncertainty analysis. The X marks are the locations of the 5 sub-samples taken within the 1m square sampling support aggregated to form a single sample.....	123
Figure 5.11	Improved variogram of pH at Bunny. Spherical model, with a fitted nugget and the semivariance at 1m added.....	126
Figure 5.12	pH value of soil 5H determined in the inter-laboratory trial including the mean result.....	128
Figure 5.13	Histograms of data from the inter- and intra- laboratory trials.....	129
Figure 5.14	pH variograms for Bunny, Portugal (Silva) and Brazil (Vieira). All variograms use the spherical model.....	130
Figure 5.15	Variogram of pH at Broom's Barn Farm. The points are the experimental semivariances, and the solid line is the best fitting exponential model; the parameters of which are shown in Table 5.6 (Webster and Oliver 2001).....	131
Figure 5.16	Diagram showing a simulated G-BASE sample using the Bunny survey. The red circles of the G-BASE samples together constitute the sample support used under G-BASE and give a single aggregated sample.....	132
Figure 5.17	Histogram of pH values for Bunny data and repeatedly simulated G-BASE sampling .....	133
Figure 5.18	Histogram of wheat grain Cd content at Bunny using the sludge soil application limit for Cd. Values calculated for the Bunny data set and for the simulated G-BASE samples are shown.....	135
Figure 5.19	Histogram of wheat grain Zn content at Bunny using the sludge soil application limit for Zn. Values calculated for the Bunny data set and for the simulated G-BASE samples are shown.....	136
Figure 5.20	Estimated free ( $Pb^{2+}$ ) ion activity at the Bunny field site derived from the full topsoil pH dataset and simulated G-	

	BASE sample values.....	138
Figure 5.21	Estimated free ( $\text{Cu}^{2+}$ ) ion activity at the Bunny field site derived from the full topsoil pH dataset and simulated G- BASE sample values.....	138
Figure 5.22	Estimated free ( $\text{Zn}^{2+}$ ) ion activity at the Bunny field site derived from the full topsoil pH dataset and simulated G- BASE sample values.....	139

## LIST OF TABLES

Table 1.1	Parameter values for the metal solubility algorithm.....	5
Table 2.1	Elements measured on the SpectrAA FAAS.....	17
Table 2.2	Elements measured on the SpectrAA and conditions used.	20
Table 2.3	Trial survey sites.....	32
Table 2.4	List of sites visited. (Sample IDs are G-BASE IDs without the location identifying prefix).....	35
Table 3.1	Parameter values and standard errors for the solubility algorithm (Equation 3.1).....	46
Table 3.2	Percentage of samples with Zn in solution predicted to be above the detection limits of the ICP-MS and ICP-AES using equation 3.2 with the data corrections described in the text.....	51
Table 3.3	Parameters of the double spherical variogram model fitted to the total Zn concentration data.....	53
Table 3.4	Parameters of the exponential variogram model fitted to the total Cu concentration data.....	55
Table 3.5	Parameters for the total Pb variogram.....	56
Table 3.6	Parameters for exponential variogram of pH.....	57
Table 3.7	Parameters for Pb solubility variogram.....	68
Table 3.8	Mean percentage error for metal solubilities calculated from cross validation kriging with respect to original G-BASE data.....	72
Table 3.9	Details of model parameters used in Crystal Ball for Pb...	79
Table 3.10	Details of model parameters used in Crystal Ball for Zn...	80
Table 3.11	Details of model parameters used in Crystal Ball for Cu...	81
Table 4.1	Parameters for the two versions of the model used to predict $p(\text{Zn}^{2+})$ by Equation 4.1: using total ( $\text{Model}_{\text{Tot}}$ ) or radio-labile ( $\text{Model}_{\text{Lab}}$ ) Zn concentration. When using the labile model, the Zn concentration is multiplied by the percentage of Zn assumed to be labile.....	95
Table 5.1	Buffer capacities for different soil textures (Rowell,	

	1994).....	108
Table 5.2	Output of ROBCOOP4 programme showing classical and robust ANOVA results.....	124
Table 5.3	pH value of soil 5H determined in the inter-laboratory trial with differences in methodology shown. The 12 participating institutions (in alphabetical order) were: BGS (British Geological Survey) ‘U-block’, BGS ‘E-block’, CEH (Centre of Hydrology and Hydrology), The University of Edinburgh, The University of Glasgow, IGER (Institute of Grassland and Environmental Research), Lancaster University, The University of Newcastle, Rothamsted Research Station, NSRI (National Soil Resources Institute), The University of Reading and The University of Nottingham (the results from the ‘control’ soil).....	127
Table 5.4	Comparison of statistics for the inter- and intra-lab data.....	128
Table 5.5	Model parameters of the three variograms – all using the spherical model.....	130
Table 5.6	Summary statistics for the Bunny data and simulated G-BASE data.....	133
Table 5.7	Parameters for the wheat uptake algorithm (Equation 5.2). a, b and c are constants.....	135
Table 5.8	Summary statistics for modelled cadmium and zinc uptake by wheat.....	136
Table 5.9	Lead, copper and zinc solubility using an estimated lead concentration across the field at Bunny (Field) and at simulated G-BASE points. The value obtained by using the mean pH value is also shown.....	139
Table 5.10	Mean wheat grain concentrations of Cd and Zn from the full Bunny data set and the simulated G-BASE samples...	142

## ABBREVIATIONS

ADAS	.....Agricultural development and advisory service
ANOVA	.....Analysis of variance
BGS	.....British Geological Survey
CEH	.....Centre for Ecology and Hydrology
DEFRA	.....Department for the Environment, Food and Rural Affairs
DOC	.....Dissolved Organic Carbon
FA	.....Fulvic Acid
FAAS	.....Flame Atomic Absorption Spectrometry
G-BASE	.....Geochemical Baseline Survey of the Environment
GPS	.....Global Positioning System
GSUE	.....Geochemical Survey of the Urban Environment
HA	.....Humic Acid
ICP-AES	.....Inductively Coupled Plasma-Atomic Emission Spectrometry
ICP-MS	.....Inductively Coupled Plasma-Mass Spectrometry
MAFF	.....Ministry of Agriculture, Fisheries and Food
Mtds	.....Million tonnes dry solids
NSI	.....National Soil Inventory
QC	.....Quality Control
RSSS	.....Representative Soil Sampling Scheme
SIPS	.....Sample Introduction Pump System
TOC	.....Total Organic Carbon
UKAS	.....United Kingdom Accreditation Service
v/v	.....By volume
WHAM	.....Windermere Humic-Aqueous Model
XRF	.....X-Ray Fluorescence Spectroscopy

The term “solubility” is used in the text and should be taken to mean free ion activity of the metal concerned

## ABSTRACT

In areas where heavy metals are introduced into or onto land where they would not normally be present at elevated concentrations, then that land could be considered to be contaminated. A simple way of determining the magnitude of contamination by heavy metals is to measure the total metal concentration in the soil. However, this simple measure is a poor way of assessing the potential risks to the environment and human health. A more effective risk assessment can be achieved by analysing the proportion of the total metal that exists in a mobile or bioavailable form, in other words, the metal solubility. Unfortunately metal solubility is more difficult and costly to measure than total metal concentration in the soil.

This thesis examines the application of a metal solubility model to geochemical survey data consisting of pH and metal concentrations. The solubility predictions were interpolated in order to produce maps; however, the interpolated data had very high uncertainties. Further analysis showed that pH was the greatest source of uncertainty in the algorithm, contributing the most for lead, with 76% of the uncertainty being due to pH. pH was least influential for copper, contributing 49% of the uncertainty, but pH was the highest contributor in each metal.

In order to examine the accuracy of the algorithm without geostatistical influences, a field work study was undertaken to measure metal solubility directly at the original survey sites. This showed that the algorithm was very good at predicting metal solubility at point sources. In order to assess the short-scale spatial variability of pH, and the errors in pH measurements, a second field work project was conducted, measuring the pH on 200 samples from a single field. This work showed that pH does vary across a field, but more importantly allowed a quantification of the uncertainty involved in sampling and measuring pH.

Results show that despite the short-scale variability in pH, point predictions are accurate (the average difference between measured and predicted  $pZn^{2+}$  is 6%),

and might be of use to land managers. However, interpolating solubility predictions for mapping produces unacceptably high uncertainties (mean values were 188% for Pb, 417% for Cu and 153% for Zn) for land management or the development of policy measures related to soil.

Further work could include calculating the measured Pb and Cu solubility and comparing these to the predictions. A study to investigate how pH and  $\text{Zn}^{2+}$  vary together across a field would also be of interest.



## ACKNOWLEDGEMENTS

I would like to thank my supervisors, Neil Crout, Scott Young and Barry Rawlins for their help and support during my PhD. I am grateful to everyone at the British Geological Survey who has helped me with equipment and information. John Corrie and Darren Hepworth at the University of Nottingham made all the practical work possible, and I am especially grateful for the days spent up to our ears in mud taking “soil” samples at Bunny.

I would also like to thank all the people at the Environmental Science department at the University of Nottingham for keeping me amused over the years. Marchello Di Bonito allowed me to share an office with him at BGS and helped me out with all the centrifugation work. Glen Cox, Catherine Morris, Lee Stapleton, Tim Reid and Imad Ahmed all helped me with field work. Melissa Morales Scott allowed me to use her wheat uptake models and Davide Tarsitano taught me how to use Crystal Ball. Andy Tye developed the solubility algorithms used in this thesis and also helped me with chemical analysis. I would also like to thank Xinxin Guo, an MSc student who worked with me on the pH field work.

Outside the department I need to thank Andy King, for being a great housemate, and again helping out with field work. Also Martin Flintham was there digging up soil when he didn't have to be.

Most of all I want to thank my family and my partner, Matt for encouraging, supporting and believing in me.

## **1. INTRODUCTION**

### **1.1 LAND CONTAMINATION**

Where substances are introduced into or onto the land where they would not normally be, then that land could be considered to be contaminated. In a small number of these situations where certain criteria are met, a site might be designated as ‘contaminated land’ which has a specific legal definition set out in Part IIA of the Environmental Protection Act (1990).

The contamination of land is of growing importance. Many potentially toxic metals are accumulated in polluted soils, with an associated risk of contamination of underlying ground waters or adjacent surface waters. Toxic metals in the soil may arise either directly from a range of anthropogenic activities or indirectly from the mobilisation of naturally occurring metals by mining, or acid rain (Cancès et al., 2003). Land is at a premium in urban areas, and in order to preserve green belt land, development often takes place on “brownfield” sites which might be contaminated by past use and where remediation might have to be undertaken before development.

On agricultural land the question is not whether the land is suitable for redevelopment but whether the food produced on that land is suitable for human consumption. Agricultural land can be contaminated, either as a result of normal agricultural practices (for example metal enrichment can occur from the application of some fertilisers) or from the application of sewage sludge (Gardiner et al., 1995) or from historical industrial activities, such as mining and smelting.

Sewage sludge is an important source of metal contamination. This is the solid waste accumulated during primary, secondary and tertiary waste water treatment. To dispose of the sludge produced in the UK,

much of it is recycled onto agricultural land. Total sewage sludge production in 1996/7 was 1.16 Mtds (Million tonnes dry solids). Production in 2005/6 was predicted to be 1.467 Mtds, of which 0.732 Mtds would be recycled to agricultural land (Environment Agency, 1999). Sewage sludge contains appreciable levels of N and P, which can replace the need for artificial fertilisers. As well as this benefit, the organic matter in sludge can improve the physical condition of soil. However, sewage sludge also often contains high levels of heavy metals, leading to an accumulation of metals such as Cd, Zn, Cu and Ni (Gardiner et al., 1995). These metals can then accumulate in crops and livestock, increasing human exposure through the food chain.

Under section 78A(2) of part IIA of the Environment Protection Act 1990, land is 'contaminated' if significant harm is being caused to a specific receptor (an end product such as food crops, livestock or humans). In the case of crops and livestock, a  $\geq 20\%$  loss is considered to be the threshold for 'significant harm'. This loss is characterised by crops or livestock that are either dead or are no longer fit-for-purpose. Food is regarded as being no longer fit-for-purpose when it fails to comply with the provisions of the Food Safety Act 1990.

## **1.2 METAL SOLUBILITY**

The suitability of land for agricultural production is called into question when heavy metal concentrations in the soil exceed specified totals (MAFF, 1998). However, these simple determinations are a rather crude way of quantifying the potential environmental and human health risks. Evaluation of the potential risks and toxicity of metals in soil may be more accurately assessed by analysing the proportion of total metal in a mobile or bioavailable form (Sauvé et al., 2000). This approach assumes that dissolved metals are mobile and could possibly be taken up by plant roots (Sauvé et al., 2000). The term bioavailable often refers to an exchangeable or extractable fraction of the metal in the soil phase, not just that dissolved in water. However, solubility is a

closer estimate of this than total metal content. Using solubility or bioavailability can lead to a direct assessment of whether significant harm might occur as set out in section 78 A(2) of the Environment Act. Although assessing levels of metal solubility appears to be a simple way of predicting any future problems with metal uptake into food, in reality, directly measuring metal solubility is time consuming and expensive. Much work has been done on methods to predict metal solubility from more easily measured parameters, for example Jopony and Young (1994), McBride et al. (1997) and Tye et al. (2003).

Metal solubility is generally thought to depend on total metal content, pH, organic matter content and ionic strength in the pore water (Sauvé et al., 2000). The importance of the effect of pH on metal solubility is well recognised but difficult to separate from the influence of other soil characteristics. However, it is known that the effect of pH dominates because it has a major influence on most of the chemical species in the soil (especially carbonates and dissolved organic matter) (Sauvé et al., 2000).

There is much circumstantial evidence for the importance of the effect of dissolved organic matter (DOM) on metal solubility. Evidence comes both from the effect of DOM on solubility observed by removing or adding organic matter to experiments and from the observation that in most situations, a majority of the dissolved metal is found in metal-organic complexes (for example, more than 98% of dissolved copper is bound to DOM in non-acidic soil solution (Sauvé et al., 2000). However, despite all the circumstantial evidence, metal adsorption experiments in soils often fail to reveal a strong correlation between DOM and metal solubility. There are several possible reasons for this. Firstly, pH is a controlling variable on metal complexation by organic matter, so there is no way to separate pH from DOM to assess the effects on solubility separately. Second DOM is heterogeneous, and is very difficult to treat as one single variable. Fresh organic materials

are chemically different from residual humus in soils and will therefore react differently with metals in the soil (McBride et al., 1997).

One commonly used index for expressing bioavailability is the distribution coefficient,  $K_d$ . This is simply the partitioning of the total metal burden between the fraction bound to the soil solids and the part that is dissolved in soil solution. However, the impact of variation in pH, DOM etc on  $K_d$  is not well described (Sauvé et al., 2000).  $K_d$  is highly variable and often soil-specific, so any expression of solubility which includes its principal determinant (pH) will give improved prediction of metal solubility. This kind of approach assumes that free metal ( $Me^{x+}$ ) and  $H^+$  compete for adsorption on the soil's exchange sites. This has been successfully applied to Cd, Cu, Pb and Zn by many workers (e.g. Tipping et al., 2003; Weng et al., 2002; McBride et al., 1997; Sauvé et al., 1997)

### 1.3 PREDICTING METAL SOLUBILITY

The algorithm used to predict metal solubility in this thesis was developed by Tye et al. (2003). Their aim was to create a simple solubility model to predict the solution activity of free metal ions requiring information commonly included in soil geochemical surveys. The algorithm was developed using data from a soil incubation experiment and a collection of historically contaminated soils, and compared to literature data sets (Tye et al., 2003)

The algorithm for estimating free metal ion activity in the soil solution (including organic matter) is shown in Equation 1.1:

$$pM^{2+} = \frac{p\left(\frac{M_{soil} \times 100}{C}\right) + a + b \times pH + c \times \log(I)}{n} \quad 1.1$$

where  $p(M^{2+}) = -\log_{10}(M^{2+})$

$C$  = organic carbon content of the soil as a %

$I$  = ionic strength; a typical or default value is 0.01.

$M_{\text{soil}}$  = metal content of the soil ( $\text{mol kg}^{-1}$ )

$M^{2+}$  = activity of the free metal ion in the soil pore water

$a, b, c, n$  = constants unique to each metal

Alternatively, soil metal content may be expressed on a “whole soil” basis, to give:

$$pM^{2+} = a + b pH - c \log_{10} M^{2+} \quad 1.2$$

The values for the parameters  $a$ ,  $b$  and  $c$  for three metals are given in Table 1.1. They are derived using “solver” in Excel to find the best fit to the data set.

	<b>Pb</b>	<b>Zn</b>	<b>Cu</b>
<b>a</b>	-2.44	-1.859	-2.766
<b>b</b>	1.531	0.913	1.255
<b>c</b>	0.979	0.628	1.253

*Table 1.1: Parameter values for the metal solubility algorithm.*

The algorithms were developed using a data set collected from a soil incubation experiment and a collection of historically contaminated soils. Comparison was made to a literature data set to validate the model using independent data. Algorithms for labile metal were also defined ('labile' is defined as 'chemically responsive to changes in the metal free ion activity within the time of the measurement'). Radio-labile Cd and Zn were determined by isotopic dilution. The radio-labile measurement discriminates between the “chemically responsive” and “fixed” pools of soil metal.

## 1.4 THE G-BASE SURVEY

The Geochemical Baseline Survey of the Environment (G-BASE) is a systematic survey to establish a geochemical baseline across the United Kingdom run by the British Geological Survey (BGS). It is a programme of systematic high-resolution geochemical mapping, and aims to have complete coverage of the UK by 2012. Geochemical data is derived from soil samples and stream sediments at an average density of 1 sample every 1-2 km<sup>2</sup> of land surface, which is dependent in the case of sediments, on drainage density. The aim is to obtain a natural background level of the various elements measured. In order to minimise the influence of anthropogenic contamination, roads, tracks, railways, human habitation and other disturbed ground is avoided. The G-BASE project does not sample in urban environments, although a related project GSUE (Geochemical Survey of the Urban Environment) does sample exclusively in the urban environment (Rawlins et al., 2002).

Soil is collected using a hand held Dutch soil auger and samples are taken from mineral top-soil (from 0 to 15 cm depth) and sub-soil (from 40 to 50 cm depth) from the centre and four corners of a 20 × 20 m square. The soil samples from each of the five holes are combined to form an aggregated sample (Rawlins et al., 2002). In this thesis only top-soil data is used because i) the solubility algorithm was developed using top soil data, and ii) top-soil is the dominant source of metals for plant growth and animal grazing.

All G-BASE samples are returned to the BGS laboratories in Keyworth for preparation and analysis. The soil samples are air dried, ground and sieved to a less than 2 mm size fraction and then ground using an agate ball mill prior to analysis by X-ray fluorescence (XRF – see section 2.4.5). A sub-sample of each soil is stored in an archive for future reference. The total concentration of a broad spectrum of elements is

measured<sup>i</sup> and Loss on Ignition (LOI), a crude proxy for soil organic matter content (see section 2.3.2), is also carried out on each sample (Rawlins et al., 2002). In the G-BASE survey of the Humber Trent region pH was measured on the sub-soil only, so samples of top-soil were retrieved from storage and their pH determined for use in this study.

G-BASE does not measure soil solution concentration and only measures total soil metal content, therefore as discussed earlier, the data does not directly relate to a risk of contamination of crops or livestock by heavy metals. However, this data can be used in conjunction with the metal solubility algorithm in order to assess the risks.

This thesis uses G-BASE data from the Humber-Trent region in the north of England (see §3.1.1).

## 1.5 SOIL GEOCHEMICAL MAPS

Most properties of the environment, pH or metal concentration for example, are contiguous but are measured at only a few points for practical and economic reasons. If we want to know what the values are where we haven't sampled they need to be predicted from the data we do have. One of the most powerful ways of making predictions based on existing data is to use geostatistics. Some of the techniques that are collectively known as geostatistics have been used in this project to describe spatial patterns and predict the values of soil properties at un-sampled locations.

Geostatistics has its roots in the 1950s South African mining industry as a method of estimating ore grades from limited data. Pioneered by

---

<sup>i</sup> The following element concentrations are measured: Mg, P, K, Ca, Ti, Mn, Fe, V, Cr, Co, Ba, Ni, Cu, Zn, Ga, As, Se, Rb, Sr, Y, Zr, Nb, Mo, Pb, Bi, Th, U, Ag, Cd, Sn, Sb, Cs, La, Ce.



D. G. Krige, the field has grown in terms of methods and application (Cressie, 1993). Formal geostatistics began life as “the theory of regionalised variables” as proposed by Matheron (1963). Geostatistics is now used in many areas, such as petroleum, forestry, ecology, farming and contaminated land. Its strength over more classical approaches to ore-reserve estimation is that it recognises spatial variability at both the large and small scale, or in other words, it models both spatial trend and spatial correlation (Cressie, 1993).

When data are abundant, most interpolation techniques (used to estimate the value of properties at un-sampled sites within the area covered by existing observations) give similar results. However, in most situations the data collected are sparse owing to constraints on resources. When data are sparse, the assumptions made about the underlying variation and the choice of method and parameters can be critical in avoiding misleading results. Comparisons of different interpolation methods on a data set will provide a variety of answers, but geostatistics is the only method that provides an estimate of uncertainty which allows the best use of the result (Burrough and McDonnell, 2000). It is the robustness of the assumptions behind geostatistics that make it such a valuable tool in comparison to simple interpolation methods such as regression, trend surface analysis, nearest neighbour methods and splines.

The main observation behind geostatistics is that samples are more likely to be similar to each other the closer they are located in space. Geostatistics uses this idea in attempting to model the relationship between points as the distance between them changes. A regionalised variable  $Z(x)$  (Matheron, 1963) is a random variable that takes different values according to its location  $x$  within some region. The term regionalised variable was coined to emphasise the two apparently contradictory aspects of  $Z(x)$  – that it combines both random and structured components. The random element comprises local

irregularities and the structured elements are large-scale trends and tendencies in the data.

The basic steps of a geostatistical analysis consist of the creation of an experimental variogram (described in §2.2), fitting a model to the variogram and using the information from this to carry out kriging (assuming the aim is to create a map). Section 2.2 details the specific methods used in this thesis. Kriging is a generic name adopted by geostatisticians for a family of generalised least-squares regression algorithms (Goovaerts, 1999). It is a technique of making optimal, unbiased estimates of regionalised variables at unsampled locations using the theory of stationarity, the structural properties of the covariance and the initial set of data values (Militano and Ugarte, 2001). The theory of stationarity states that the moments of a distribution of a random variable are the same everywhere (Webster, 2000). Kriging divides spatial variation into three components – (i) deterministic variation (different levels or trends), (ii) spatially autocorrelated variations, and (iii) uncorrelated noise (Burrough and McDonnell, 2000).

Kriging provides a solution to the problem of estimation based on a continuous model of stochastic spatial variation. It makes the best use of existing knowledge by taking account of the way that a property varies in space through the variogram model (Webster and Oliver, 2001). There are many kinds of kriging, some developed to tackle specific problems in areas such as mining and petroleum engineering. Ordinary punctual kriging is the most common form of kriging. It was used in this thesis because it predicts values at the same scale or support of the original data and the predictions can be easily compared to the original values. It is also a relatively simple technique.

### 1.5.1 Previous studies

Many studies have used geostatistics to analyse heavy metal concentration in soil (e.g. Atteia et al., 1994; Steiger et al., 1996; Saldaña et al., 1998) but there does not appear to have been much work on using derived values (solubility in this case) within geostatistics. In this thesis it is proposed to use geostatistics to interpolate metal solubility values derived from G-BASE data in order to create maps of solubility to assess the risk of food contamination.

## 1.6 THESIS SUMMARY

In summary, the availability of metals depends on their free ion concentration ( $M^{2+}$ ) in the soil solution. Equations predicting ( $M^{2+}$ ) have to be simple if they are to be used with geochemical survey data. The spatial resolution of large geochemical surveys is often not down to a field scale that would be useful to individual farmers. When completed with full coverage of the UK, G-BASE will be the highest resolution geochemical survey. The objective of this thesis is to test the viability of applying metal availability models to a large scale geochemical survey and attempt to quantify the separate sources of prediction error.

Chapter 2 outlines details of methods used throughout the investigation. This includes all the analytical methods, details of geostatistical analysis and procedures used in the two fieldwork campaigns.

Chapter 3 describes the initial investigation into the G-BASE data and the geostatistical analysis and mapping of total soil metal concentration and pH. The metal solubility algorithm was then applied to the G-BASE data and the resulting metal solubility predictions were kriged and mapped. The kriging results indicated that the uncertainty of the predicted solubility values were very high, so an uncertainty analysis of

the solubility algorithm was carried out. The analysis in Chapter 3 showed that the sampling scale of the G-BASE survey misses much of the short-scale variability, and that pH is the greatest contributor to total uncertainty.

Chapter 4 presents the results of fieldwork conducted to assess the accuracy of the solubility algorithm by returning to G-BASE sampling sites and measuring the zinc concentration in the soil solution to compare with predicted zinc solubility.

Chapter 5 presents the investigation into the short-scale spatial variability of pH prompted by the results in Chapter 3. The pH across a field was measured and analysed using geostatistics. Metal uptake by plants was estimated using the pH values across the field compared to using the average for the field.

Chapter 6 provides a summary of the key findings of the thesis.

## 2. METHODS

### 2.1 ANALYTICAL METHODS

#### 2.1.1 pH

##### 2.1.1.1 *Introduction*

In this thesis pH has been measured using two different procedures, one for measuring the pH of archived G-BASE samples and one for a short-scale spatial variability study.

The G-BASE project only measured the pH of sub-soil samples for the Humber-Trent study region, using a salt solution (0.01 M  $\text{CaCl}_2$ ) as a suspending electrolyte. This gives rise to two problems with respect to utilising survey pH values to predict metal solubility. Firstly, G-BASE measures metal concentrations on the top-soil samples and secondly the metal solubility algorithm has been calibrated using pH values determined with water as the suspending electrolyte. Therefore, the pH values of the archived G-BASE top-soil samples for the region of interest had to be measured in water.

In a second study, examining the short scale variability in pH, greater care was taken in establishing a reliable method. The theory of pH measurement is discussed briefly below, before the methods used to measure pH in the short scale variability study and in the G-BASE sample pH measurement are outlined.

##### 2.1.1.2 *pH theory and measurement*

pH is defined as the negative logarithm of the hydrogen ion activity,  $\text{pH} = -\log_{10} \text{H}^+$ . It is a direct measure of acidity according to the Brønsted definition of acids as substances that are able to donate hydrogen ions, and bases as substances that are able to combine with hydrogen ions (Linnet, 1970).

Despite pH measurements being a routine part of any soil survey it is difficult to quantify the errors involved in measurement. pH values of colloidal suspensions such as soils have often been measured with little attention being paid to the operational factors which affect the electrochemical measurements that result. These problems arise primarily from uncertainties associated with liquid junction potentials, and the heterogeneity of soil suspensions resulting in the '*suspension effect*' and '*salt effect*' amongst others (Sumner, 1994). There is also a great deal of uncertainty in the literature over the length of time required to establish an equilibrium between the solid and solution phases.

As one of the aims of the short-scale pH study was to minimise uncertainty in pH measurement, an understanding of the suspension effect and salt effect is needed in order to design the best method for pH measurement.

A pH measurement is usually carried out using a combined electrode containing a pH sensitive glass electrode and a reference electrode. The reference electrode is filled with a concentrated KCl solution which slowly leaks into the test solution through a porous liquid junction. The filling solution makes a contact between the internal reference element and the liquid junction (and hence the test solution outside the electrode) and so is sometimes referred to as a salt bridge. KCl is used as  $K^+$  and  $Cl^-$  have nearly equal mobilities, so that each conducts almost the same amount of current (Bloom, 2000). A 'liquid junction potential',  $E_j$ , is the result of the salt bridge solution containing different concentrations of ions to the test solution. The interdiffusion between the two solutions carries electrical charge unequally across the liquid junction affecting the pH measurement (Sumner, 1994). Soils are cation exchangers, so can have a disproportionate effect on the rate of  $K^+$  diffusion compared to  $Cl^-$  diffusion into solution. The effect increases with increasing suspension concentration, and results in a decrease in the measured pH. This is known as the '*suspension effect*'. The common practice of stirring soil water suspensions while measuring pH greatly increases the suspension effect (Sumner, 1994). The effect can be minimised by measuring pH in salt solutions greater than 0.01 M and by placing the electrode in the supernatant.

The salt effect can be illustrated as follows: the pH value of an aqueous solution of 0.01 molal hydrochloric acid would be exactly 2.00 if no salt effect was present, i.e. if the hydrogen ion activity was equal to its concentration. However, the pH of this solution is actually 2.05 (at room temperature) owing to the salt effect of the hydrochloric acid itself (Linnet, 1970).

All soils will produce a certain level of electrolyte in their pore water, which might have an effect on the soil pH measured. It has been demonstrated that when the pH of a soil is measured in an electrolyte such as KCl or CaCl<sub>2</sub>, the pH value for a negatively charged soil is lower than when measured in water (Sumner, 1994; Blake et al., 2000). There are two reasons for the difference between pH measured in salt solution and water. First, when water is added to a soil in order to measure the pH, the concentration of electrolyte which would have been present under field conditions is diluted. This reduces the salt effect and gives a lower pH measurement than the soil should produce. Secondly, when a salt solution such as 1M KCl is added to a soil, there is an exchange of the added cations and anions with H<sup>+</sup> (and Al<sup>3+</sup>) and OH<sup>-</sup> on solid surfaces, lowering the pH measured (Sumner, 1994).

Sumner (1994) and Blake et al. (2000) conclude that pH should preferably be measured in a 0.01 M CaCl<sub>2</sub> solution, (which approximates the salt concentration of the natural soil solution) to minimise the liquid junction potential. However, we are limited to measuring pH in water, as all the pH measurements used in the creation of the metal solubility algorithm (Tye et al., 2003) have been measured in water. If using water is unavoidable, Sumner proposes that as small a soil:water ratio as possible is used and that the suspension is allowed to settle so that the calomel electrode salt bridge can be placed in the clear supernatant liquid.

Contrary to Sumner's conclusions, many pH measurements are now carried out in de-ionised water (for example Blake et al (2000), Webb et al (2001), Zhang et al(2002)). Gascho et al (1996) found that the correlation between pH values measured in water and those measured in CaCl<sub>2</sub> was high ( $r = 0.97$ ) and

concluded that there was no clear reason to use salt over water for soil pH measurements.

#### *2.1.1.3 Method used for measuring pH of archived G-BASE samples*

A 1:2.5 volume ratio of soil to water was used. Ten grams of air dried soil was mixed with 25 ml of deionised water. This was mixed well and left to stand for 30 minutes. After this time the slurry was re-suspended by mixing with a glass rod. The electrode was rinsed thoroughly and stirring applied to the solution at a constant rate until a stable pH reading was obtained. Soils were tested in batches of 10 samples and the highest and lowest of each batch was re-tested as a check.

#### *2.1.1.4 Method of pH measurement for electrode selection*

Three ‘Red Rod’ combined electrodes from Radiometer Analytical (pHC2005, pHC2401 and pHC2701) were tested to see which was most suitable to use for testing the samples from the fieldwork. The electrodes are characterised by the relative flow rate of the internal filling solution across the liquid junction: ‘slow’ (pHC2005), ‘medium’ (pHC2401) and ‘fast’ (pHC2701). Red Rod electrodes use silver/silver chloride reference electrodes. The ‘slow’ electrode had a porous pin liquid junction and was designed to be “robust”. The ‘medium’ electrode had an annular ring liquid junction. These two are both classed as “general purpose” by the manufacturer. The ‘fast’ electrode was classed as “high KCl flow” and also had an annular ring. The pH meter used was a Radiometer Analytical pHM82 Standard pH meter with a chart reader.

Two soils, ‘U’ and ‘Q’ were chosen from archived control soils used in a previous study (Tye et al., 2003). ‘U’ had a pH of 4 and ‘Q’ a pH of 7 in order to see if the electrode responses were pH-dependant.

The soils were made into a slurry in 50 ml plastic centrifuge tubes using a 10 ml scoop of soil and 25 ml of deionised water. The tubes were placed on an end-over end shaker for an hour. The tubes were centrifuged to separate the



soil from the supernatant. The first measurement was carried out with the electrode in the supernatant and was left for at least 10 minutes before recording the final reading. The tube was then shaken vigorously and a second measurement was carried out on the re-suspended slurry. The electrode was placed with the bulb near the bottom of the tube and the sediment allowed to settle around it. For each electrode, the pH of two samples of each soil were measured, resulting in 12 samples, and 24 measurements, in total.

#### *2.1.1.5 Method of pH measurement for short-range field study*

Based on an investigation into electrode response (the results of which can be found in Chapter 3) the following method was chosen. A combined pH electrode (the 'slow' 'Red Rod' pHC2005 described above) from Radiometer Analytical was used with the same meter for the duration of the project. The electrode was selected because it had the minimum difference between measurements on the supernatant and the slurry and had the fastest response time.

Ten ml of soil was mixed with 25 ml deionised water in a centrifuge tube and mixed on an end-over-end shaker for one hour. The reading was taken by inserting the electrode to the bottom of the tube, allowing the sediment to settle, and taking the reading after 6 minutes. The measurement was taken using the slurry rather than the supernatant because in general the slurry gave a more consistent reading in the electrode test. It also saved time by cutting out a centrifugation step to separate the supernatant. The equilibration time was chosen after monitoring the drift in soil pH for 2 soils with contrasting pH values. The soils were randomised and split into batches of 10, with a QC sample in each batch.

#### **2.1.2 Loss on Ignition**

Soil samples were dried overnight at 105 °C. Approximately 10 g of oven-dry soil was weighed into a crucible and heated at 500 °C in a muffle furnace over

night. The loss of mass recorded between 105 and 500 °C is the loss on ignition (LOI) and is an estimate of organic matter content (Rowell, 1995).

### 2.1.3 Analysis of total soil metal content

An aqua regia digest was used to extract the metals from the soil samples for the subsequent determination of pseudo-total concentrations. Between 1 and 2 g of finely ground soil were digested in a mixture of 15 ml concentrated hydrochloric acid and 5 ml concentrated nitric acid. The solutions were boiled on a hot plate until reduced to approximately 5 ml. When cool, deionised water was added and the samples filtered and made up to 50 ml.

The resulting solutions were analysed for several trace metals using a Varian SpectrAA 220FS Atomic Absorption Spectrometer with a SIPS auto-dilution attachment. The SpectrAA has two thermal devices for atomisation, flame atomisation and thermoelectric atomisation. Table 2.1 shows the elements measured and the methods used.

Element	SIPS matrix	Instrument Type	Instrument Mode	Top calibration	Wavelength (nm)	Modifier
Cd	N/A	Furnace		10 µg L <sup>-1</sup>	228.8	(NH <sub>4</sub> ) <sub>2</sub> HPO <sub>4</sub> 2%
Cu	7.5%	Flame (Air)	Absorbance	5 mg L <sup>-1</sup>	324.8	None
Pb	HCl and	Flame (Air)	Absorbance	10 mg L <sup>-1</sup>	217.0	None
Zn	2.5% HNO <sub>3</sub>	Flame (Air)	Absorbance	5 mg L <sup>-1</sup>	213.9	None

*Table 2.1: Elements measured on the SpectrAA FAAS*

### 2.1.4 Soil pore water extraction for large scale field study

Total soil metal content alone is not a good measure of short-term bioavailability and is not a useful tool to determine potential risks from soil contamination (Hough et al., 2004). Analysis of the soil pore water can provide a better measure, with the assumption that rates of transfer across biological membranes are proportional to the free ion activity of trace metals in solution

(Sauvè et al., 2000). Centrifugation is one method of extracting pore water from soil (di Bonito, 2004).

A preliminary study found that soil at field conditions was not wet enough to yield sufficient pore water for analysis. Therefore the following method was devised. Field-moist soils were sieved to less than 4mm and initially stored in plastic food boxes with air holes to avoid changing the redox status of the soil. Field capacity was determined on re-packed cores using a sand bath at 0.005 MPa for 48 hours. Moisture contents were determined gravimetrically by drying sub-samples overnight at 105°C. De-ionised water was added to each soil in order to create a moisture content of 110% field capacity. The soil and water were mixed in a plastic bag and incubated for a further 48 hours to allow the added water to reach equilibrium with the soil. Each day the boxes were weighed to check for evaporation, and any water lost was replaced by spraying de-ionised water onto the surface of the soil. After the incubation time the soils were centrifuged to extract the soil pore water.

Six polyoxymethylene (Acetal) tubes with 316 stainless steel 20 µm mesh filters were manufactured at the BGS (see Figure 2.1) to fit in the fixed-angle rotor available with a Beckman J2-21 high speed refrigerated centrifuge. The tubes consist of a bottom cup (part 1 in Figure 2.1), to collect the extracted pore water, into which is screwed a plastic filter (part 4 in Figure 2.1). A stainless steel filter is placed on top, followed by a filter paper; the top section (part 2 in Figure 2.1) is screwed on and filled with soil. The 6 tubes are weighed to ensure they are of equal weight. A lid is screwed on firmly before centrifugation (part 3 in Figure 2.1). The soils were centrifuged for 1 hour 30 minutes at 3000 rpm at 16°C (the temperature of the soil storage room). Six tubes of soil yielded on average about 100 ml of solution per soil. The centrifugation method was adapted from di Bonito (2004)

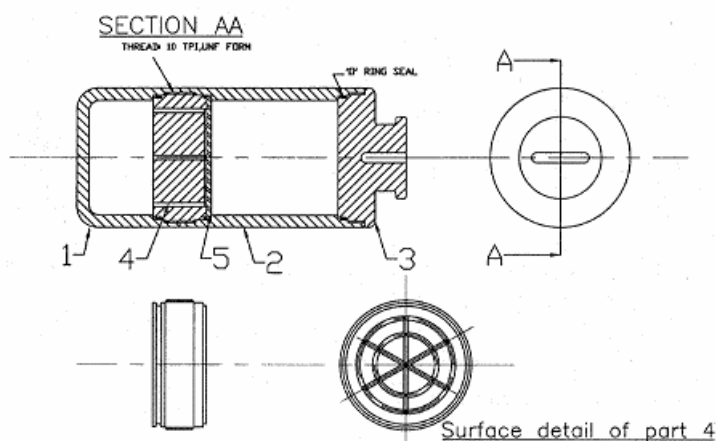


*Figure 2.1: Centrifuge tubes for soil pore water separation, designed and manufactured by R&D Workshop. BGS, Keyworth.*

Each sample was split into sub-samples for the different analyses required; some were acidified to 1%  $\text{HNO}_3$  v/v and the unacidified sub-samples were frozen to preserve them until all samples were collected. The acidified sub-samples were stored in the fridge.

### **2.1.5 Analysis of soil pore water**

The extracted soil pore water was analysed for trace metal content, carbon content and major anions and cations.

Trace element analysis was carried out using inductively coupled plasma mass spectrometry (ICP-MS), at the BGS, Keyworth. Samples were acidified to 1%  $\text{HNO}_3$  using aristar grade concentrated acid. The quadrupole ICP-MS instrument used was a VG Plasmaquad PQ 2+ in combination with a Gilson 222 autosampler. The system was controlled by a PC through dedicated software.

Major elements were also measured at the University of Nottingham using a Varian SpectrAA 220FS Atomic Absorption Spectrometer with a SIPS (sample introduction pump system) auto-dilution attachment. As with the ICP-

MS measurements, the samples were acidified. Table 2.2 shows the elements measured and the methods used.

Element	SIPS matrix	Instrument Type	Instrument Mode	Top calibration	Wavelength (nm)	Modifier
Ca	1% HNO <sub>3</sub>	Flame (N <sub>2</sub> O)	Emission	50 mg L <sup>-1</sup>	422.7	Cs/Sr 10%
Mg		Flame (Air)	Absorbance	10 mg L <sup>-1</sup>	202.6	
K		Flame (Air)	Emission	50 mg L <sup>-1</sup>	766.5	
Na		Flame (Air)	Emission	100 mg L <sup>-1</sup>	589.0	

Table 2.2: Elements measured on the SpectrAA and conditions used.

Ion chromatography was used to measure major anions (Cl, NO<sub>3</sub>, SO<sub>4</sub> and PO<sub>4</sub>). The analysis was carried out using a Dionex DX500 with AS-14 4 mm anion exchange column. A standard eluent of Na<sub>2</sub>CO<sub>3</sub> (0.371 g/l) and NaHCO<sub>3</sub> (0.084 g/l) was used.

Total organic carbon (TOC) in the filtered pore water was determined using a Shimadzu TOC-V CPH/CPN Total Organic Carbon Analyser using a carrier gas of O<sub>2</sub>.

#### 2.1.5.1 Speciation of soil pore water using WHAM-VI

Total dissolved Zn in soil solutions [M<sub>Sol</sub>] was speciated using the Windermere Humic Aqueous Model (WHAM) which incorporates the ‘Humic Ion Binding Model VI’ (Tipping, 1998). Input files included the variables [Cu], [Pb], [Zn], [Cd], [Cl], [NO<sub>3</sub>], [SO<sub>4</sub>], [Ca], [K], [Mg] and [Na], pH, and the temperature was set at 14°C. In addition estimated values of (Fe<sup>3+</sup>) were included in the input data set, calculated from the solubility product of Fe(OH)<sub>3</sub> and its standard enthalpy (S. Lofts, *personal communication*). Instead of using atmospheric CO<sub>2</sub>, the inorganic carbon value measured by TOC was used. This gives a more accurate measurement of the total carbonate (CO<sub>3</sub>) than the atmospheric CO<sub>2</sub>.

Organic speciation within WHAM allows for complex formation with both humic acid (HA) and fulvic acid (FA). It is assumed that 30% dissolved

organic carbon (DOC) is HA, 30% is FA and 40% is inert (Weng et al., 2002). 50% of the HA and FA is assumed to be carbon. Output from WHAM VI includes the free metal ion activity, ( $M^{2+}$ ) and an inventory of all inorganic and organic (FA) complexes; ionic strength (I) in solution was also calculated from the output of the speciation model.

#### **2.1.6 Analysis of solid soil samples by XRF**

Solid soil samples were analysed for selected elements. Determination of major, minor and trace element content was carried out by wavelength-dispersive X-ray fluorescence spectrometry and energy-dispersive X-ray fluorescence spectrometry at BGS (Rawlins et al., 2003). Two Philips PW2400 sequential x-ray fluorescence spectrometers fitted with rhodium-anode X-ray tubes (3 kW 60 kV) were used for Na<sub>2</sub>O, MgO, Al<sub>2</sub>O<sub>3</sub>, SiO<sub>2</sub>, P<sub>2</sub>O<sub>5</sub>, K<sub>2</sub>O, CaO, TiO<sub>2</sub>, MnO, Fe<sub>2</sub>O<sub>3</sub>, Sc, V, Cr, Co, Cs, Ba, La, Ce, Nd and Sm as one suite and Ni, Cu, Zn, Ga, Ge, As, Se, Br, Rb, Sr, Y, Zr, Nb, Mo, Hf, Ta, W, Tl, Pb, Bi, Th and U as another. The spectrometers were controlled using Philips X40 application software package, version 3.2 and 4.01 (PW1480) and version 3.9F and 4.02 (PW2400) running under DEC VMS operating system on a VAX4000 computer. The laboratory operates under UKAS.

Samples were prepared for analysis by grinding 12 g of sample and 3 g of Elvacite 2013 (n-butyl methacrylate copolymer, Dupont & Co) in an agate planetary ballmill (Fritsch P5) for 30 minutes. The mixture was then pressed at 25 t load into 40 mm diameter pellets using a Herzog (HTP-40) semi-automatic press.

Calibration was carried out using numerous reference materials. Analytical results for six reference materials for each element, covering the analytical concentration range compared with their recommended values (Govindaraju, 1994), have been published elsewhere (British Geological Survey, 2000).

## 2.2 GEOSTATISTICS

### 2.2.1 Introduction

The techniques that are collectively known as geostatistics have been used in this project to describe spatial patterns and predict the values of soil properties at un-sampled locations. In this section some aspects of geostatistical theory and the processes involved in a geostatistical analysis are explained.

Land management decisions are usually made on a field scale, which can be predicted from the G-BASE data using geostatistics. Interpolating G-BASE data using geostatistics can create continuous surface maps which can be used to visualise spatial trends and distributions. In certain circumstances, a geostatistical approach can also provide a measure of the uncertainty associated with estimates at unsampled locations.

The central theory behind geostatistics is that of the regionalised variable ( $Z(x)$ ), a random variable that takes different values according to its location  $x$  within a region. The value of  $Z$  is given in 2.1.

$$Z(x) = m(x) + \varepsilon'(x) + \varepsilon'' \quad 2.1$$

where  $m(x)$  is a deterministic function describing the “structural” component of  $Z(x)$ ;  $\varepsilon'(x)$  is the term denoting the stochastic, locally varying but spatially dependant residuals from  $m(x)$  – the regionalised variable and  $\varepsilon''$  is a residual, spatially independent Gaussian noise term having zero mean (Burrough and McDonnell, 2000).

The variogram, described in detail in §2.2.4, is a central part of a geostatistical analysis. It gives a picture of the relationship (difference) between sample values versus the distance between their locations.

### 2.2.2 Exploratory Data Analysis

The first stage in the geostatistical analysis is to explore the data. Boxplots are an ideal graphical way to describe the frequency distribution, showing the interquartile range and any outliers. Histograms and descriptive statistics highlight any skewness in the data. Any obvious outliers are removed to reduce the skewness of the data. Skewness is a measure of the asymmetry of the data, the most common departure from normality in environmental data. If the data is skewed then there is doubt over which measure of centre to use, causing uncertainty in further analysis. The estimates obtained with the usual computing formula for the variogram are sensitive to outliers and strong skewness in distributions. If data are skewed then the confidence limits on the variogram are wider than they would otherwise be, and as a result the semi-variances are less reliable (Webster and Oliver, 2001).

If the data is strongly skewed (i.e.  $> 1$ ) the variances are considered too unstable to compute a variogram, and the data must be transformed using a function that produces data closer to a normal distribution. The transformation used in this thesis is the log transform. Data is transformed back to the original scale at the end of the analysis.

It is very important to ensure that there are sufficient data points to produce reliable estimates of the regionalised variable. The larger the sample size, the more precisely the variogram is estimated. The number of individual samples should always be greater than 50 and preferably greater than 100 (Webster and Oliver, 2001) for calculating a reliable variogram.

### 2.2.3 Assessment of Trend

Variation in  $Z(x)$  might contain a systematic component in addition to the random one, in which case.

$$Z(x) = u(x) + \varepsilon(x)$$

2.2



where  $u(x)$  is the drift. The presence of drift or trend present means that the assumptions of the random function model no longer hold. Semi-variances computed on data with trend will be biased. The variogram describing random variation in the presence of trend must be calculated on the residuals after removal of the trend. In order to separate the trend from the data a multiple regression analysis is carried out. The predictors are the spatial coordinates, such that

$$Z(x_1, x_2) = f(x_1, x_2) + \varepsilon_1 \quad 2.3$$

where  $Z(x_1, x_2)$  is the predicted value at  $\{x_1, x_2\}$  and  $f$  denotes a function of the spatial coordinates at this location. The model also contains an error term,  $\varepsilon_1$ . Plausible functions, usually simple polynomials such as planes, quadratics and cubics are fitted by least squares to the spatial coordinates thereby minimising the sum of squares. The equation used in this study is the quadratic function

$$Z = b_0 + b_1x_1 + b_2x_2 + b_3x_1^2 + b_4x_2^2 + b_5x_1x_2 \quad 2.4$$

Geostatisticians generally remove trend if it accounts for more than 20% of the variance (R. Webster, personal communication).

## 2.2.4 The Variogram

### 2.2.4.1 Estimating the Variogram

Once the data has been examined and determined fit for geostatistical analysis, the experimental variogram can be computed. Three variograms can be distinguished: the experimental variogram, the regional variogram and the theoretical variogram (the experimental variogram summarises the spatial distribution of  $z$  in the absence of trend). The experimental variogram is the variogram computed from the data and is represented by symbols in Figure 2.2.

The semivariance (half a variance) is the variance per sample point when the points are considered in pairs. As a function of  $\mathbf{h}$  (the distance between the points, or the ‘lag’) it is the semivariogram, now usually termed the variogram (Webster and Oliver, 2001). The semivariance can be estimated from sample data

$$\hat{\gamma}(h) = \frac{1}{2n} \sum_{i=1}^n \{z(x_i) - z(x_i + h)\}^2 \quad 2.5$$

where  $n$  is the number of pairs of sample points of observations of the values of attribute  $z$  separated by distance  $h$ . A plot of  $\hat{\gamma}(h)$  against  $h$  is known as the experimental variogram (see the symbols in Figure 2.2).

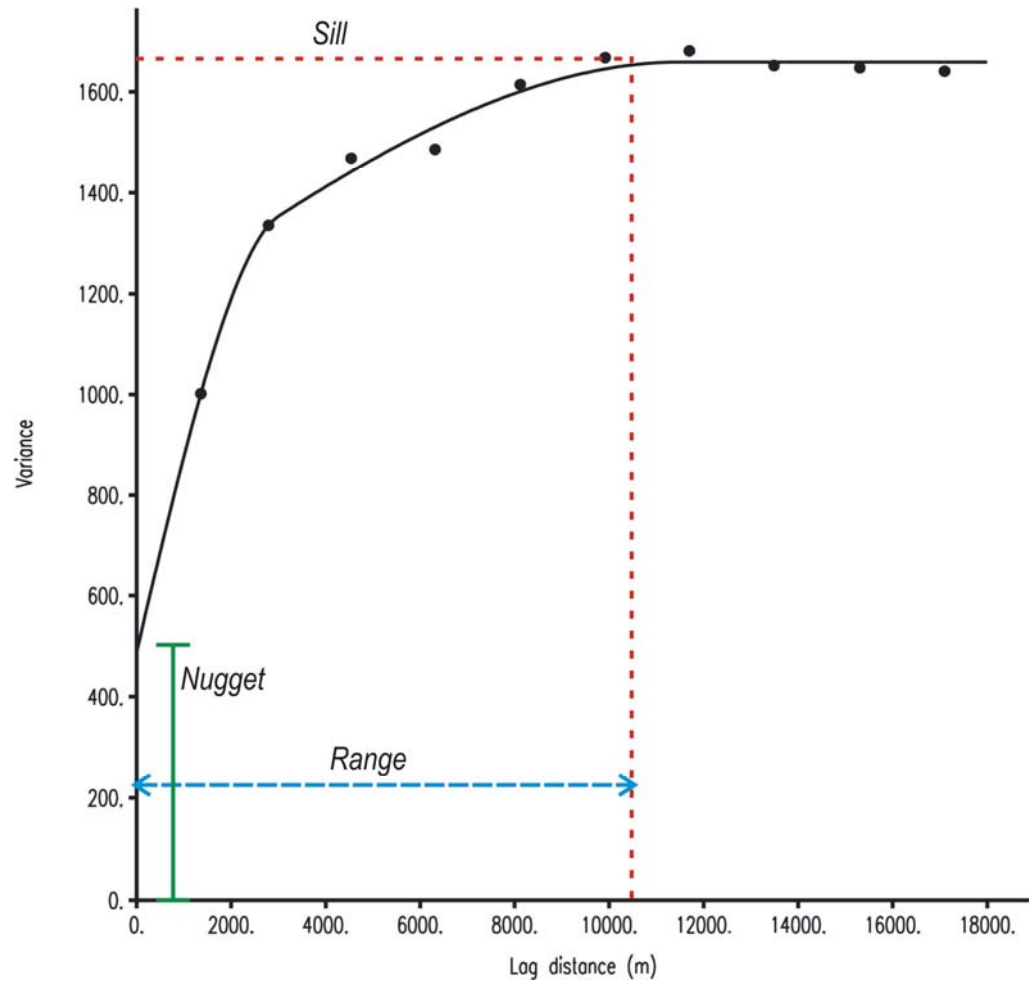


Figure 2.2: Sample variogram with key features highlighted. Symbols (●) show the experimental variogram, and the solid black line is the model of the theoretical variogram, in this case a double spherical model.

#### 2.2.4.2 Modelling the Variogram

The regional variogram is the variogram that would be computed if the complete information for a region was available. As this is never the case, this is approximated by the theoretical variogram. The theoretical variogram is the variogram of the process that you imagine generated the field of which the measured data are a sample. A mathematical function must be fitted to the experimental variogram as a model or approximation to the theoretical variogram (Webster and Oliver, 2001).

A variety of simple, authorised models can be used (authorised in the sense they cannot return negative variances (Oliver and Webster, 1991)), and the fit (percentage of variance accounted for) of these is calculated by a conventional regression analysis. The most commonly used models are described below.

Figure 2.2 shows an example variogram from this research with a fitted curve. The curve shows three important features. (i) At large values of the lag  $h$ , it levels off. This horizontal part is known as the sill and implies that at these values of the lag there is no spatial dependence between the data points. The lag is the separation between the two samples in a pair, in two dimensions this is a vector, with both distance and direction (Webster and Oliver, 2001). (ii) The curve rises from a low value of  $\hat{\gamma}(h)$  to the sill, reaching it at a value of  $h$  known as the range. This describes how inter-site differences are spatially dependent within the range, the closer sites are together the more similar they are likely to be. (iii) The fitted model does not pass through the origin, but cuts the  $y$ -axis at a positive value of  $\hat{\gamma}(h)$ . This is an estimate of  $\varepsilon''$ , the residual, spatially uncorrelated noise, known as the ‘nugget’ (Burrough and McDonnell, 2000). The nugget consists of two components: i) analytical error and ii) short-scale variability that occurs at scales smaller than the shortest sampling interval.

#### 2.2.4.3 Commonly used variogram models

There are a number of different models that can be fitted to the variogram. Spherical, double spherical, exponential and linear models have been used in this study.

The spherical model was first proposed by Matheron (1963) and represents the non-overlap of two spheres of influence. The formula is cubic since it represents volumes, and relies on two parameters, the range of influence (radius of the sphere) and the sill which the experimental variogram reaches at the range. In addition to these there may also be a nugget effect.

$$\gamma(0) = 0$$

$$\gamma(h) = C_0 + C \left\{ \frac{3}{2} \frac{h}{a} - \frac{1}{2} \frac{h^3}{a^3} \right\} \quad \text{when } 0 < h < a$$

$$\gamma(h) = C_0 + C \quad \text{when } h > a \quad 2.6$$

where  $\gamma$  is the semi-variogram and  $h$  the distance between the two points of interest. The parameter  $a$  represents the range of influence of the semi-variogram.  $C$  is the sill of the spherical component and  $C_0$  the nugget effect on the  $\gamma$  axis (Clark and Harper, 2000).

There are modifications that may be made to the standard spherical model. There are often cases where the semi-variogram reaches a definite sill but does not quite match the shape of a single spherical model. It is possible to mix spherical components with different ranges of influence and/or sill values. Hence the formula for a double spherical model is

$$\gamma(0) = 0$$

$$\gamma(h) = C_0 + C_1 \left\{ \frac{3}{2} \frac{h}{a_1} - \frac{1}{2} \frac{h^3}{a_1^3} \right\} + C_2 \left\{ \frac{3}{2} \frac{h}{a_2} - \frac{1}{2} \frac{h^3}{a_2^3} \right\} \quad \text{when } 0 < h < a_1$$

$$\gamma(h) = C_0 + C_1 + C_2 \left\{ \frac{3}{2} \frac{h}{a_2} - \frac{1}{2} \frac{h^3}{a_2^3} \right\} \quad \text{when } 0 < h < a_2$$

$$\gamma(h) = C_0 + C_1 + C_2 \quad \text{when } h > a_2 \quad 2.7$$

(Clark and Harper, 2000).

The exponential model was developed to represent the notion of exponential decay of “influence” between two samples. It has two main parameters: the range of influence and the sill, which the graph tends to at large distances. There is also a possible nugget effect.

$$\gamma(0) = 0$$

$$\gamma(h) = C_0 + C \left\{ 1 - \exp\left(-\frac{h}{a}\right) \right\} \quad \text{when } h > 0 \quad 2.8$$

Where  $\gamma$  is the semi-variogram and  $h$  the distance between the two points of interest. The parameter  $a$  represents the range of influence of the semi-variogram.  $C$  is the sill of the exponential component and  $C_0$  the nugget effect on the  $\gamma$  axis (Clark and Harper, 2000).

The linear model is the simplest model for a semi-variogram, a straight line with a positive (or zero) intercept with the y-axis.

$$\gamma(0) = 0$$

$$\gamma(h) = C_0 + jh \quad \text{when } h > 0 \quad 2.9$$

where  $\gamma$  is the semi-variogram and  $h$  the distance between the two points of interest. The parameter  $j$  represents the slope of the line and  $C_0$  the nugget effect on the  $\gamma$  axis.

The fit of models can be improved by changing the step length, which determines the lag distance ( $\lambda$ ) and maximum lag distance.

The geostatistical analysis in this project has been carried out using GenStat® for Windows (5<sup>th</sup> and 6<sup>th</sup> editions). An example of the code used to create a variogram is in Appendix I and its output in Appendix II.

### 2.2.5 Kriging

The aim of kriging is to estimate or predict the values of  $z$  at unsampled places from the data. Ordinary kriging is used in approximately 90% of cases. The original data and the model of the variogram are used. When the nugget variance  $\varepsilon$  so dominates the local variation that the experimental variogram shows no tendency to diminish as  $h \rightarrow 0$ , the interpretation is that the data are so noisy that interpolation is not sensible. In this situation, the best estimate of  $z(x)$  is the overall mean computed from all sample points in the region, without taking spatial dependence into account.

In this study punctual kriging has been used – where the predictions made are for points. Block kriging is also commonly used where the predictions made are for areas of specified dimensions.

Ordinary kriging computes a weighted average of the data and is the most commonly used form of kriging. Given that the spatially dependent random variations are not swamped by uncorrelated noise, the fitted variogram can be used to determine the weights  $\lambda_i$  needed for local interpolation. The procedure is similar to that used in weighted moving average interpolation except that now weights are derived from a geostatistical analysis (i.e. the shape of the variogram) rather than a general model.

The value  $z(x_0)$  is given by:

$$\hat{z}(x_0) = \sum_{i=1}^n \lambda_i \bullet z(x_i) \quad 2.9$$

With  $\sum_{i=1}^n \lambda_i = 1$ . The weights  $\lambda_i$  are chosen so that the estimate  $\hat{z}(x_0)$  is unbiased, and that the estimation variance  $\sigma_e^2$  is less than for any other linear combination of observed values. The minimum variance of  $[\hat{z}(x_0) - z(x_0)]$ , the prediction error, or kriging variance is given by:

$$\hat{\sigma}_e^2 = \sum_{i=1}^n \lambda_i \gamma(x_i, x_0) + \phi \quad 2.10$$

And is obtained when

$$\sum_{i=1}^n \lambda_i \gamma(x_i, x_0) + \phi = \gamma(x_j, x_0) \text{ for all } j \quad 2.11$$

$\gamma(x_i, x_j)$  is the semivariance of  $z$  between sampling points  $x_i$  and  $x_j$ :  $\gamma(x_i, x_0)$  is the semivariance between the sampling point  $x_i$  and the unvisited point  $x_0$ . Both are obtained from the fitted variogram. The quantity  $\phi$  is a lagrange multiplier

required for minimisation. Ordinary kriging is an exact interpolator in the sense that the interpolated values, or best local average, will coincide with the values at data points. In mapping, values will be interpolated for points on a regular grid that is finer than the spacing used for sampling (Burrough and McDonnell, 2000).

Another form of kriging is Simple Kriging. This is prediction by generalised linear regression under the assumption of 2<sup>nd</sup> order stationarity with a known mean. This is often too restrictive for most data and is therefore not commonly used.

### **2.2.6 Cross-Validation**

Cross-validation has often been misused (and confused with jackknifing), but its primary use in geostatistics is to find the “best” model for a variogram (Davis, 1987). Cross-validation uses kriging retrospectively to check the variogram model. It involves computing the moments of the distribution of residuals for all data points when each data point is successively left out and predicted from the rest of the data (Burrough and McDonnell, 2000). In this thesis cross-validation has been used as a way of estimating the uncertainty of the kriging predictions when a transformation has taken place and kriging variances are not produced.

### **2.2.7 Is kriging better than simple interpolation?**

Kriging is referred to as a Best Least squares Unbiased Estimator (BLUE) and as such provides more reliable predictions than other interpolators. Laslett and McBratney (1990) showed that geostatistical methods are superior to other interpolator methods for a variety of reasons. Kriging is used when the variation of an attribute is so irregular, and the density of sampling is such that simple interpolation methods may give unreliable predictions (Burrough and McDonnell, 2000). As such is it more flexible than some other methods. Kriging also has a number of other advantages. It provides probabilistic estimates of the quality of the interpolation; allows predictions for blocks of



land greater than the support; allows interpolation of indicator functions and can incorporate soft data to guide interpretation (Burrough and McDonnell, 2000).

## 2.3 FIELD WORK

### 2.3.1 Large scale validation of the metal solubility algorithm

#### 2.3.1.1 Preliminary field work

The aim of this section of the project was to conduct a sampling program returning to G-BASE sites in order to measure the metal solubility and compare this to the predictions made from the solubility algorithm. A trial survey revisiting four G-BASE sites was conducted in order to develop the methods for the final programme. The four sites were selected to give the following combinations of relevant soil properties: high pH and large metal concentration (HH); high pH and small metal concentration (HL); low pH and small metal concentration (LL) and low pH and large metal concentration (LH). ‘High’ values were chosen to be those in the upper quartile range, and ‘low’ values those in the lower quartile range of pH or soil metal concentration. A short-list of sites was created using these criteria. The short-list was further refined on the basis of land-use. The selected area was predominantly (75%) agricultural (arable or pasture) with an even split between the two uses. The four sites finally selected (see Table 2.3) were chosen for ease of access and the absence of hazards.

Sample Number	Easting	Northing	OS map no.	Landuse	pH /Metal	Location/soil type
408380	440310	373090	120	pasture	HH	Footpath behind pub in Brimington. Soil 541f
408588	440750	365320	120	arable	LH	Bridleway behind school, north wingfield.
402805	447800	394400	111	arable	LL	Near sunnyside mine. Soil 541f
408115	450310	383870	120	pasture	HL	Todwick (near M1 J31) Kiveton Park. Soil 541f

*Table 2.3: Trial survey sites*

A handheld GPS was used to locate the sample sites. Soil was collected using the method employed by G-BASE (Rawlins et al., 2003). A soil auger was used to take 5 samples from the centre and corners of a 20 m x 20 m square sampling 'support'. The samples were aggregated to yield one bulk sample for each site. Aggregated samples were sieved while field moist to remove stones and placed in plastic boxes with air holes to prevent anaerobic conditions developing. Owing to the fact that it was not possible to dry the soil prior to sieving, the largest available sieve was used (approx. 8 mm), and with some soils the removal of stones had to be done by hand.

Soil pore water was extracted using centrifugation. Purpose made centrifuge tubes made by BGS were used to extract the pore water from the soil (see §2.1.4). Initially, extraction of pore water under field conditions was attempted. However, it proved difficult to recover sufficient water to carry out all the analysis required. Increasing the speed of centrifugation led to leaking from the containers, and repeating the centrifugation to recover smaller increments of water was too time consuming. It was concluded that water would have to be added to the soil and re-equilibrated in order to extract the amount of soil solution required.

### *2.3.1.2 Final large-scale study*

It was decided to re-sample 25 G-BASE sites. This figure was a compromise between the need for as large a data set as possible and the need to collect and process the field soil samples within a restricted period of time.

The first step in choosing the sample locations was to remove global and local outliers from the G-BASE data set. Local outliers indicate 'hotspots' of metal concentration and on the basis of experience with the preliminary study it was decided to avoid these to reduce the chance of missing the hotspot and finding different results from those recorded by G-BASE. The variogram cloud function in S+ was used to identify local outliers, see Figure 2.3. The variogram cloud is a plot of the squared differences between pairs versus the distances, i.e. a scatterplot of the set of pairs. It is useful for the detection of

global outliers and local outliers. Global outliers are measurements that are distinctly separate from the main part of the data and are easily spotted by a number of methods. They stand out in a variogram cloud because for every distance, the squared differences of pairs that were formed with such an outlier will be significantly larger than the rest of the cloud. Local outliers are hidden in the main bulk of the observed data, but differ markedly from the neighbouring values. Local outliers are more difficult to identify than global outliers, as they will result in large squared differences for small distances close to the origin only (contributing to a high nugget), but will behave normally for medium to large distances. (Ploner, 1999). The local outliers for Pb, Cu and Zn were identified and removed.

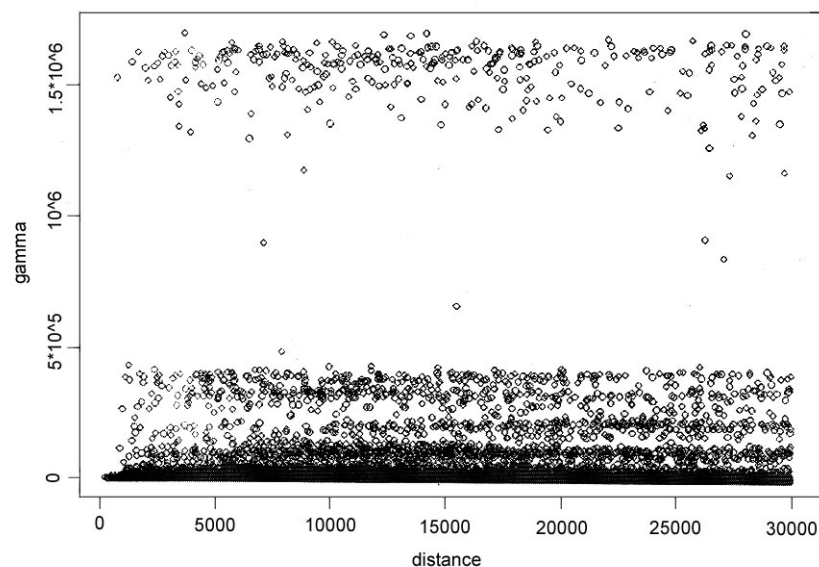


*Figure 2.3: Variogram cloud for Pb across the Westphalian region. Points at the top of the graph represent local outliers.*

Any sites that were not pastoral or arable land use were removed as in the preliminary study, to keep the samples representative of the area as a whole (75% of the area is pastoral or arable).

The remaining samples were ordered by pH and split into 8 groups. These were then ordered by metal concentration, and 5 sites selected from each group

to represent a range of pH and metal concentration. These 40 sites were examined for location and ease of access and 25 sites were selected. A number of alternative sites were held in reserve. In the process of sampling a number of problems were encountered with access. For example, one land owner refused to allow sampling (even after speaking to the BGS), one site had been built over, a number of sites were home to very angry bulls and a few appeared to have no means of access. One was on the green of the first hole of a golf course! The final number of samples collected was 21, even after visiting all the reserve sites. Table 2.4 shows the 21 sites visited.

Sample	OS sheet	GPS easting	GPS northing	date	current landuse	G-BASE land use
2857	SK	46281	91202	15/08/03	Arable	Arable
2860	SK	48128	93361	26/08/03	Recreation	
7012	SK	33679	74523	11/08/03	Pasture	Arable
7020	SK			28/08/03		
7046	SK	34391	75813	12/08/03	Pasture	Pasture
7089	SK	34600	73806	11/08/03	Pasture	Pasture
7100	SK	30538	77314	12/08/03	Pasture	Pasture
7757	SK	38786	56046	16/07/03	Pasture	Pasture
7770	SK	36206	59293	17/07/03	Pasture	Pasture
7772	SK	36825	55176	16/07/03	Arable	Pasture
8149	SK	43930	86509	14/08/03	Pasture	Pasture
8194	SK	43838	88481	14/08/03	Arable	Pasture/Recreation
8336	SK	40600	81800	13/08/02	Arable	Arable
8370	SK	38207	81910	13/08/03	Pasture	Pasture
8374	SK	43212	64510	27/08/03	Arable	Arable/Pasture
8448	SK	50786	91599	26/08/03	Arable	Arable
8464	SK	49776	88364	15/08/03	Arable	Arable
8490	SK	51443	84201	27/08/03	Arable	Arable
8722	SK	41142	58602	18/07/03	Pasture/Arable	Arable
8786	SK	40402	59509	18/07/03	Pasture	Arable
8982	SK	37758	52259	15/07/03	Pasture	Arable

*Table 2.4: List of sites visited. (Sample IDs are G-BASE IDs without the location identifying prefix).*

### 2.3.2 Relocating G-BASE sample sites

A major factor in any study requiring temporal monitoring is the reliability with which sampling sites can be revisited. Apparent variation in soil characteristics can result from spatial errors as well as the passage of time. Experience with fieldwork in re-sampling National Soil Inventory (NSI) sites suggested that whilst someone familiar with an area can relocate sites accurately, others may find it very difficult (DEFRA, 2003).

In this project G-BASE sites were revisited using Global Positioning System (GPS) technology. The original G-BASE samples were collected during the summers of 1994, 1995 and 1996 (Rawlins et al., 2003) and located using OS Landranger 1:50,000 scale maps. Grid references were recorded to the nearest 10 m and extra information on location recorded at the site. The DEFRA study found that GPS gave a positioning accuracy of better than  $\pm 2.7$  m. Any problems in location are therefore most likely to be due to inaccuracies in the original grid references.

The original NSI requirement states that *“location accurate to 20 m on enclosed land and 50 or even 100 m on open land is reasonable”*. The DEFRA study found that the ability to get as close as possible to the target site varied from 3 m in a relatively small grassland field to 77 m on an open heath. The overall mean accuracy was 15 m, which meets the original NSI requirement (DEFRA).

The question then becomes: does it matter if we are not sampling at the target, but at 10 or even 50 m away? The DEFRA study attempts to address this question by taking samples at the target point and also sampling at 10 m and 50 m away from the target. Samples were collected from a depth of 15 cm and from the intersects of a 4 m  $\times$  4 m grid within a 20 m  $\times$  20 m square. The sites covered a range of land-uses and soil types. Analysis of the whole data set showed significant differences between the target samples and those recovered from 10 and 50 m distance for: carbon, available P, available Mg, Pb and Zn concentrations. When the sites were examined individually, a greater range of parameters where the effect of distance was significant was discovered. The uniformity of the land (i.e. rough, varied heath-land is less uniform than a managed arable field) had an impact on whether distance has a significant effect on the values (DEFRA, 2003).

### 2.3.3 Short scale spatial variation of pH

#### 2.3.3.1 Sampling error estimation

One of the aims of the investigation was to understand the propagation of errors in pH sampling. Analysis of the solubility algorithm shows that pH contributes the most variance to the metal solubility. This means that it is important to understand where errors occur in the process and to minimise them if possible. This investigation was looking at possible ways of minimising the errors involved in the various stages of sampling. There are two main areas requiring investigation, errors caused by field sampling, and errors caused by laboratory technique.

In contaminated land investigations it has been shown that it is field sampling, rather than chemical analysis, that contributes the largest source of measurement error and will therefore limit the measurement uncertainty (Ramsey et al., 1997). It is often quoted that an analysis can never be of better quality (in terms of understanding how accurate the result is) than the sample upon which it is made. However, the means with which to estimate the uncertainty introduced by field sampling has been lacking (Ramsey et al., 1997).

Ramsey's "single sampler/single protocol" method (Ramsey et al., 1997) for estimating sampling and analytical precision is the one most appropriate for this survey. This involves taking duplicate samples at some proportion of the sampling locations, typically 10%. Duplicates are not taken at exactly the same position as the original, but displaced by a distance that represents the uncertainty of locating the sample point by the particular surveying technology used. This distance will produce differences between sample duplicates caused by small scale local variation, which represents variation that may arise randomly in locating the sample location. There are three components of variation, which can be separated using analysis of variance. Two components represent uncertainty; these are the sampling and the analytical variance ( $s^2_{\text{samp}}$  and  $s^2_{\text{anal}}$ ). The third component is the between-location variance due to real

variation of the contaminant (e.g. lead) across the sites; this is termed the geochemical variance ( $s^2_{\text{geochem}}$ ). The total variance can then be expressed by:

$$S^2_{\text{total}} = s^2_{\text{geochem}} + s^2_{\text{samp}} + s^2_{\text{anal}}$$

The sampling uncertainty,  $s^2_{\text{samp}}$ , will be partly owing to small scale geochemical variation within the location and represents the uncertainty of returning to the location specified (in this case within a 1 m radius due to the care taken in setting up the grid) (Ramsey et al., 1997). In this particular case,  $s^2_{\text{samp}}$  could be generalised to ‘within the area of the sample support’ because of the way the duplicate samples were taken. This gives us an idea of the variability caused by differences in sampling within the sample support.

The errors at the laboratory stage can be examined by re-testing a reference soil at various intervals throughout the procedure.

#### *2.3.3.2 Sample collection*

Sampling was carried out on a field that is part of the University Farm at the village of Bunny near Keyworth, Nottinghamshire (see Figure 2.4). The grid consisted of 200 soil samples at 10 m intervals, see Figure 2.5. It has been shown (Webster and Oliver, 2001) that in order to establish a reliable variogram, around 150 samples are needed.

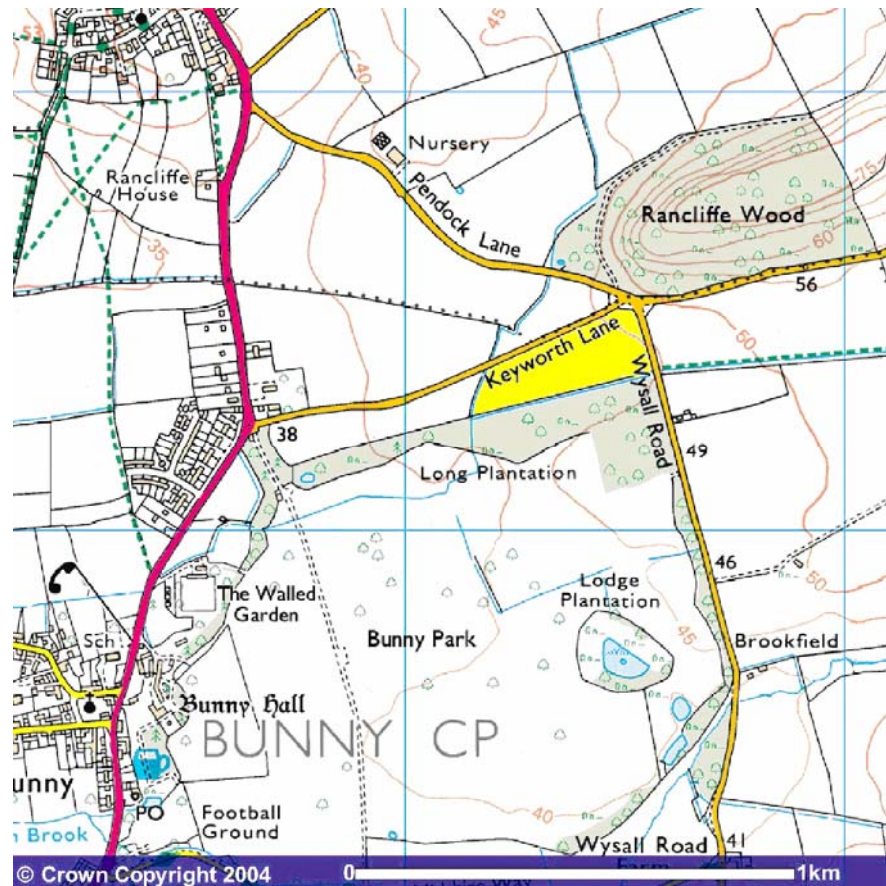


*Figure 2.4: Location of the sample site for the pH survey. National grid reference SK 594 303. The field used is highlighted in yellow and bounded by Keyworth Lane and Wysall Road on two sides, a boundary with a neighbouring field on the west and a wall with woodland beyond on the southern side.*

Parent material at the site is Mercia Mudstone (Cropwell Bishop formation) and the soil association is Dunnington Heath (drift over Permo-Triassic reddish mudstone).



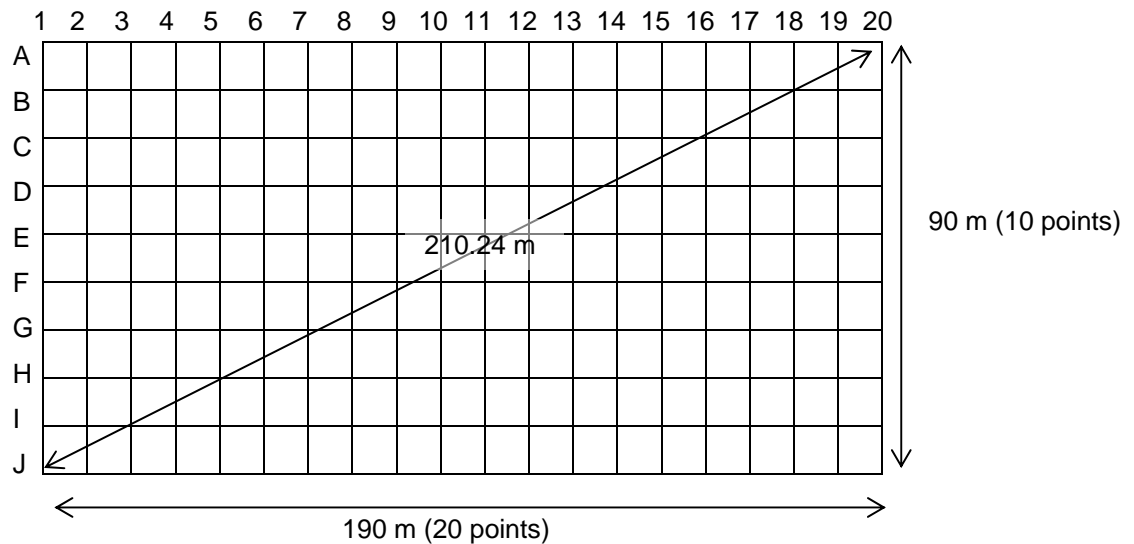


*Figure 2.5: Grid layout and numbering system for pH field sampling.*

Sampling was undertaken using a 1 m x 1 m support. A 1 m quadrat was placed on the ground at each sample point, and 5 samples of topsoil (down to 15 cm depth) taken from the corners and centre of the square using a hand corer. At 20 randomly selected sites duplicate samples were taken, following Ramsey's method discussed above. At these 20 sites, the samples and duplicate samples were sub-sampled to give 4 measurements for each site: original sample (2 subsamples - giving 2 analyses) and duplicate sample (2 subsamples - giving 2 analyses). The random duplicate sites are shown in Figure 2.6 and include a random site used as a Quality Control. This sample was tested with each batch of pH measurements to provide an estimate of the consistency of pH determination after re-calibration, and was tested 29 times. The sample was larger than the other samples and well mixed to ensure it was homogenous. The samples were selected using the random number analysis tool in Microsoft Excel.

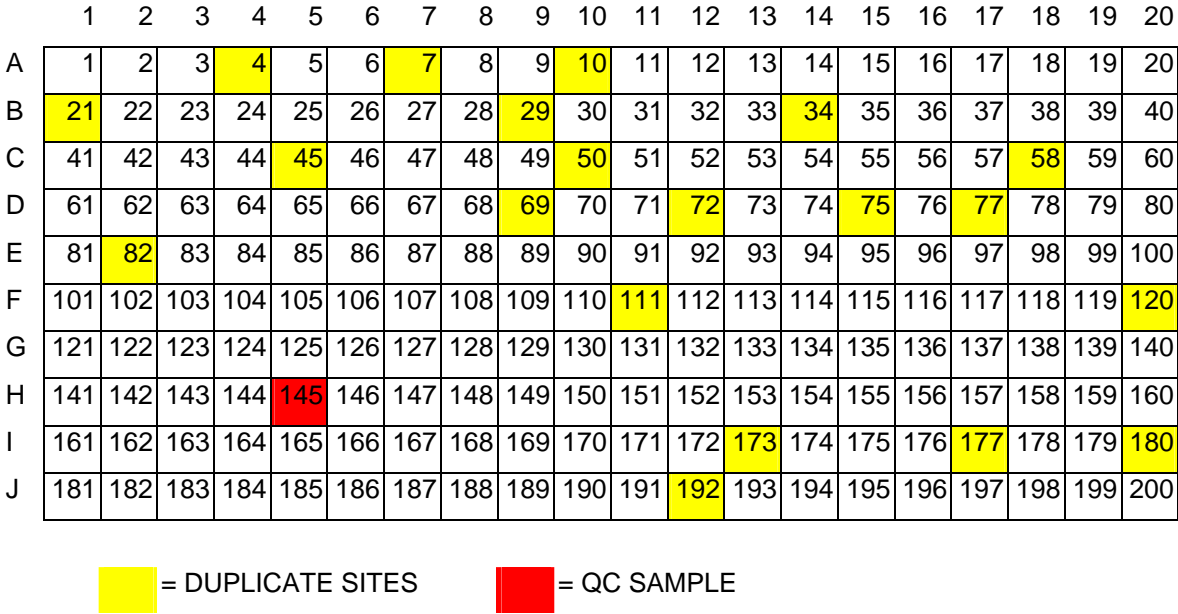


Figure 2.6: Location of random duplicate sites

The grid was set up in the field using canes as markers. A 100 m tape was used. The diagonals of sections were measured as they were laid out to ensure the sections were square.

Self-seal bags were used for the samples, double-labelled clearly with permanent marker pen. Approximately 250 g of soil was collected from each point

In the lab the soil aggregates were roughly broken up and placed in foil trays to dry for 2 days. After the drying time the soils were crushed in the tray, sieved to <2 mm and placed in labelled bags ready for pH measurement.

### **3. MAPPING METAL SOLUBILITY AND ANALYSIS OF SOLUBILITY ALGORITHM**

#### **3.1 INTRODUCTION**

An understanding of soil solution metal concentrations is of more value to researchers in attempting to predict metal uptake in comparison to total metal concentrations in the soil. As well as predicting metal solubility at G-BASE sample points, it is an objective of this work to use geostatistics to predict solubility between sample locations. The objectives of this chapter are to analyse the G-BASE data and to map the metal concentrations and metal solubilities across the area.

The chapter starts with an investigation into the G-BASE data and the kriging and mapping of the heavy metal and pH data. Metal solubility is then calculated and this data is kriged and mapped. The sensitivity of the solubility algorithm is investigated to find the greatest source of uncertainty.

##### **3.1.1 Introduction to the data**

Details of the aims and methods of the G-BASE survey can be found in Chapter 1. For the purposes of this study, G-BASE data from the Humber-Trent region was made available. The data set is derived from 6400 topsoil samples across an area of approximately 3,260 km<sup>2</sup> stretching from Nottingham in the south to York in the north (British Geological Survey, In Press). Figure 3.1 shows the extent of the region with the parent materials underlying the area. Figure 3.2 shows the Pb, Zn and Cu concentrations across the area. Land use data was obtained from the CEH land cover map (Fuller et. al., 1994).

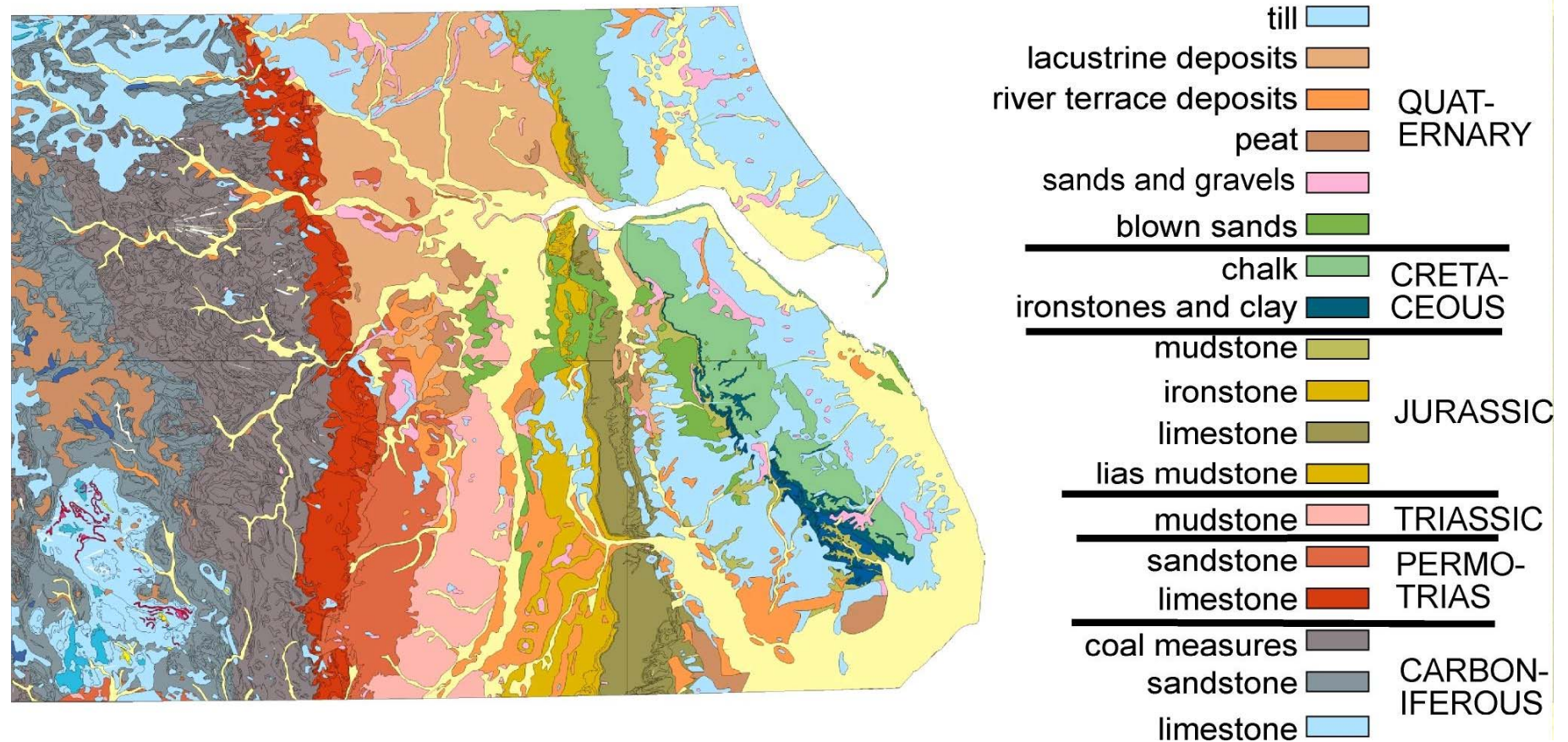


Figure 3.1: Parent material map of the Humber-Trent region ©BGS. Source: combined maps of bedrock geology (1:625k for England) and drift geology (1:625k for England), Institute of Geological Sciences, 1977 & 1979

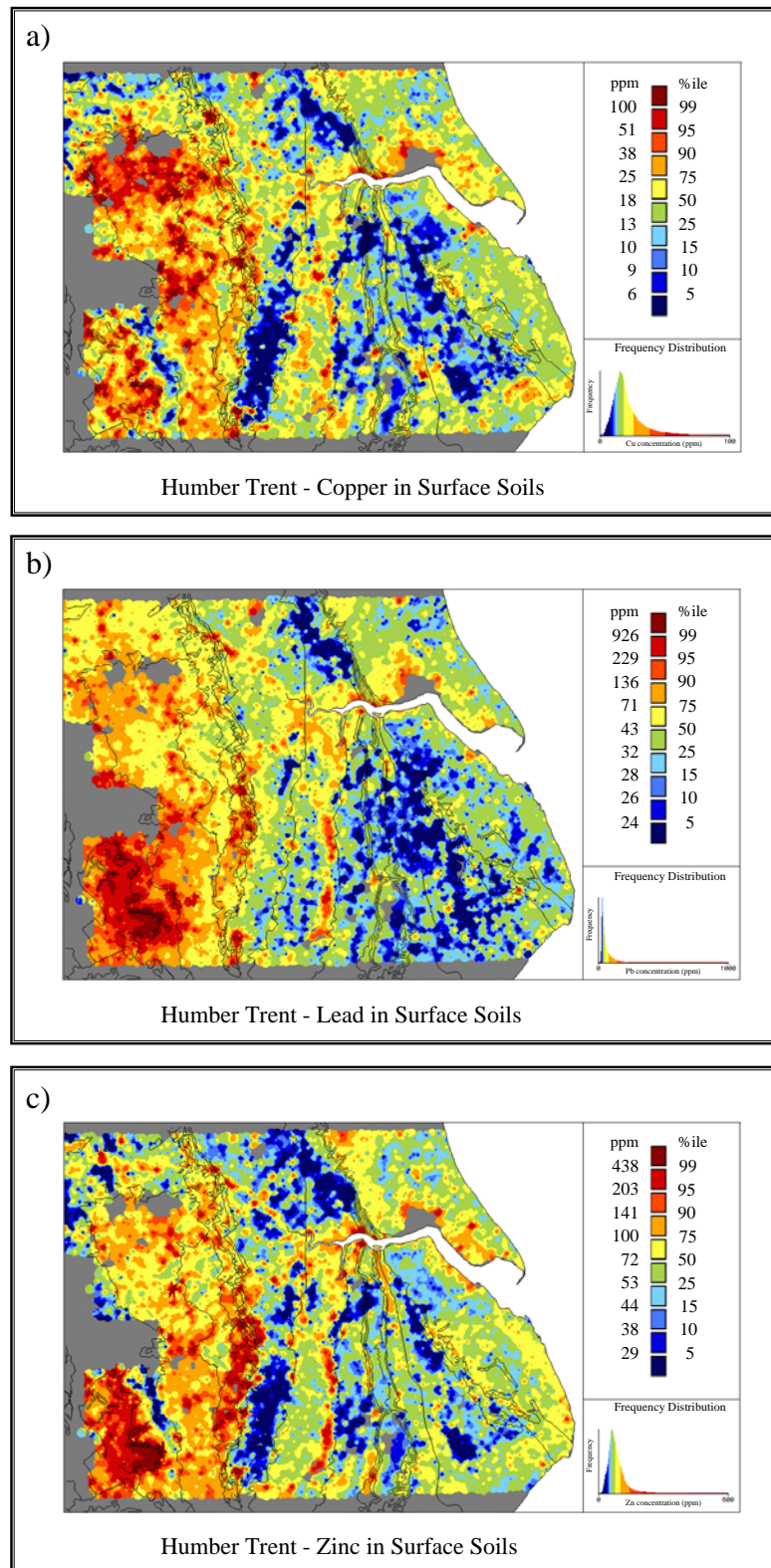


Figure 3.2: Topsoil (0-15 cm depth) metal concentrations across the Humber-Trent region for a) Cu, b) Pb and c) Zn. Source: British Geological Survey, © NERC 2005.

Maps generated using inverse distance weighted interpolation. The calculations are for predictions on a grid of  $250\text{m} \times 250\text{m}$  based on all samples within 1500m. the weighting is proportional to the inverse square of the distance.

### 3.1.2 Metal solubility algorithm

The development of the metal solubility algorithm used in this project is discussed in Chapter 1. As there was no soil organic carbon data available, the form of the algorithm based solely on  $M^{2+}$  and pH was used (Equation 3.1, Tye et al, 2003). Table 3.1 shows the parameters for Pb, Cu and Zn, and their standard errors.

$$pM^{2+} = a + bpH - c \log_{10} M^{2+} \quad 3.1$$

	<b>Pb</b>	<b>Zn</b>	<b>Cu</b>
<b>a</b>	-2.44 ± 0.77	-1.859 ± 0.65	-2.766 ± 0.92
<b>b</b>	1.531 ± 0.08	0.913 ± 0.07	1.255 ± 0.08
<b>c</b>	0.979 ± 0.20	0.628 ± 0.18	1.253 ± 0.30

*Table 3.1: Parameter values and standard errors for the solubility algorithm (Equation 3.1).*

## 3.2 SELECTION OF STUDY AREA

### 3.2.1 Introduction

Preliminary attempts at modelling the variograms for metal concentration over the entire Humber-Trent region produced unsatisfactory results with very high nugget values. This is unsurprising, as the primary control on trace-metal contents of undisturbed soil in temperate regions such as the United Kingdom is typically the geochemical composition of the soil parent material (the bedrock geology or quaternary deposit from which it is formed) (Rawlins et al, 2002). In the Humber-Trent region the parent material was found to account for between 14 and 47% of the variance of 13 different elements (Rawlins et al, 2003). As can be seen in Figure 3.1, the parent material varies considerably across the Humber-Trent region, including lithologies ranging from carboniferous limestone and coal measures in the west to cretaceous chalk in the east, and several

types of unconsolidated, quaternary deposit. By focusing on a smaller area with a single parent material the data is more likely to belong to a single population and therefore a more descriptive variogram could hopefully be achieved. Webster (2000) in a previous work, found that variograms for different classes of soil on the Jurassic outcrops of central England differed substantially from one to another, and advised people to be aware that this may occur over large areas of land and to model each area separately for kriging.

A smaller study area is not only useful for the geostatistical accuracy of predictions that can be achieved, but is also more amenable to field work.

For the purposes of validating the algorithm, the study area needs to represent as much variation in soil metal concentration and soil pH as possible. It was also necessary to ensure that the resulting metal solubilities would be above the detection limits of the analytical method available (ICP-MS).

While parent material is the primary influence on trace-metal concentration in soil, metal concentration is not the only influence on solubility. Organic carbon and pH are major factors in metal solubility. Land use in particular can have a significant impact on factors such as pH and organic carbon content (Clark and Harper, 2000). The land use data showed that over the Humber-Trent region 90% of the land was arable (tilled) land, with the majority of the rest being either meadow or suburban. The small amount of woodland was not clustered in one area, but scattered around. When choosing sample sites for the field work only arable and pasture was considered, in order to minimise sources of variation.



### 3.2.1.1 pH data

In analysing soils from the Humber-Trent region, the BGS determined pH only on the sub-soil samples. However, the metal solubility algorithm has been developed using top-soil pH values. There is not always a direct correlation between top-soil and sub-soil pH levels, so it may not be valid to use sub-soil pH to predict metal solubilities in top-soil. In order to test this, pH data from the National Soil Inventory (NSI) was used to compare top-soil with sub-soil pH values.

The NSI is at a resolution of a 5km grid square rather than every other 1km grid square (G-BASE). A random area of the Humber-Trent was chosen for the exercise, which contained 35 NSI sample points. The G-BASE sub-soil pH data were kriged to the location of the NSI data points to enable a comparison of sub-soil and top-soil pH values. The G-BASE data were kriged to the NSI data as it was felt that this would be more accurate than interpolating the sparser data of the NSI to the denser data of G-BASE. The mean kriging variance was 0.424. The comparison between the two data sets is shown in Figure 3.4. The correlation was poor ( $r^2 = 0.1$ ). Therefore pH determinations were undertaken on the G-BASE archived top-soil samples.

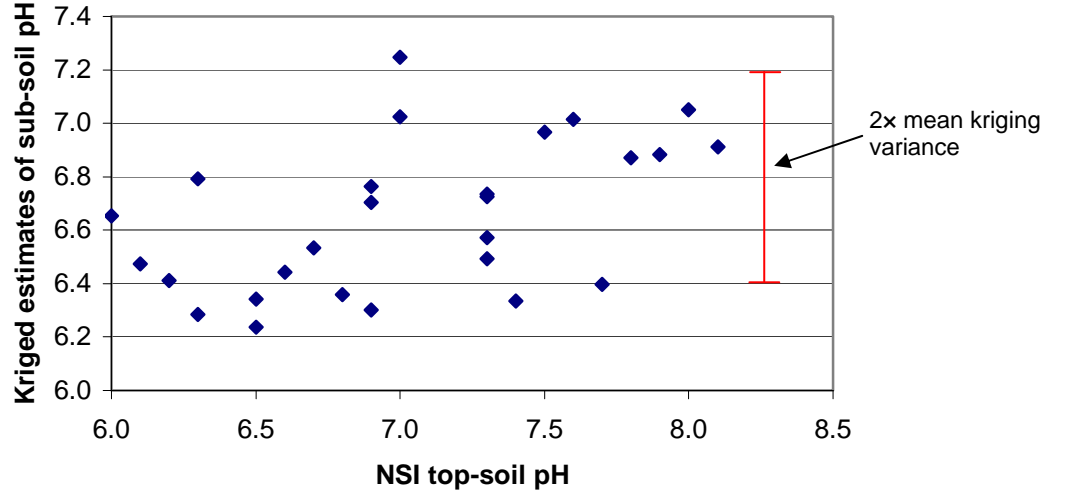


Figure 3.3: Relationship between NSI top-soil pH measurements and G-BASE sub-soil pH measurements kriged to NSI locations ( $n = 35$ ).

#### 3.2.1.2 Concentration of Zinc in solution

Metal concentration was an important consideration when choosing the study area. The intention was to measure soil solution concentrations in the field work and it was important that these were detectable by the measurement techniques available. In order to estimate which areas would yield measurable metal solubilities, Zn concentration in solution was predicted. The sub-soil pH values had to be used as this was the only data available at the time. G-BASE measure pH in 0.01M  $\text{CaCl}_2$ , but the algorithm has been calibrated using pH measured in water. The pH of the same soil measured in water is usually about 0.5 pH units higher than when measured in  $\text{CaCl}_2$  (Rowell, 1995), so 0.5 pH units were added to the G-BASE values before using the algorithm.

The result of previous research shows that the average difference (on a log scale) between  $\text{pZn}$  (solution) and  $\text{pZn}^{2+}$  (activity) is 0.49 (Scott Young, *Personal Communication*), so:

$$\text{Zn}_{\text{sol}} = \frac{10^{-(\text{pZn}-0.49)}}{6.53 \times 10^7} \quad 3.2$$

where  $[Zn_{sol}]$  is the solution concentration of Zn in all chemical forms, in  $\mu\text{mol L}^{-1}$  (ppb).

The Humber-Trent region was divided up into areas based on parent material. Six areas contained enough sample points in a contiguous unit to be used for the geostatistical analysis. The six areas were: the Chalk Group, Lower Coal Measures Formation, Middle Coal Measures Formation, Lacustrine Deposits, Sherwood Sandstone Group, and the Mercia Mudstone Group. A seventh area combining both Middle and Upper Coal Measures (Westphalian) was also selected as it covered an area with a wide range of pH and metal concentrations. Zn solution estimates were estimated using Equation 3.2 for each area and these are shown in Table 3.2. The Lower Coal Measures and the Westphalian area were those with the highest proportion of samples predicted to have detectable Zn in solution. The Westphalian area has slightly lower detection levels than the Lower Coal Measures but the Westphalian area was nevertheless chosen as it is a contiguous area for mapping. Figure 3.4 shows the Westphalian region and the G-BASE sample locations included in it.

Data	Measurement method	% samples detectable
<b>LCM</b>	ICP-MS	87.91
	ICP-AES	73.95
<b>MCM</b>	ICP-MS	65.60
	ICP-AES	51.20
<b>LDE</b>	ICP-MS	24.63
	ICP-AES	13.43
<b>SSG</b>	ICP-MS	49.73
	ICP-AES	33.16
<b>CK</b>	ICP-MS	0.00
	ICP-AES	0.00
<b>MMG</b>	ICP-MS	27.65
	ICP-AES	15.67
<b>West</b>	ICP-MS	83.92
	ICP-AES	70.85

**CK** = Chalk Group,  
**LCM** = Lower Coal Measures Formation  
**MCM** = Middle Coal Measures Formation  
**LDE** = Lacustrine Deposits,  
**SSG** = Sherwood Sandstone Group  
**MMG** = Mercia Mudstone Group  
**West** = Westphalian

*Table 3.2: Percentage of samples with Zn in solution predicted to be above the detection limits of the ICP-MS and ICP-AES using equation 3.2 with the data corrections described in the text.*

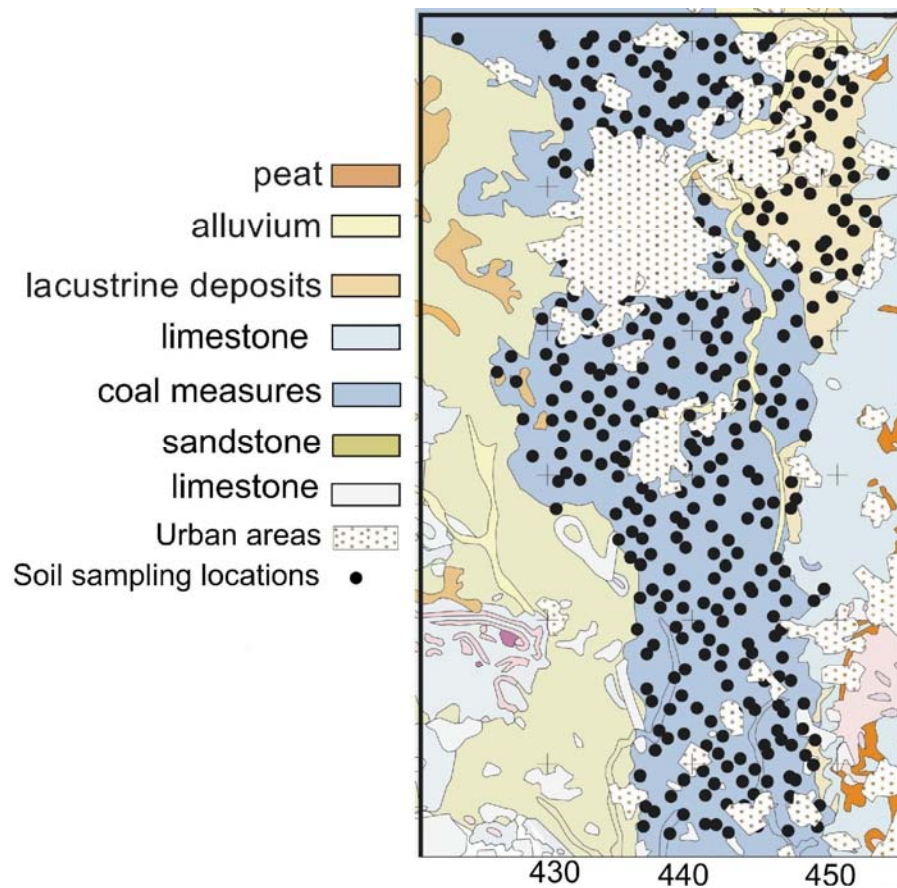


*Figure 3.4: Sample locations in the Westphalian region chosen for further investigation overlying the parent material. Westphalian region is over the coal measures.*

### 3.3 MAPPING

#### 3.3.1 Variograms

The method of analysing data to plot variograms is described in §2.2.

##### 3.3.1.1 Total zinc concentration

The total Zn concentration data has a minimum of  $10 \text{ mg kg}^{-1}$ , a maximum of  $289 \text{ mg kg}^{-1}$  and mean of  $111.5 \text{ mg kg}^{-1}$ . Although the distribution was somewhat skewed (skew = 1.0) this is within the limits of skewness for which most geostatisticians consider data

transformation unnecessary. A regression analysis involving fitting linear and quadratic functions to the spatial co-ordinates showed that the percentage of variance accounted for is 6.4%, suggesting that there is a minimal trend present. The data was also checked for anisotropy. The model fitted to the variogram is a double spherical model, which accounted for 95.4% of the variance (Figure 3.5 and Table 3.3).

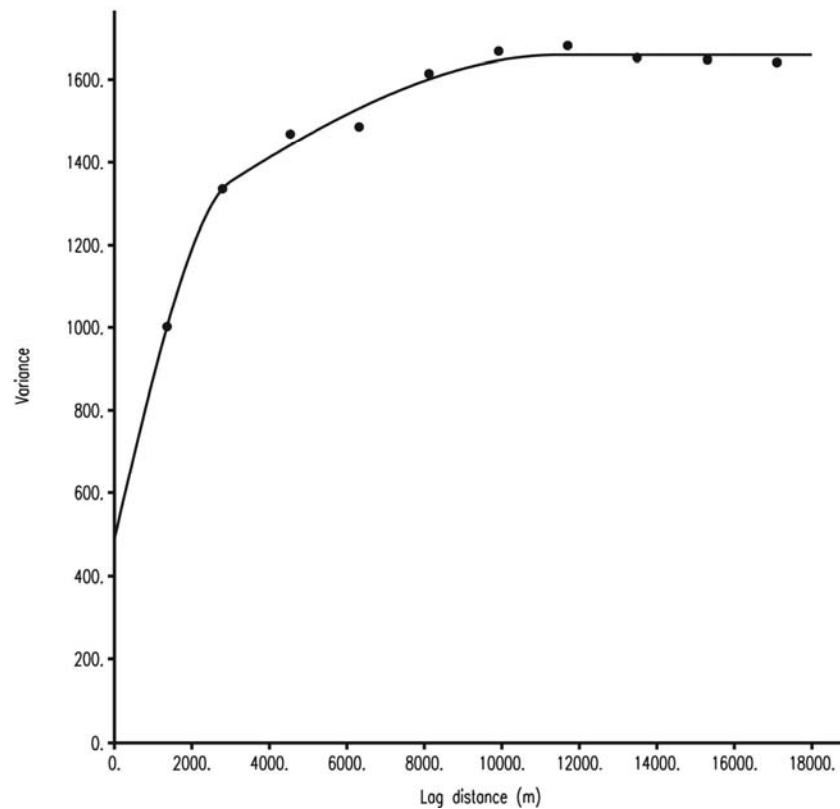


Figure 3.5: Isotropic semivariances (symbols) of total Zn concentrations and a double-spherical model fitted through them (line).

Parameter	Value
Range <sub>1</sub>	3014
Range <sub>2</sub>	11516
Sill <sub>1</sub>	676.2
Sill <sub>2</sub>	494.6
Nugget	488.2

Table 3.3: Parameters of the double spherical variogram model fitted to the total Zn concentration data.

### 3.3.1.2 Total copper concentration

The total Cu concentration data has a minimum of  $4.0 \text{ mg kg}^{-1}$ , maximum of  $161 \text{ mg kg}^{-1}$  and a mean of  $33.6 \text{ mg kg}^{-1}$ . The data is positively skewed, with a skewness coefficient of 2.82. Therefore the data required a logarithmic transformation prior to plotting the variogram. By applying a logarithmic transformation the skewness was reduced to 0.37. A regression analysis involving fitting linear and quadratic functions to the spatial co-ordinates to check for trend showed that the percentage of variance accounted for is 10%. The model with the best fit for the variogram was the exponential model, which accounted for 97.6% of the variance (Figure 3.6 and Table 3.4).

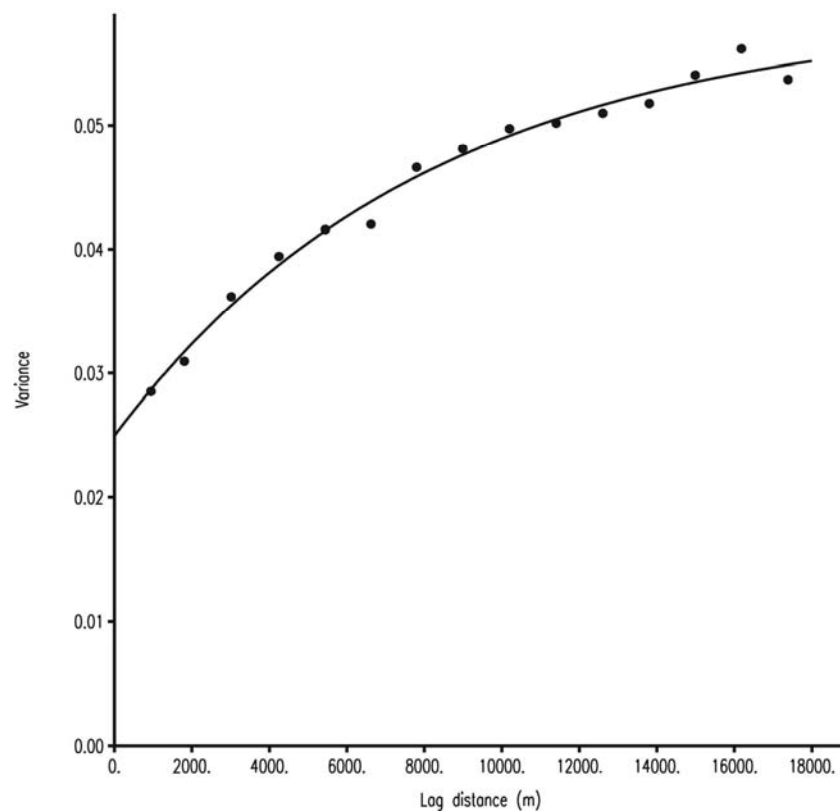


Figure 3.6: Isotropic semivariances (symbols) of total Cu concentrations and an exponential model fitted through them (line). Data has been log transformed.

Parameter	Value
Range	8166
Sill	0.339
Nugget	0.025

*Table 3.4: Parameters of the exponential variogram model fitted to the total Cu concentration data.*

### 3.3.1.3 Total lead concentration

The total Pb concentration data has a minimum of 21 mg kg<sup>-1</sup>, a maximum of 245 mg kg<sup>-1</sup> and a mean of 97.2 mg kg<sup>-1</sup>. Although the distribution was somewhat skewed (skew = 1.08) this is within the limits of skewness for which most geostatisticians consider data transformation unnecessary. A regression analysis involving fitting linear and quadratic functions to the spatial co-ordinates to check for trend showed that the percentage of variance accounted for is 27%, suggesting a regional trend in the data (co-ordinates are resolved to an origin for the purpose of estimating trend). The presence of such a long-range trend implies that the assumptions of the random function model no longer hold. Raw semi-variances will be biased estimates; so the variogram used to describe the random variation is that of the residuals after trend removal. It is possible to kriging with the presence of trend using the method of universal kriging. However, by removing the trend and working with the residuals it is possible to use ordinary kriging as with the other metals. The trend equation is shown in Equation 3.3,  $x$  and  $y$  are the spatial co-ordinates of each sample point. Parameters are calculated using regression analysis.

$$u(x) = 199.7 - 0.0090x + 0.00088y + (0.1 \times 10^{-6})x^2 - (0.29 \times 10^{-7})y^2 + (0.45 \times 10^{-7})xy \quad 3.3$$

The value of the trend component is calculated at each point and subtracted from the original value to create a data set of residuals. The variogram is then estimated from the residual data. The resulting



variogram and parameters are shown in Figure 3.7 and Table 3.5 respectively. The relatively large nugget is because the variogram is modelled on the residuals rather than the original data. The optimum model (an exponential function) accounted for 94.1% of the variance.

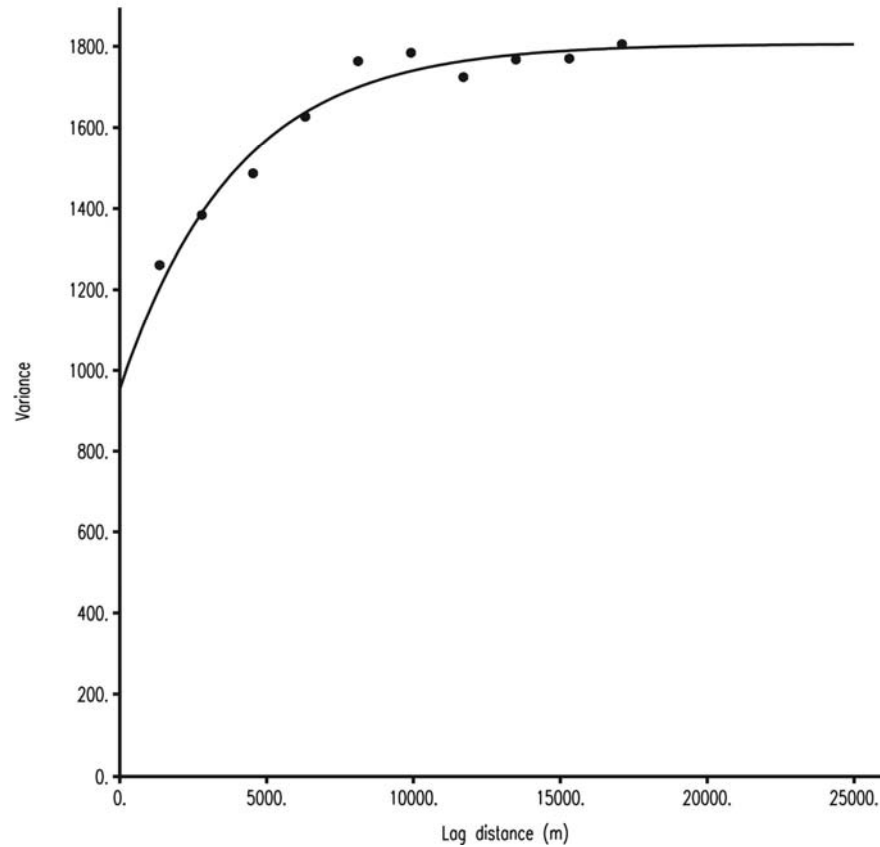


Figure 3.7: Isotropic semivariances (symbols) of total Pb concentrations and an exponential model fitted through them (line). Data has had the trend removed.

Parameter	Value
Range	3908
Sill	852.9
Nugget	953.5

Table 3.5: Parameters for the total Pb variogram.

#### 3.3.1.4 pH

The archived G-BASE top-soil samples were measured for pH (see §2.1.1.3); the data has a minimum of 3.2 and a maximum of 7.92 pH

units. The mean is 6.09 and the data is not significantly skewed (-0.672). A regression analysis of the spatial co-ordinates fitting both linear and quadratic functions to the pH data found a trend of 15.4%. An exponential model was fitted, with the optimum authorised model parameters shown in Table 3.6. The variance accounted for is 96.3%.

Parameter	Value
Range	23812
Sill	0.481
Nugget	0.678

*Table 3.6: Parameters for exponential variogram of pH*

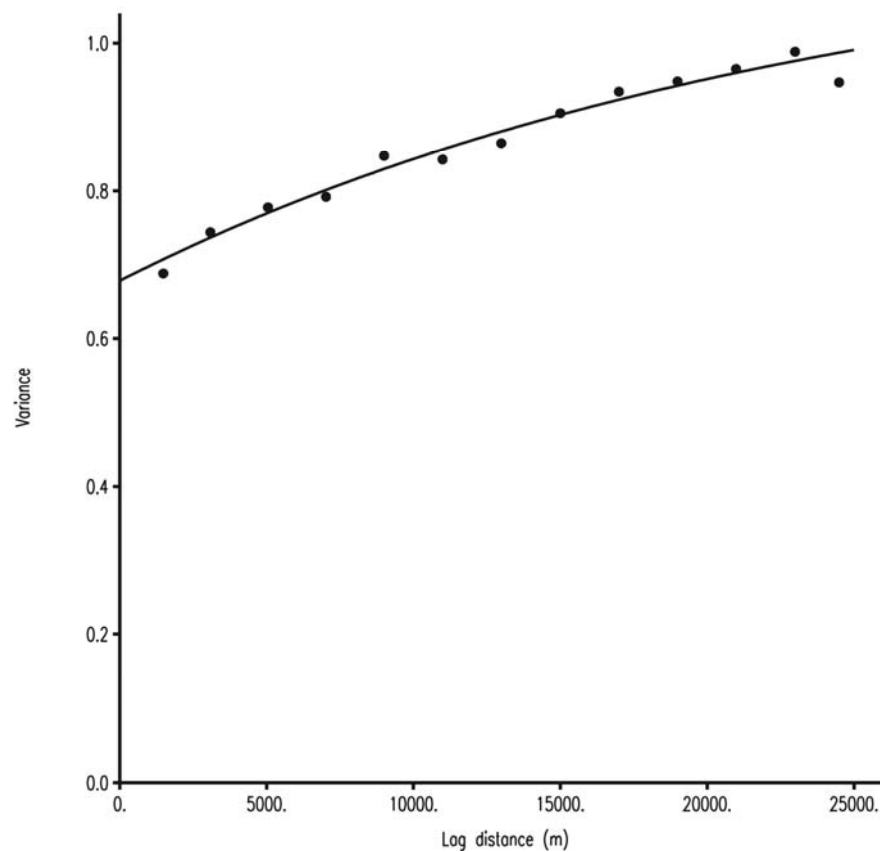


*Figure 3.8: Isotropic semivariances (symbols) of soil pH values and an exponential model fitted through them (line). Parameters shown in Table 3.6.*

### 3.3.2 Kriging and Mapping

In order to create maps of the G-BASE data, the variograms are used to krig the data. This produces estimates of the data in the areas where there are no samples and therefore produces a more detailed map than mapping the raw data. The details of kriging are in Chapter 2. Kriged Cu and Zn concentrations are shown in Figures 3.9 and 3.10 respectively.

The Pb variogram was modelled using the residuals after removal of the trend, so the kriging procedure is more complicated. For the Pb data, estimates of the residuals were made on a regular grid and added to the trend component calculated for each location on the grid. This is then mapped (Figure 3.10). Figure 3.11 is the map of kriged soil pH estimates.

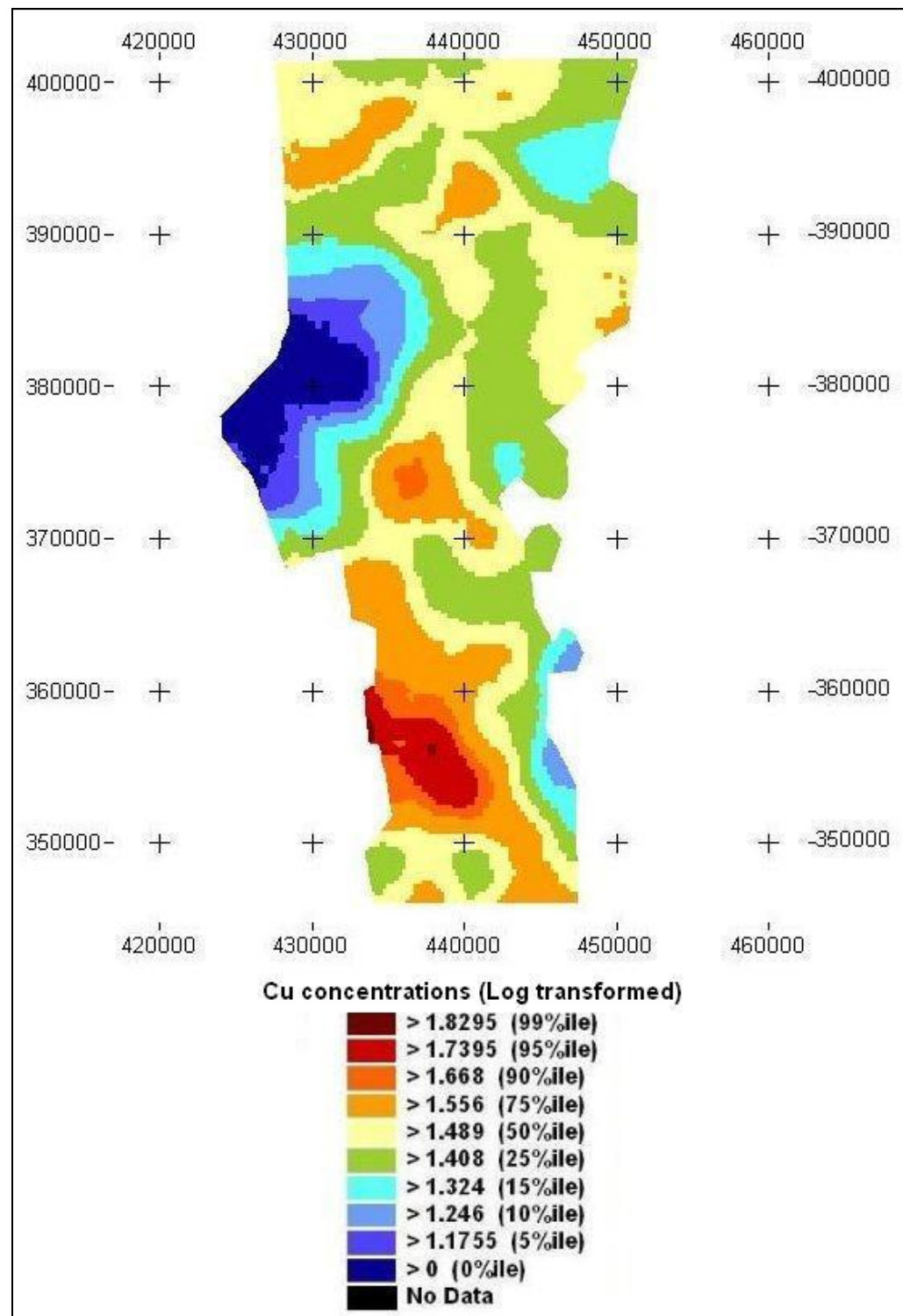


Figure 3.9: Map of kriged Cu concentration (log transformed  $\text{mg kg}^{-1}$ ).

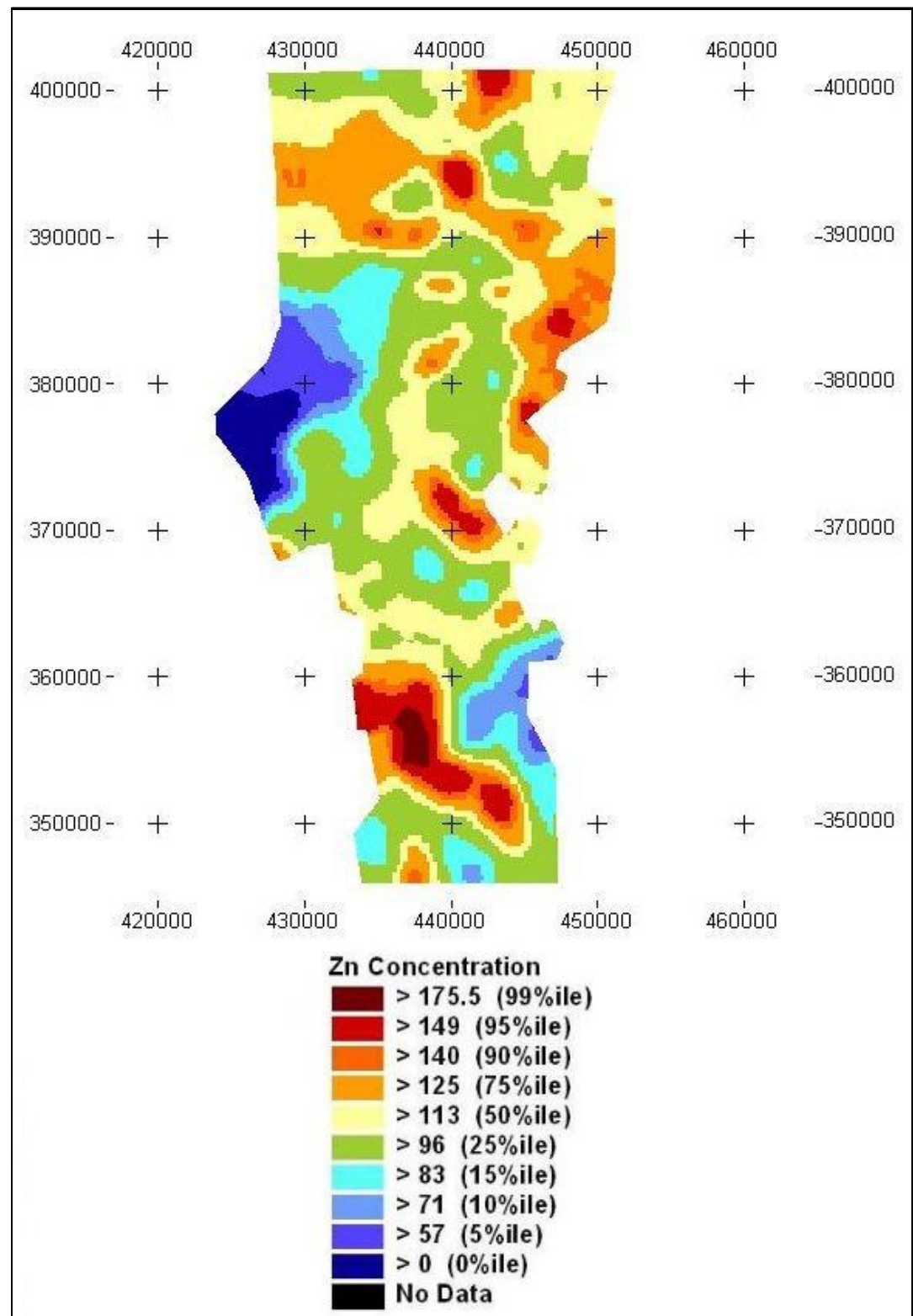


Figure 3.10: Map of kriged Zn concentration ( $\text{mg kg}^{-1}$ ).

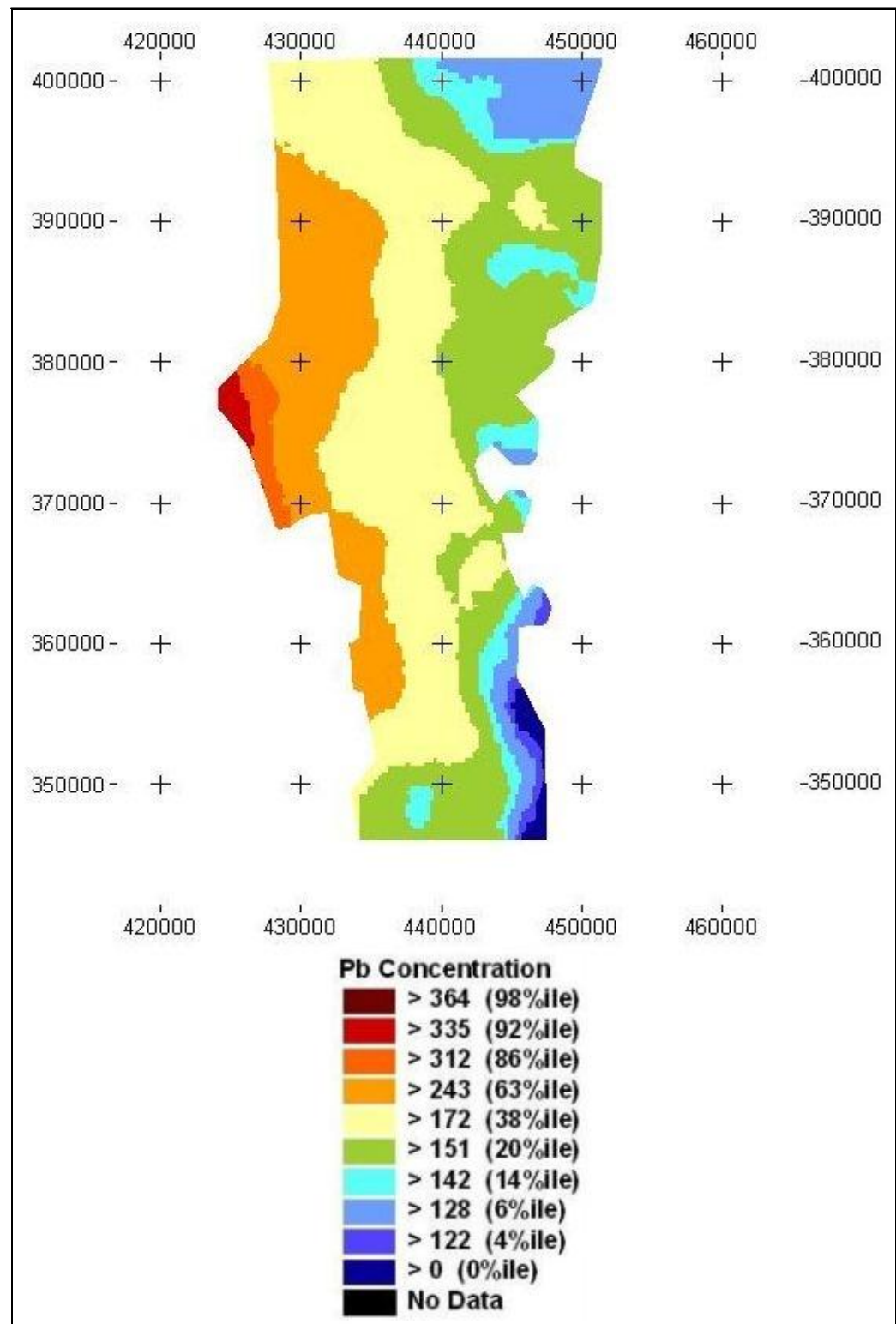


Figure 3.11: Map of kriged Pb concentration ( $\text{mg kg}^{-1}$ ).

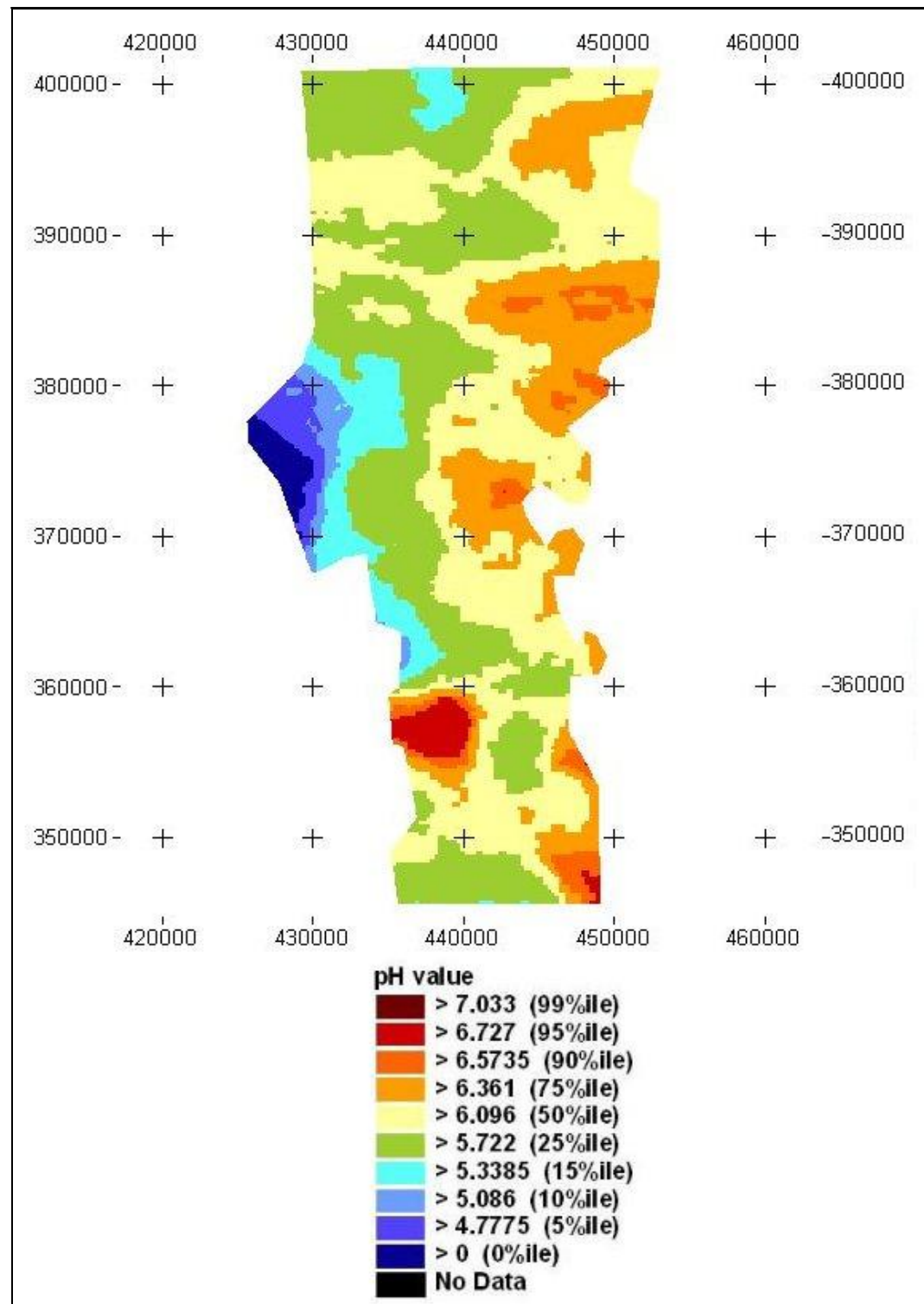


Figure 3.12: Map of kriged soil pH.

The maps for Zn (3.10) and Cu (3.9) show a similar distribution of metal concentration, with high and low spots in the same place. Pb (3.11) however, shows a very different distribution. There is a clear east-west trend, which was also revealed by the analysis. Some of the trend can be seen in the map of pH (3.12), with mainly lower values in the west and higher values in the east. You would usually expect Pb to have a similar distribution to Zn as the two elements often occur together and are mined together.

### **3.3.3 Estimation uncertainty**

One of the benefits of geostatistics is that the kriging procedure returns a quantity referred to as the kriging variance at each kriged location. The square root of this quantity is the kriging error, providing a measure of the uncertainty in the actual estimate. More precisely, on 95% of occasions the actual sample value will be within the kriged value, plus or minus twice the kriging error estimate. Figure 3.13 is a map of the kriging variances of the pH map (Figure 3.12). The variances are highest at the corners of the map, where there are fewer samples used in the interpolation.



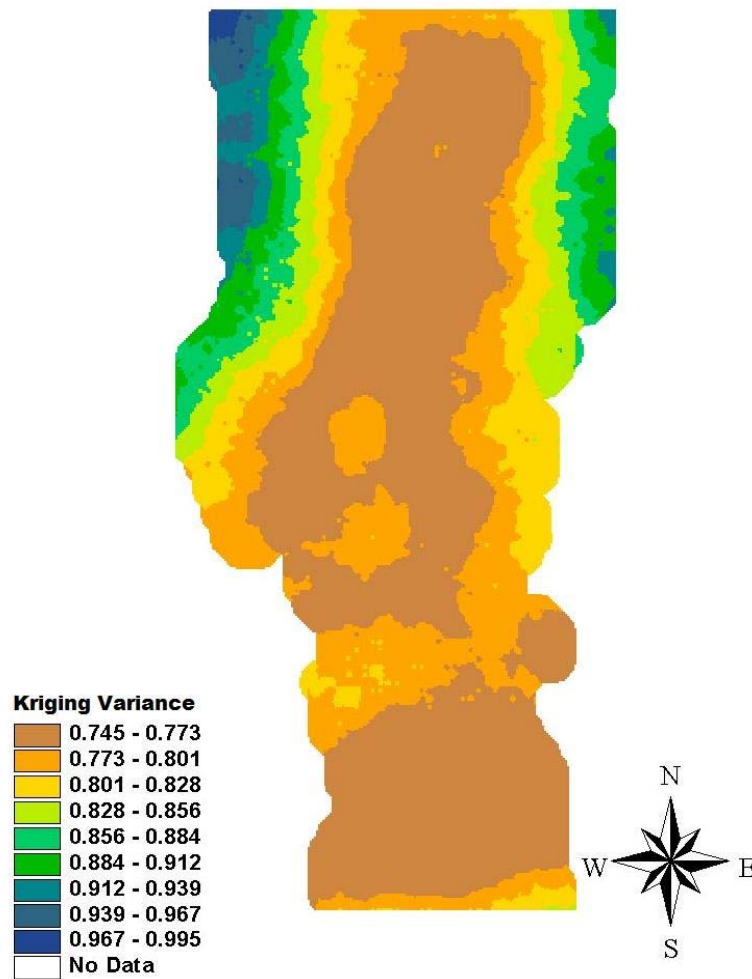


Figure 3.13: Kriging variances for soil pH.

The variances of pH and Zn are produced automatically by the kriging procedure. In the case of Pb, as the kriged estimates are based on the residuals, the kriging variances do not reflect the uncertainty on the actual data due to the presence of trend. However, it is possible to estimate uncertainty using the mean squared error from cross validation. This method removes a single point from the data set and uses the remaining points to estimate the value at the point that has been removed. This gives a variance for each original point, rather than for each of the kriged points, but serves to provide an estimate of the errors involved in the kriged predictions. Cross validation is also carried out for Cu, as the data is log-transformed and the back-transform procedure cannot be applied to the variances. Figure 3.14 shows graphs of the error as a percentage of the estimates for Zn and

pH. As the error estimates for Zn and pH are produced by the ordinary kriging procedure there are 6720 data points based on the kriging grid. Figure 3.15 shows the comparable graphs for Pb and Cu. These estimates were produced by cross validation so have the same number of points as the original data set. Zn, Pb and pH show a higher percentage error where the estimate is lower. The trend is stronger in Zn and pH. Cu shows no real trend in the distribution. The mean percentage errors were 29.14% for Pb, 11.1% for Cu, 19.68% for Zn and 15% for pH.

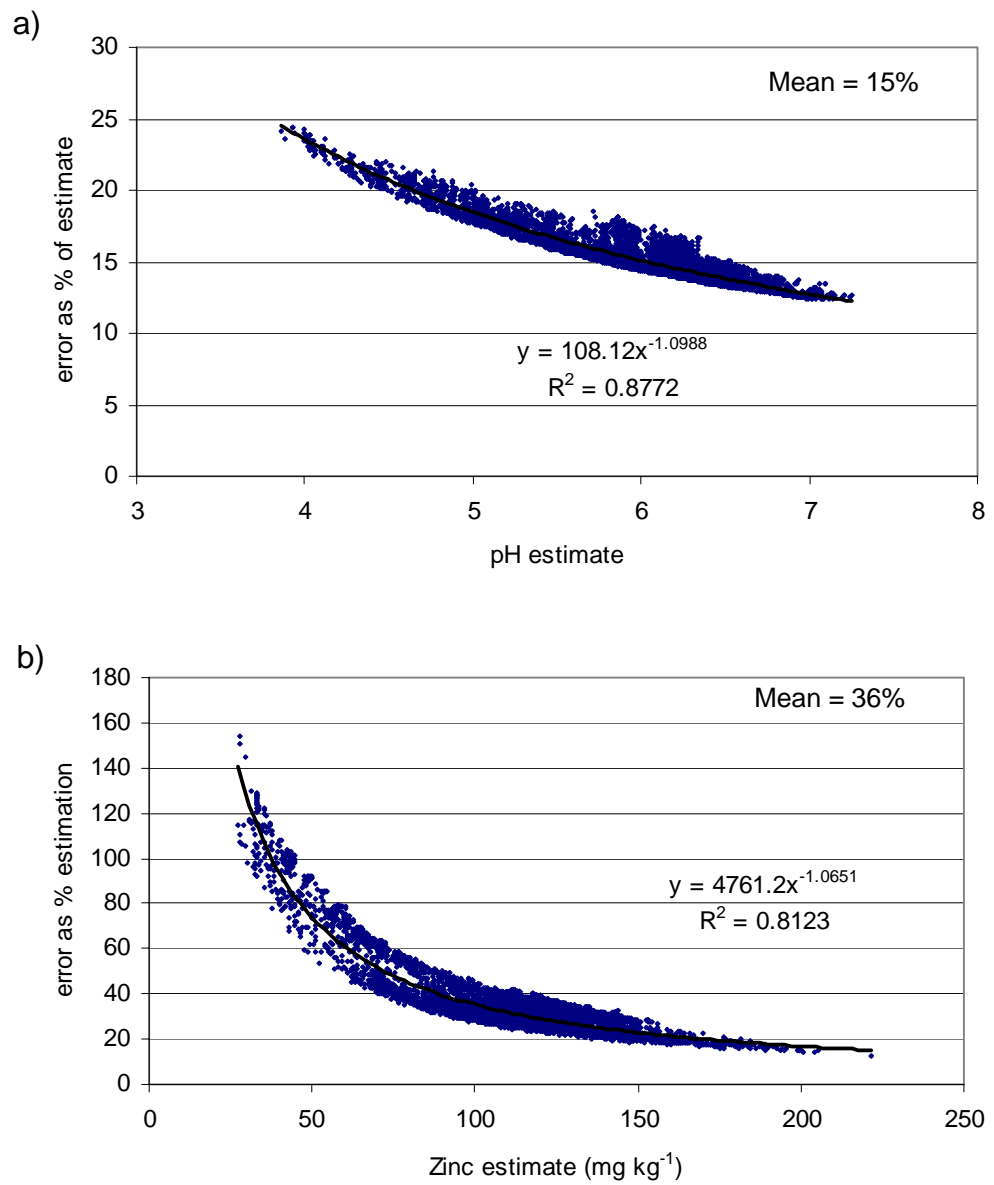


Figure 3.14: Kriging error as a percentage of the kriging estimate for  
a) Zn and b) pH.

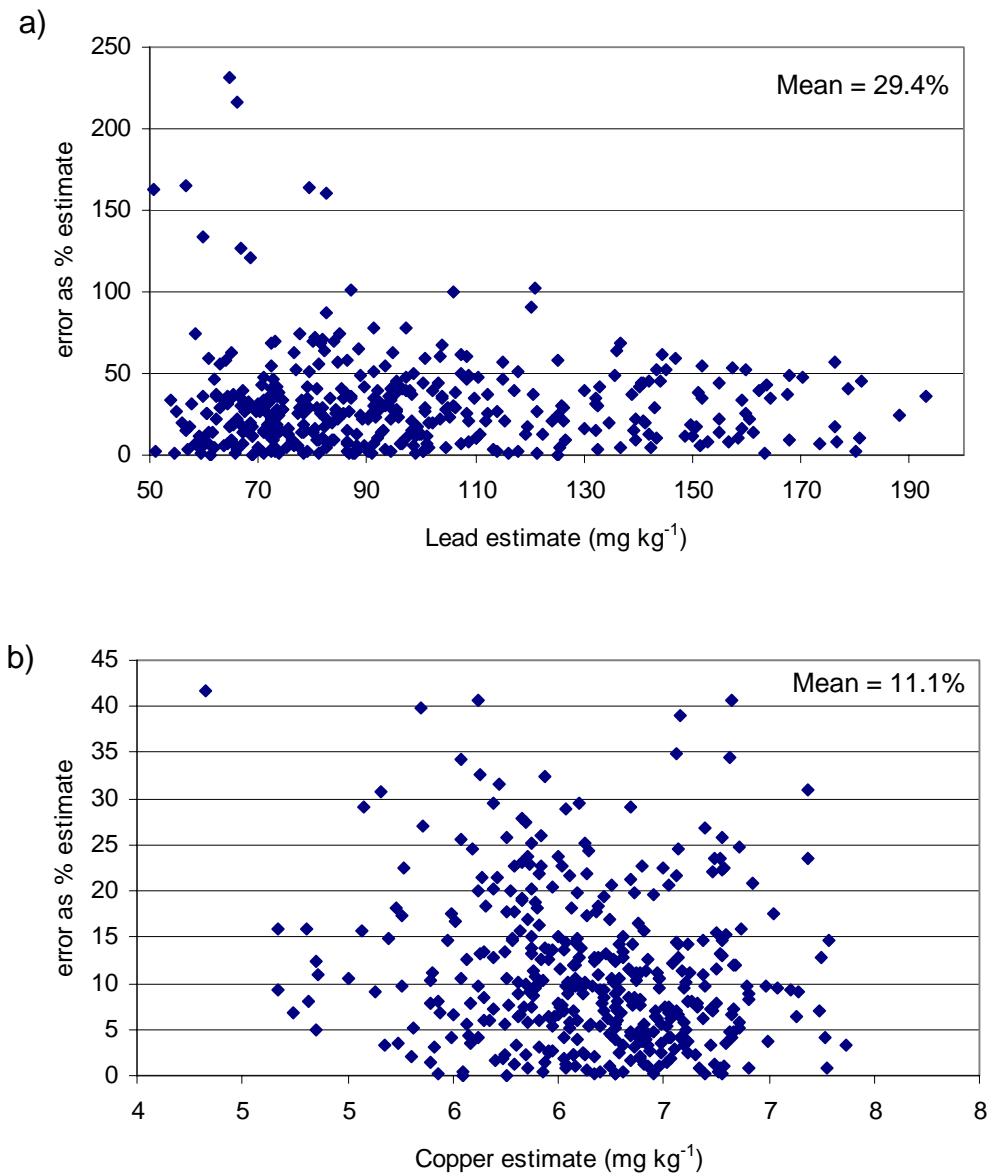


Figure 3.15: Cross Validation error as a percentage of the kriging estimate for a) Pb and b) Cu.

### 3.4 MAPPING METAL SOLUBILITY

#### 3.4.1 Modelling the variograms

Solubility was calculated for Pb, Cu and Zn using the algorithm in Equation 3.1 for each G-BASE sampling location, and the variograms modelled. There are 405 samples in the chosen area.

##### 3.4.1.1 Lead solubility

The minimum Pb solubility is  $2.94 \times 10^{-13}$  mmol l<sup>-1</sup> and the maximum is  $2.69 \times 10^{-8}$  mmol l<sup>-1</sup>, with a mean value of  $1.15 \times 10^{-9}$  mmol l<sup>-1</sup>. A regression analysis involving fitting linear and quadratic functions to the spatial co-ordinates showed that the percentage of variance accounted for is 5.4%, suggesting that there is a minimal trend present. The data is skewed (5.2), so the data is log-transformed. The data was also checked for anisotropy. The model fitted to the variogram is a spherical model with a fit (percentage variance accounted for by the model) of 95.5%. Figure 3.16 shows the variogram of Pb solubility and Table 3.7 shows the parameters.

Parameter	Value
Range	18402
Sill	3.485
Nugget	4.803

*Table 3.7: Parameters for Pb solubility variogram*

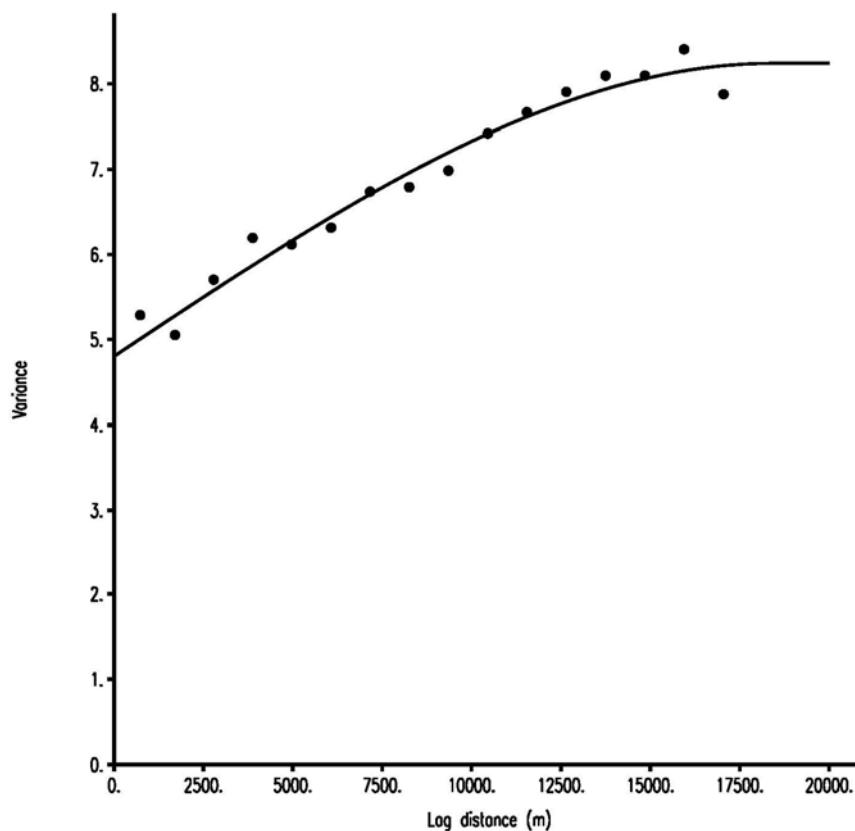


Figure 3.16: Isotropic semivariances (symbols) of Pb solubility and a spherical model fitted through them (line).

#### 3.4.1.2 Zinc solubility

The minimum Zn solubility is  $2.54 \times 10^{-7} \text{ mmol l}^{-1}$  and the maximum is  $2.84 \times 10^{-4} \text{ mmol l}^{-1}$ , with a mean value of  $2.17 \times 10^{-5} \text{ mmol l}^{-1}$ . A regression analysis involving fitting linear and quadratic functions to the spatial coordinates showed that the percentage of variance accounted for is 13.5%, suggesting that there is a minimal trend present. The skewness of the data is 3.86, so the data is log-transformed using the natural logarithm. The data was also checked for anisotropy. The model fitted to the variogram is a linear model with a fit (percentage variance accounted for by the model) of 96.1%. Figure 3.17 shows the variogram of Zn solubility.

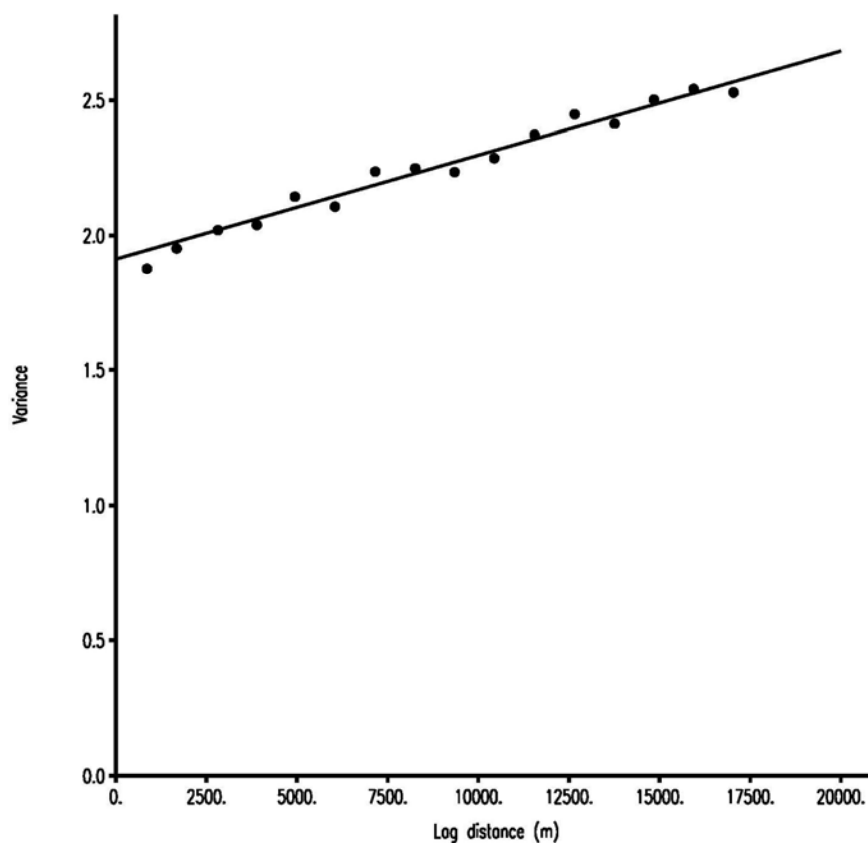


Figure 3.17: Isotropic semivariances (symbols) of Zn solubility and a linear model fitted through them (line). The model has a gradient of  $3.85 \times 10^5$  and a nugget value of 1.913.

#### 3.4.1.3 Copper solubility

The minimum Cu solubility is  $8.54 \times 10^{-12}$  mmol l<sup>-1</sup> and the maximum is  $8.48 \times 10^{-7}$  mmol l<sup>-1</sup>, with a mean value of  $2.30 \times 10^{-8}$  mmol l<sup>-1</sup>. A regression analysis involving fitting linear and quadratic functions to the spatial coordinates showed that the percentage of variance accounted for is 1.0%, suggesting that there is minimal trend present. The skewness of the data is 6.42, so the data is log-transformed using the natural logarithm. The data was also checked for anisotropy. The model fitted to the variogram is a linear model with a fit (percentage variance accounted for by the model) of 96.4%. Figure 3.18 shows the variogram of Zn solubility.

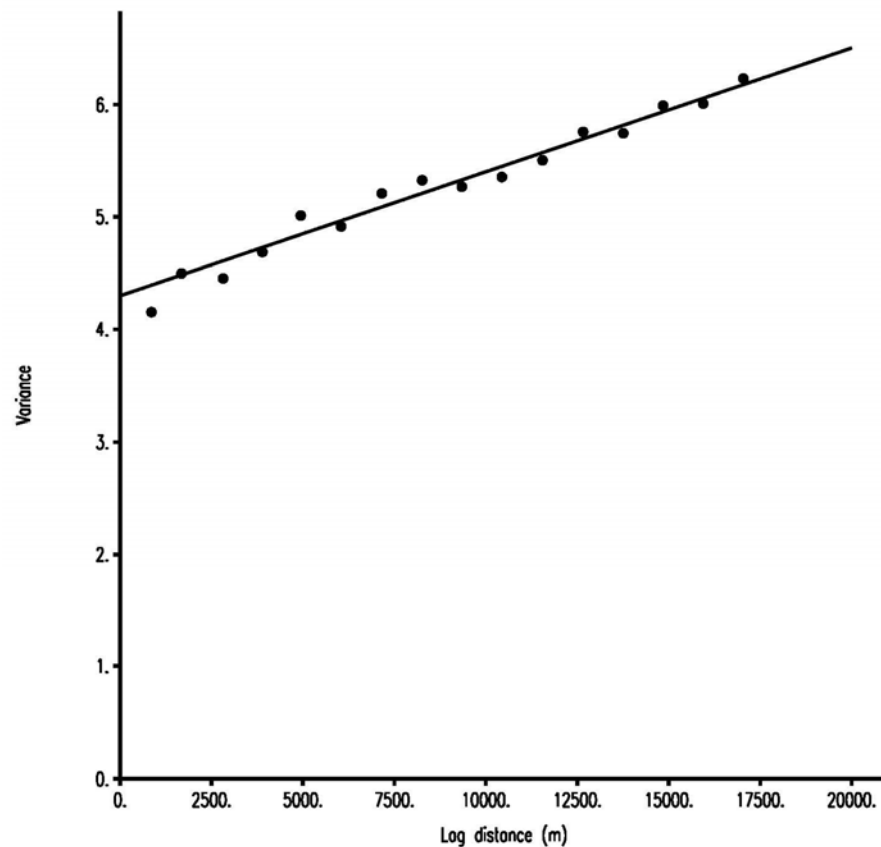


Figure 3.18: Isotropic semivariances (symbols) of Cu solubility and a linear model fitted through them (line). The model has a gradient of  $1.10 \times 10^{-4}$  and a nugget value of 4.2964.

#### 3.4.1.2 Kriging and mapping of solubility

Figures 3.19, 3.20 and 3.21 show maps of metal solubility for Pb, Cu and Zn. All three metal solubilities required a log transformation before modelling the variogram and kriging, so the backtransform procedure does not produce any kriging variances. In order to estimate the error, a cross validation was undertaken for each metal. This produces kriged estimates for each G-BASE point and calculates the error by subtracting the estimate from the original value at each point. The error is then calculated as a percentage with respect to the kriging estimate and the mean values are shown in Table 3.8.



<b>Metal Solubility</b>	<b>% error</b>
Pb <sup>2+</sup>	188.2
Zn <sup>2+</sup>	153.2
Cu <sup>2+</sup>	417.5

*Table 3.8: Mean percentage error for metal solubilities calculated from cross validation kriging with respect to original G-BASE data.*

The uncertainties on all three metals are very large, and this brings into question the value of the maps that can be created. It also raises the question of the accuracy of the point predictions before kriging. Figure 3.19 shows graphs of the error as a percentage of the estimate in the same way as for the metal concentration in Figure 3.14 and 3.15. The graphs are dominated by extreme percentage errors in a few cases.

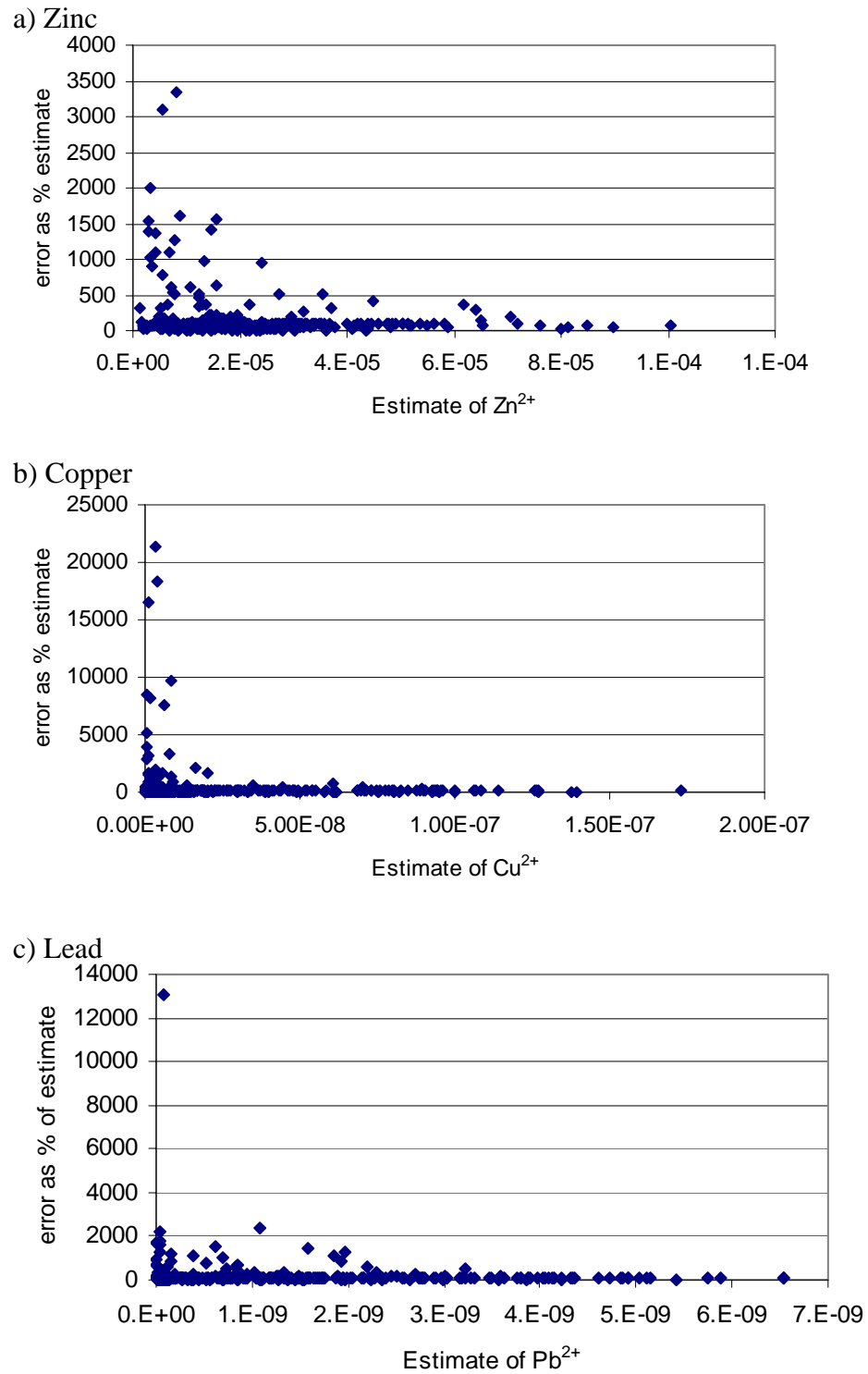


Figure 3.19: Graphs of error as a percentage of the kriging estimate as a result of cross validation for a) Zn solubility, b) Cu solubility and c) Pb solubility.

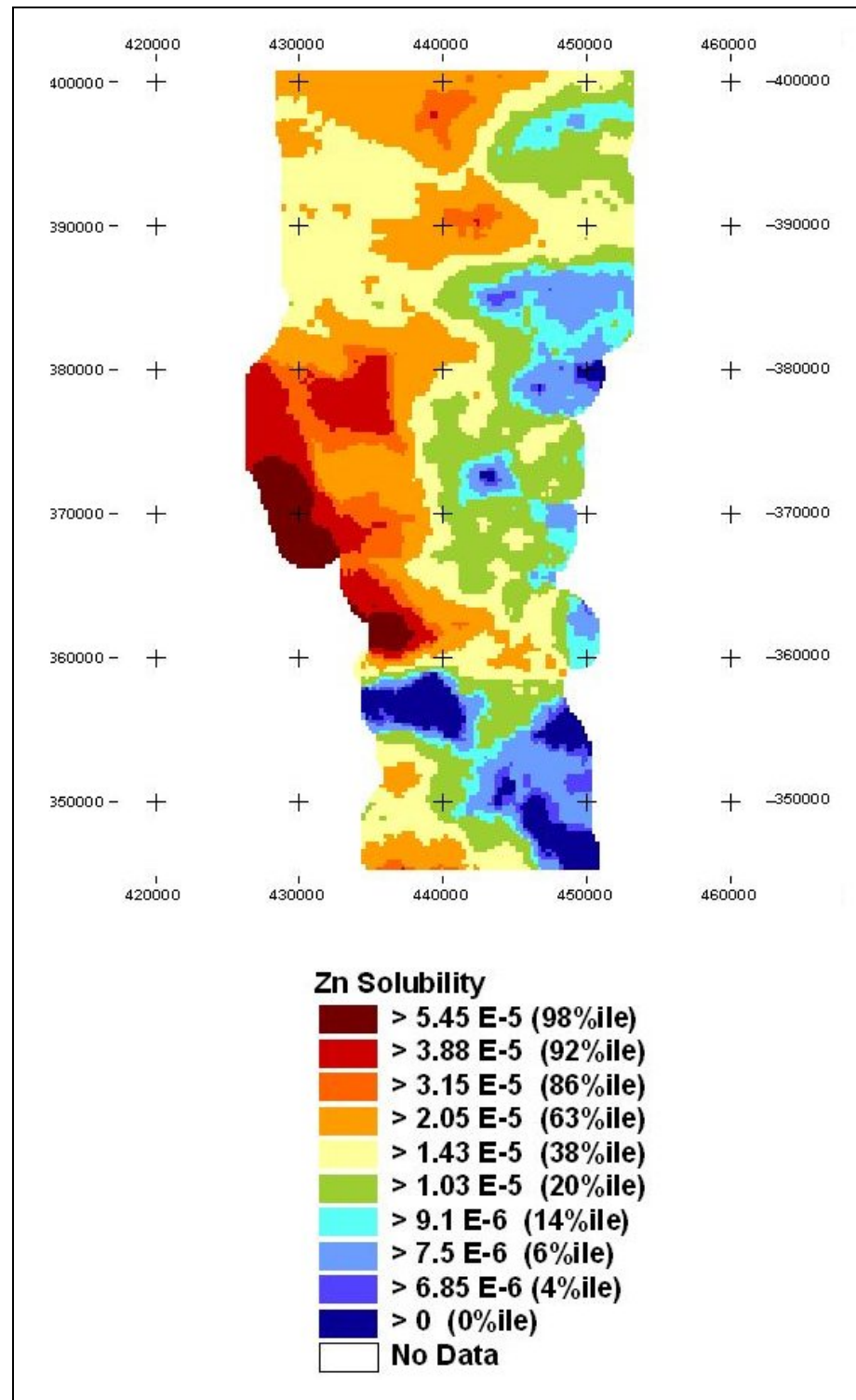


Figure 3.20: Kriged predicted Zn solubility values ( $\text{mmol l}^{-1}$ ).

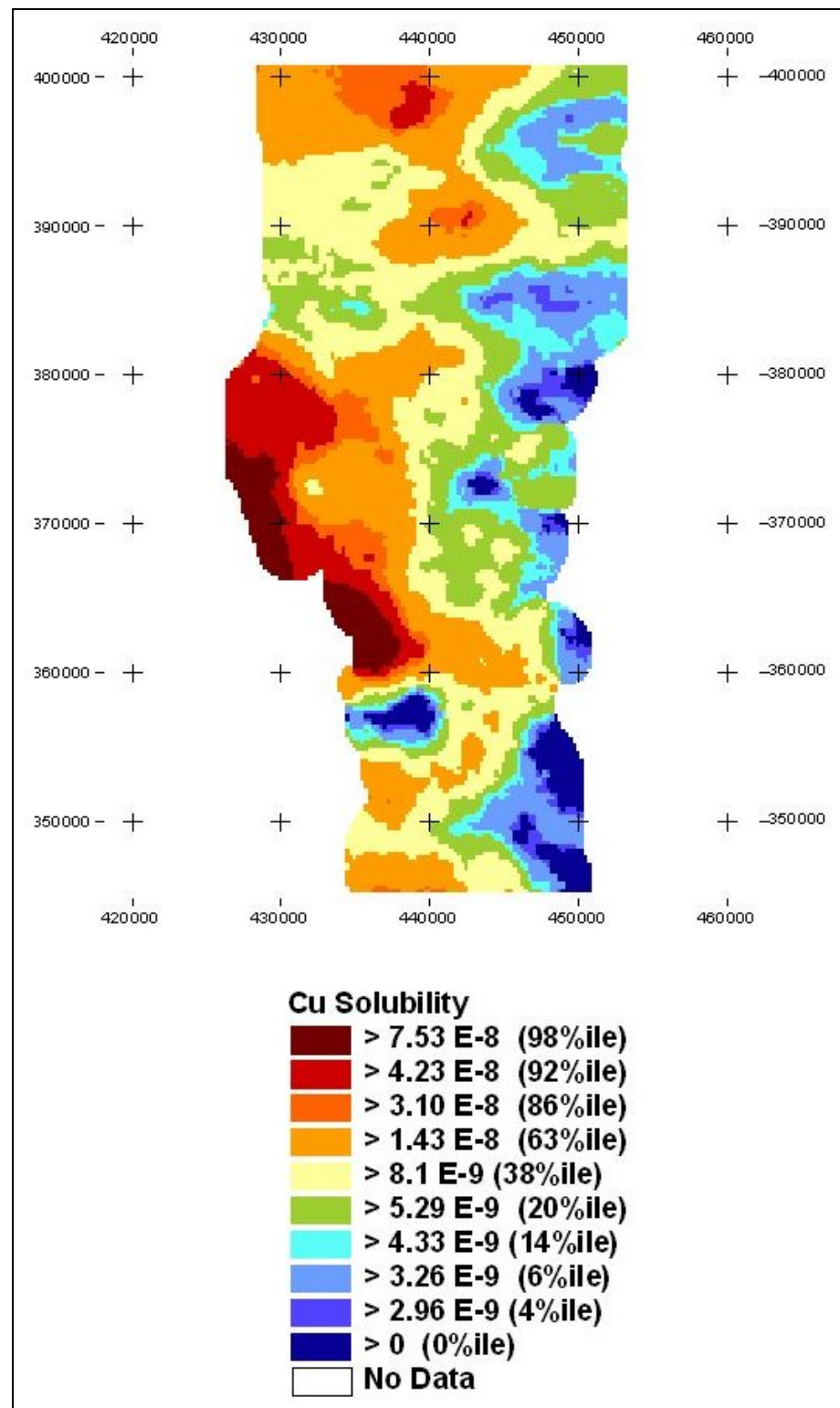


Figure 3.21: Kriged predicted Cu solubility values ( $\text{mmol l}^{-1}$ ).

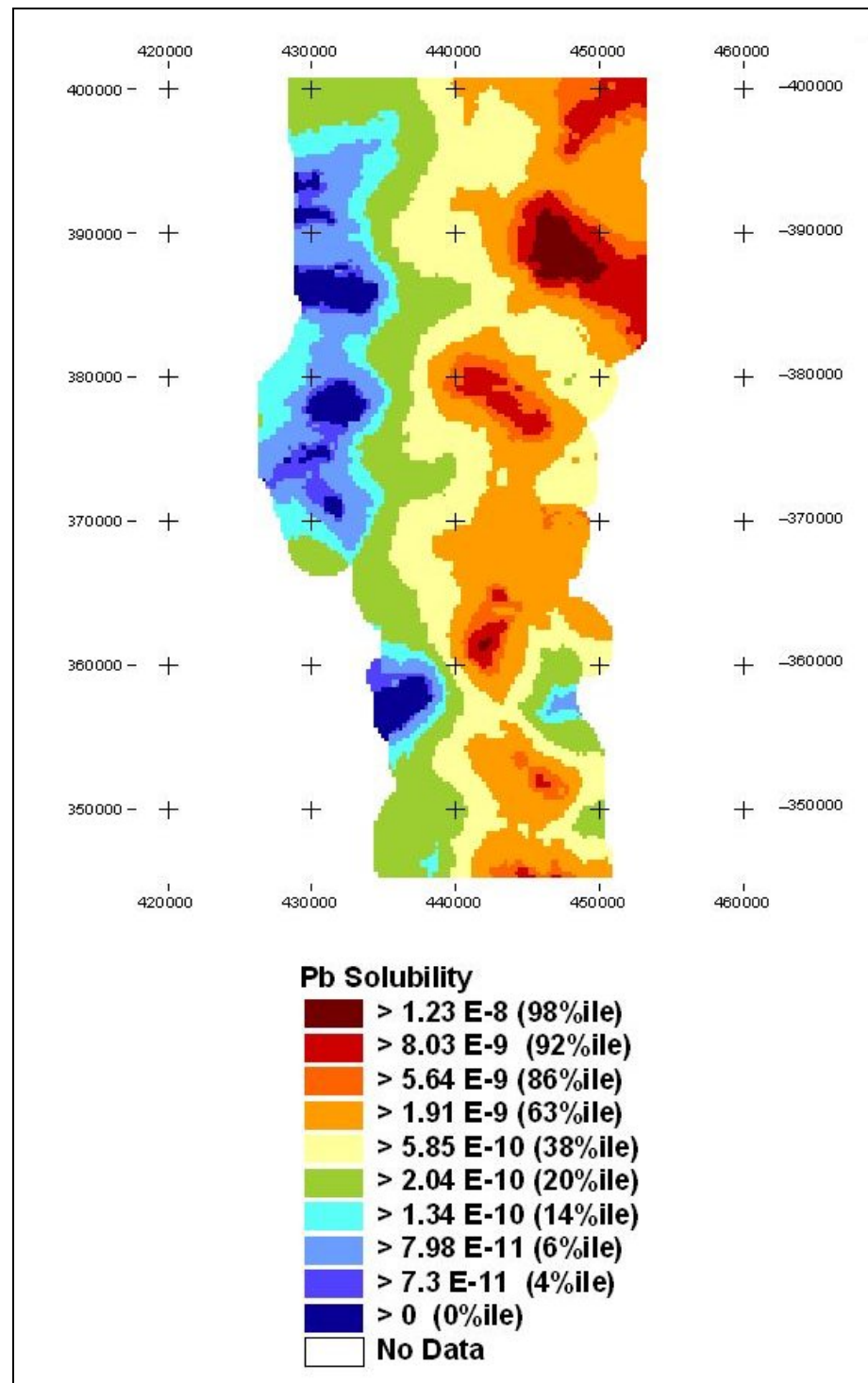


Figure 3.22: Kriged predicted Pb solubility values ( $\text{mmol l}^{-1}$ ).

Lead solubility (Figure 3.22) shows the opposite pattern to lead concentration (Figure 3.11) concentration. This could be due to the strong influence of pH on the lead solubility algorithm (see Figure 3.23).

### 3.4.2 Uncertainty analysis of metal solubility algorithm

As the uncertainty on the solubility kriged values are so high, an investigation into the uncertainty from the solubility algorithm was undertaken.

Most practical problems involving elements of uncertainty are too complex to solve analytically. There are simply too many combinations of input values to calculate every possible result. Monte Carlo Simulation is an iterative process using a random number generator to select a value for each iteration. For each variable the possible values are defined by a probability distribution, from which the value to be used each time is selected.

Crystal Ball is a model simulation programme used in conjunction with Excel. It allows the user to specify the distribution of each model parameter. Using Monte Carlo Simulation, Crystal Ball displays results in a forecast chart showing the entire range of possible outcomes and their probability.

The forecast chart is invaluable for risk analysis and assessing the certainty of a particular event occurring. The tool which is most valuable in this case however, is the sensitivity chart. The overall sensitivity of a forecast to an assumption is a combination of two factors – the model sensitivity and of the forecast to the assumption and the assumption's uncertainty. Crystal Ball calculates sensitivity by computing rank correlation coefficients between every assumption and every forecast while the simulation is running. Correlation coefficients provide a meaningful measure of the degree to which assumptions and forecasts change together. If an assumption and a forecast have a high correlation coefficient, it means that the assumption has a significant impact on the forecast (both through its uncertainty and the model sensitivity). Crystal Ball can also calculate the sensitivities as a percentage of the contribution to the variance of the target forecast.

This is an approximation calculated by squaring the rank correlation coefficients and normalising to 100%. It is these Contribution to Variance values that are most useful in this case. Running simulations of the solubility algorithm using probability distributions modelled on the data for the Westphalian region will provide a sensitivity chart for each metal indicating which parameter is the most influential on the prediction.

Tables 3.9, 3.10 and 3.11 show the model parameters used in Crystal Ball to carry out the uncertainty analysis. The metal and pH distributions were fit to the Westphalian data. The algorithm parameters a, b and c are shown in Table 3.1. The standard error was used as the standard deviation, and a normal distribution was used.

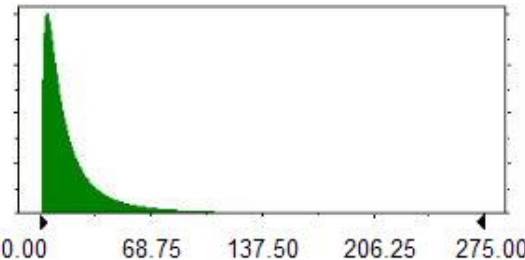
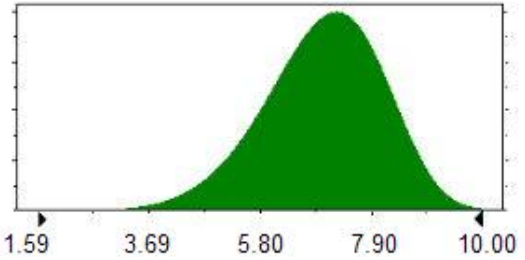
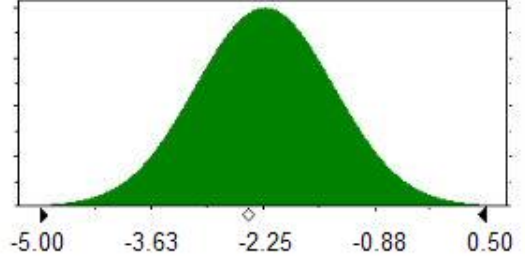
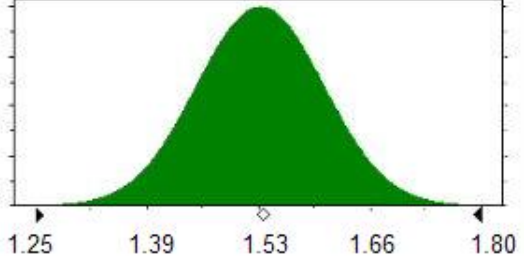
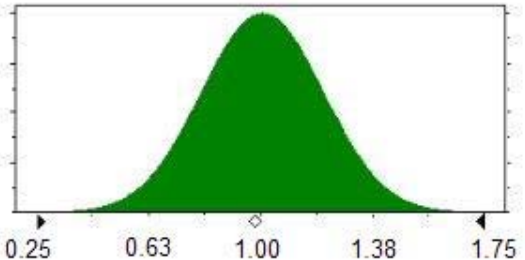
Assumption	Distribution	Parameters
Pb (mg kg <sup>-1</sup> )	Lognormal	Mean = 21.00, Standard Deviation = 29.14 
pH	Weibull	Location = 1.59, Scale = 5.81, Shape = 5.56 
A	Normal	Mean = -2.44, Standard Deviation = 0.77 
b	Normal	Mean = 1.53, Standard Deviation = 0.08 
c	Normal	Mean = 0.98, Standard Deviation = 0.20 

Table 3.9: Details of model parameters used in Crystal Ball for Pb



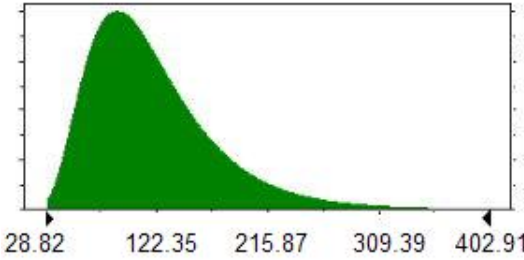
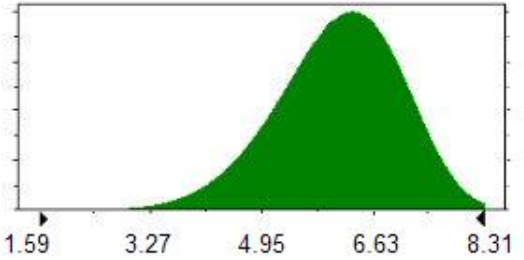
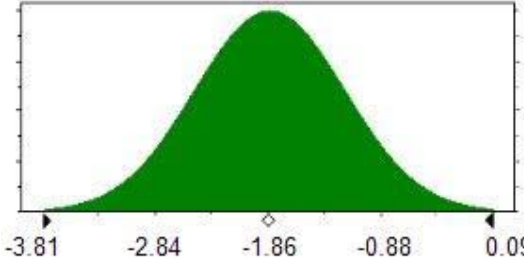
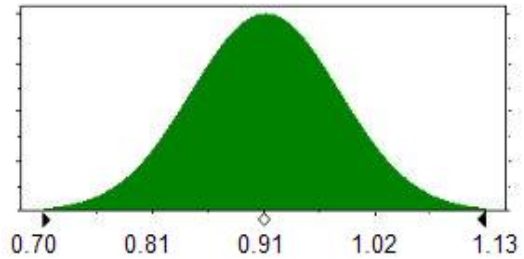
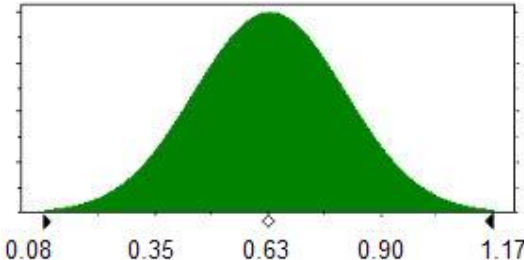
Assumption	Distribution	Parameters
Zn ( $\text{mg kg}^{-1}$ )	Lognormal	Mean = 118.70, Standard Deviation = 54.80 
pH	Weibull	Location = 1.59, Scale = 5.81, Shape = 5.56 
a	Normal	Mean = -2.44, Standard Deviation = 0.77 
b	Normal	Mean = 1.53, Standard Deviation = 0.08 
c	Normal	Mean = 0.98, Standard Deviation = 0.20 

Table 3.10: Details of model parameters used in Crystal Ball for Zn

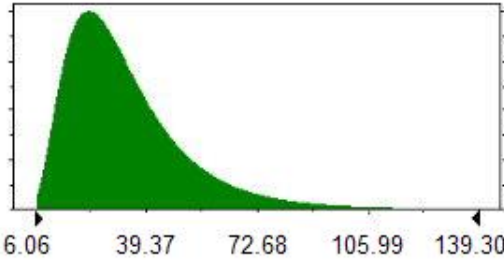
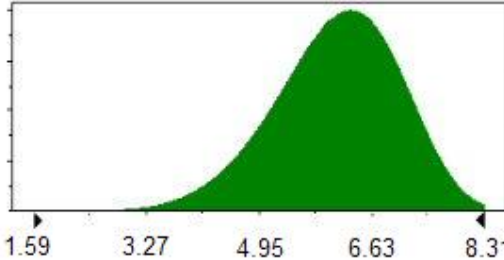
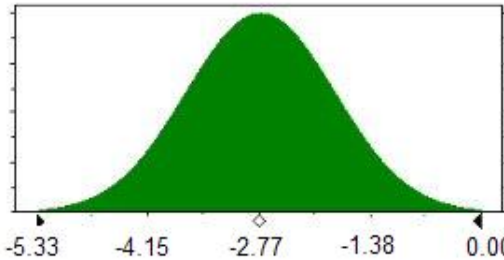
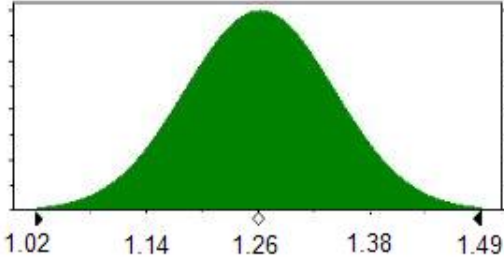
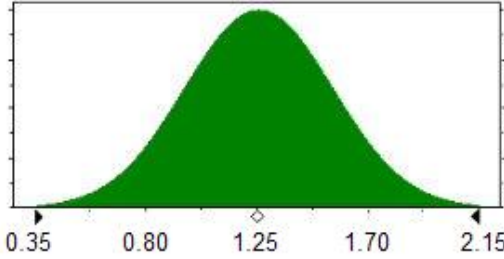
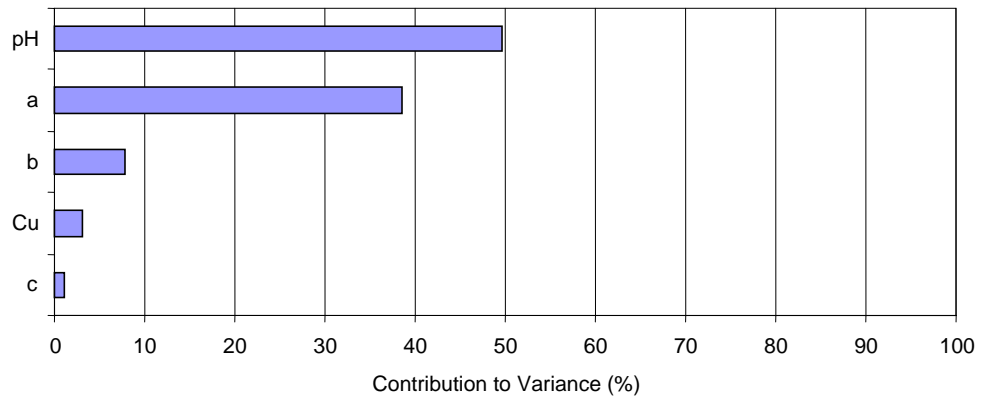
Assumption	Distribution	Parameters
Cu (mg kg <sup>-1</sup> )	Lognormal	Mean = 118.70, Standard Deviation = 54.80 
pH	Weibull	Location = 1.59, Scale = 5.81, Shape = 5.56 
a	Normal	Mean = -2.44, Standard Deviation = 0.77 
b	Normal	Mean = 1.53, Standard Deviation = 0.08 
c	Normal	Mean = 0.98, Standard Deviation = 0.20 

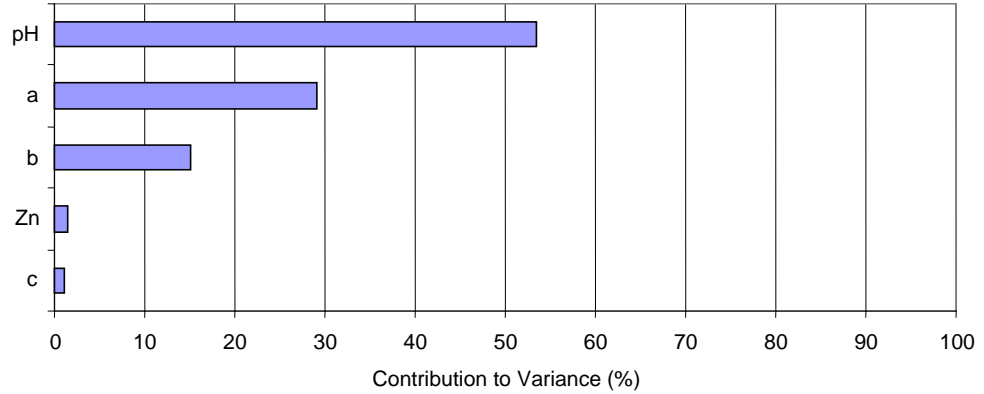
Table 3.11: Details of model parameters used in Crystal Ball for Cu

### 3.4.2.2 Results of Crystal Ball analysis

#### a) Copper



#### b) Zinc



#### c) Lead

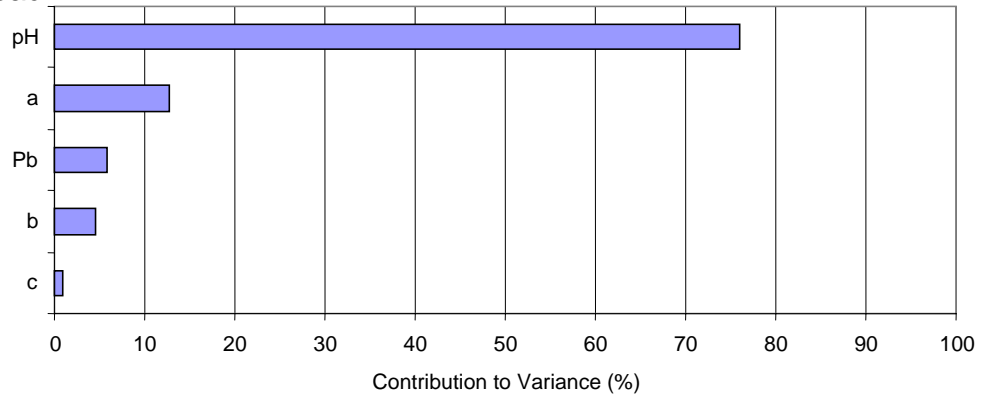


Figure 3.23: Percentage contribution to Variance for the metal solubility algorithm parameters for a) Cu, b) Zn and c) Pb.

The sensitivity charts for each metal are shown in Figure 3.23. In all cases pH is the greatest contributor to the variance in all three metals. Pb is slightly different from Cu and Zn in that the parameters  $a$ ,  $b$  and  $c$  (Equation 3.1) are not as influential. pH has a greater percentage of the variance, and the metal is the third highest contributor to variance, whereas with Cu and Zn metal is the forth. So for all cases metal concentration makes a small contribution to the variance. Parameters  $a$ ,  $b$  and  $c$  represent the model uncertainty and so are intrinsic. From these results it appears that effort should be made to ensure uncertainty in pH measurement is kept to a minimum, as any uncertainty at this early stage will be magnified by the contribution to the variance of the model predictions that pH makes.

### 3.5 CONCLUSIONS

Variograms of the total metal concentrations for the Humber-Trent region capture very large proportions of the spatially correlated variance; the variogram for Zn captures the greatest correlated variance (75%), Cu has a higher nugget of 40%. The nugget for the Pb variogram is higher, at 60%, but this is mainly due to being modelled on the residuals. When the data is kriged for mapping the errors as a percentage of the estimate are between 11 and 30%. Pb had the highest error percentage, at 29.4%, which could be due to the presence of trend in the data which has to be removed before kriging. This adds an extra stage to the process and therefore more opportunities to introduce error. The errors are also calculated in a different way (cross validation) to Zn and Cu as the kriging process for Pb does not produce a kriging variance. Zn and Cu concentration maps show similar low and high concentration spots, whereas Pb shows a different distribution, with a marked east-west trend. This could be due to Pb mining and smelting in the area (see §3.6 and Figure 3.24).

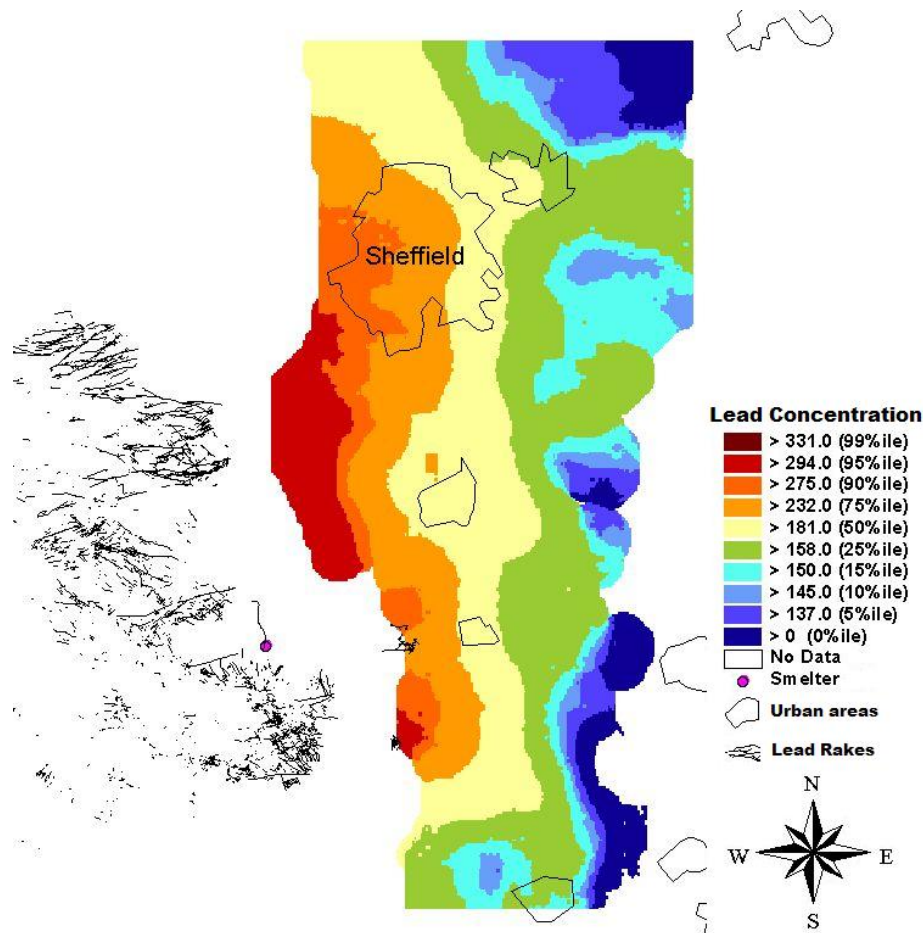


Figure 3.24: Map of Pb concentration showing location of Pb rakes and the location of the Darley Dale smelter.

The pH variogram does not capture as large a proportion of the spatially correlated variance as the total metals; the nugget is 70% of the sill. This shows that the G-BASE sampling scale misses much of the short-scale variation (this prompts the investigation in Chapter 5). The mean kriging error for mapping is 15%.

The variograms for metal solubility showed much larger nuggets than those for the total concentrations. All three metals needed a log transformation because the distributions were skewed. The errors after kriging range from 55% for Cu to 292% for Zn. These errors seem too high for the data to be considered useful.

Analysis by Crystal Ball showed that pH is the greatest contributor to uncertainty in all three metals. The G-BASE sampling scale has been shown above to miss much of the short-scale variation in pH. The sensitivity of the model combined with the uncertainty of the G-BASE pH values means that pH is the crucial element when trying to predict metal solubility from this data, and is the main contributor to the high percentage errors in kriging the solubility predictions. pH probably requires sampling on a finer scale than metals do, perhaps down to a field scale.

### **3.6 INFLUENCE OF HISTORIC CONTAMINATION ON LEAD CONCENTRATION AND SUGGESTIONS FOR FURTHER WORK**

As already discussed, the strong trend present in the Pb concentrations differs from Cu and Zn. One reason for this could be contamination from the Pb mining and smelting industry that has been present in the region for hundreds of years. Of particular interest is the Darley Dale smelter, located to the west of the study area (National grid reference: SK 258 621). Emissions of Pb from the smelter could be the source of Pb forming a strong regional trend.

The Darley Dale smelter has a long history of non-ferrous metal smelting, and between the wars was one of the largest smelters in England. In 1981 a soil survey was undertaken by Sheffield City Polytechnic (Wild and Eastwood, 1992) in North East Derbyshire, covering the area studied in this thesis. This survey discovered that 25% of the area had values of Pb classed as “anomalously high” (based on a “natural” background concentration of Pb of 30-250 mg kg<sup>-1</sup> in NE Derbyshire) with 10% of the values falling above the Department of the Environment’s 1983 trigger value for allotments of 500 mg kg<sup>-1</sup>. A study of Pb levels in tree bark around the Darley Dale smelter in 2001 (Bellis et al., 2001) also found extremely high Pb concentrations in the area. The concentration of Pb found in the tree bark varied from

100 mg kg<sup>-1</sup> to over 25 000 mg kg<sup>-1</sup>, compared to “typical” concentrations of 30-100 mg kg<sup>-1</sup> Pb recorded in South Yorkshire.

The trend present in the other major trace elements was calculated in order to see if this trend was isolated to Pb. A significant trend was only found in Mo, but when the trend surface was mapped it did not show the same distribution as that seen in Pb. It is therefore thought that the most likely source of the Pb trend is the transport and deposition of Pb in dust from the Peak District, more specifically that associated with the processing of mined ore at the Darley Dale smelter.

One way to investigate the source further would be to undertake Pb isotope analysis on individual soil samples along one or more transects from the south and west of the area (close to the possible source) towards the north and east (in the direction of the prevailing wind). This would determine whether the Pb isotope signatures were consistent with a Pb source in the Peak District.

## **4 LARGE SCALE FIELD WORK**

### **4.1 INTRODUCTION**

Chapter 3 represented an attempt to predict metal solubility in topsoil from an area of the Humber-Trent region using data from G-BASE, measured pH values and a metal solubility algorithm (Tye et al, 2003). Large uncertainties occurred when the solubility predictions were kriged to produce maps. In order to examine the accuracy of the metal solubility algorithm without the added uncertainties involved with kriging, a field work programme was designed. This involved returning to original G-BASE locations and taking new samples in order to obtain a direct measure of the metal solubilities as well as top soil pH and total metal concentration. This produced three values for metal solubility – direct measurement from the soil pore water, prediction from newly measured pH and total metal concentration, and prediction from original G-BASE data. These can then be compared to assess the accuracy of the algorithm. A preliminary study was undertaken on four sites (see Table 2.3) in order to refine the sampling and extraction methods, followed by a larger study of 21 further sites (see Table 2.4).

#### **4.1.1 Materials and Methods**

The methods used in this chapter are described in detail in Chapter 2. The analytical methods are described in §2.1 and the field work methods in §2.3. Section 2.3.1.1 describes the preliminary study of four sites, and includes the method of selection of these sites and the methods used for sample collection and pore water extraction.

The process of site selection for the final survey involved the removal of global and local outliers of original G-BASE metal concentration values and analysis of the G-BASE data to ensure a range of pH and metal concentrations, (described in detail in §2.3.1.2). Table 2.4 shows the site locations where samples were collected. The problems encountered with relocating sample



sites which were not originally recorded using GPS technology are described in §2.3.2. The results of the preliminary survey, which are presented below, illustrate the problems described in §2.3.2.

## **4.2 RESULTS**

### **4.2.1 Results of Preliminary Field Work**

The metal concentrations in the four test soils, measured by acid digestion and flame atomic absorption spectrometry (FAAS) (§2.1.3), were in some cases significantly different from the original G-BASE values, which were determined by XRF (§2.1.6). In order to determine whether the difference in values was owing to the measurement technique or a failure to relocate the original sample location, both the G-BASE samples and the new samples were analysed by XRF. The results are shown in Figure 4.1.

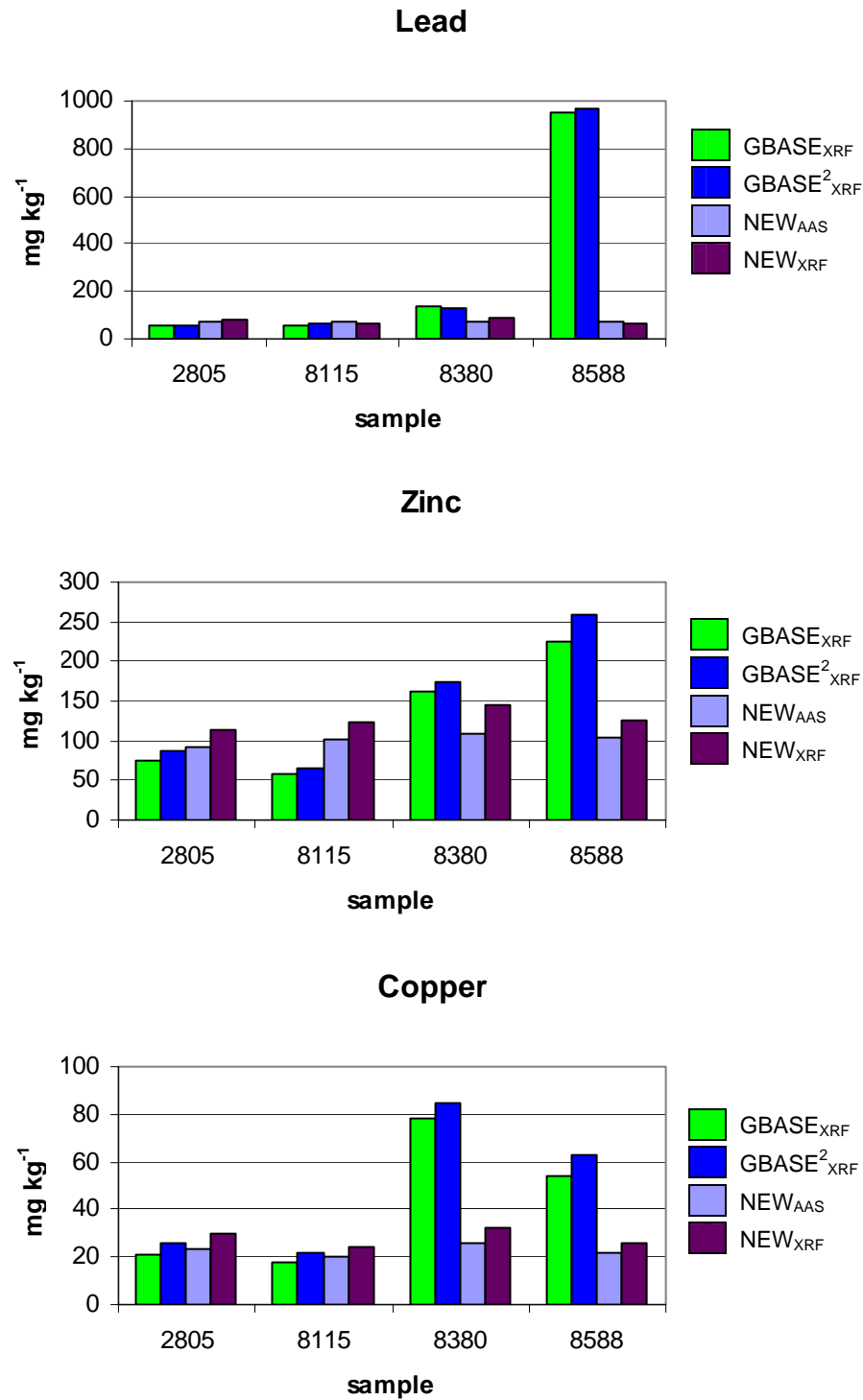


Figure 4.1: Pb, Zn and Cu concentrations at the four test survey sites showing G-BASE results and new sample results. 'GBASE<sub>XRF</sub>' are the original GBASE values, 'GBASE<sup>2</sup><sub>XRF</sub>' are the archived G-BASE soils re-analysed by XRF, 'NEW<sub>AAS</sub>' are the new soil samples measured by aqua regia digest and FAAS, and 'NEW<sub>XRF</sub>' are the new soils measured by XRF.

The results suggest that the measurement techniques are quite consistent. The mean change from  $\text{GBASE}_{\text{XRF}}^{(\text{ii})}$  to  $\text{GBASE}_{\text{XRF}}^2$  is 12%, which shows that the measurement by XRF is consistent between the same samples following a period of storage. The mean change from  $\text{NEW}_{\text{AAS}}$  to  $\text{NEW}_{\text{XRF}}$  is 22%. The difference shown between these two methods is to be expected because of incomplete extraction of metals by aqua regia digest. Research on industrial soils found that for Cu, Pb and Zn the concentrations estimated with XRF were similar to the results obtained when aqua regia digests were analysed with ICP-AES (which produced the same results in the study as FAAS) (Anderson et al, 1998). The model has been calibrated on ‘labile’ and total metal measured by aqua regia digest, so despite the difference to original G-BASE measurement methods it is still the best method to use for testing the model.

$\text{GBASE}_{\text{XRF}}^2$  was compared to  $\text{NEW}_{\text{XRF}}$  to highlight any difference between the original values and those measured on returning to the site. Using these two values minimises both differences in analysis techniques (both use XRF) and instrument differences (the XRF analysis for  $\text{GBASE}_{\text{XRF}}^2$  and  $\text{NEW}_{\text{XRF}}$  was carried out at the same time). The mean change from  $\text{NEW}_{\text{XRF}}$  to  $\text{GBASE}_{\text{XRF}}^2$  for all metals is 170%. The large difference between G-BASE samples and new samples is most obvious at site 8588, where the difference between measurements is 1438%. It is probable that the original G-BASE survey point was over an isolated hotspot of Pb (with elevated levels of Zn and Cu as well), and that on re-locating the site with GPS the hot spot was missed. This sort of phenomenon is supported by the DEFRA (1993) findings that pre-GPS grid references are hard to relocate. The accuracy of relocation was found to be highly dependent on the size of the field and availability of landmarks, but varied between 3 and 77 m. In areas with a history of mining and mine spoil, which could be the case here, contamination can be very localised, and so a difference of a few tens of metres could potentially have a large effect on the value of soil metal concentration measured.

---

<sup>ii</sup>  $\text{GBASE}_{\text{XRF}}$  refers to the original GBASE data which was analysed at the time of collection by XRF;  $\text{GBASE}_{\text{XRF}}^2$  refers to the G-BASE archive soil samples that were re-analysed by XRF;  $\text{NEW}_{\text{AAS}}$  refers to the samples taken as part of the preliminary survey and analysed by FAAS;  $\text{NEW}_{\text{XRF}}$  refers to the new samples analysed by XRF.

As a result of the preliminary survey, it was decided to try and minimise the ‘hot spot’ effect on the larger field study by removing G-BASE sites that were ‘local’ outliers (i.e. significantly different in concentration to their neighbours) from consideration of re-sampling.

The variogram cloud is a diagnostic tool that can be used to identify potential outliers or trends, and to assess variability with distance. Here it was used to remove ‘local’ outliers from the selected region in order to avoid localised hotspots that might prove difficult to re-locate. This exercise revealed that site 8588 was indeed a local outlier for Pb, and that 8380 was a local outlier for Cu. When the values of Pb and Cu concentrations, at sites 8588 and 8380 respectively, were removed, the mean difference in metal concentration between sampling occasions falls to 44% (from 170%) for all metals bulked together.

## **4.2.2 Re-sampling of G-BASE survey sites**

### *4.2.2.1 Total soil concentrations*

The comparison between the concentrations of metal in topsoil at the 21 sites re-sampled (measured by aqua regia digest and FAAS, see §2.1.3) and the original G-BASE values (measured by XRF) is illustrated in Figure 4.2. The results are shown as the percentage change from G-BASE to new values. Figure 4.2 is dominated by the large difference in Pb concentration at site 408982. Figure 4.3 has this site removed in order to see more clearly the differences in the other samples. Pb shows the largest difference between the sites, and there are many sites where the differences show that the original G-BASE site may not have been accurately re-sampled. If a difference of up to 20% is taken as an acceptable measurement variance, 20 of the 21 sites appear to have been ‘missed’ for at least one metal. The preliminary study showed that a small percentage of the difference could be owing to a difference in measurement technique, but that the majority is likely to be due to errors in re-location. The majority of concentrations measured are lower in the new

samples than the original G-BASE samples. This could be partly due to incomplete extraction of the metals by acid digestion.

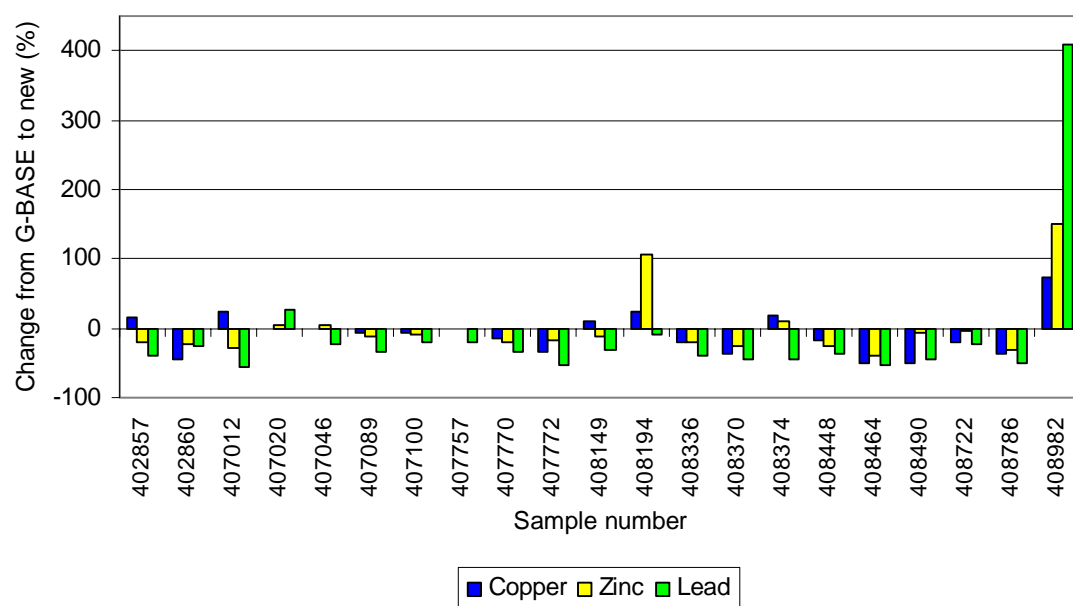


Figure 4.2: Graph showing the percentage change from G-BASE values (XRF) to new sample values (aqua regia digest and FAAS).

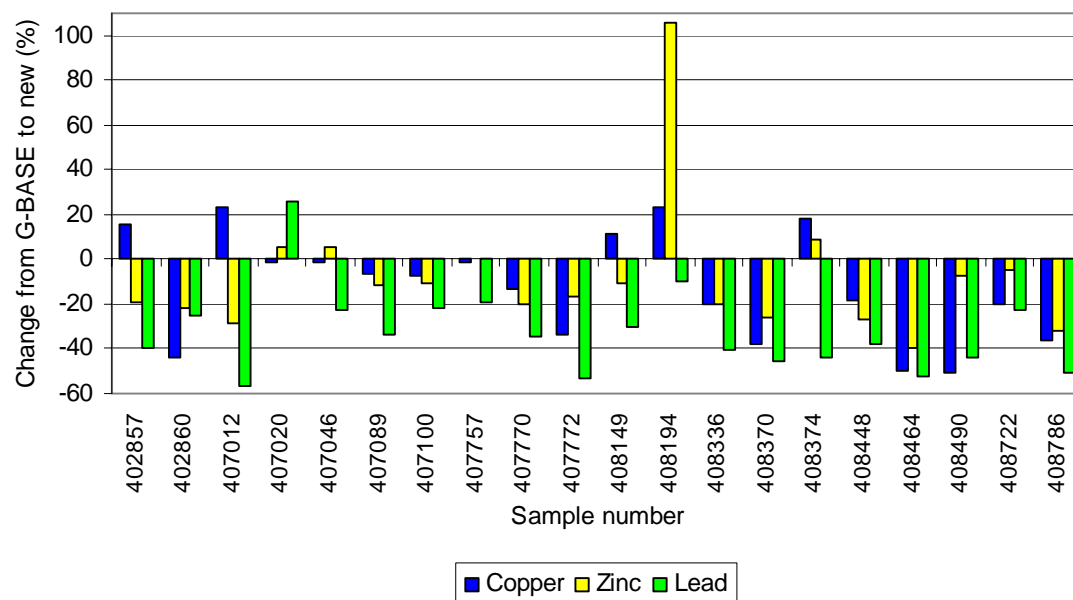


Figure 4.3: Graph showing the percentage change from G-BASE values (XRF) to new sample values (aqua regia digest and FAAS) with sample 408982 removed in order to show the detail of the other sample sites.

Figure 4.4 shows scatter plots of soil metal concentrations measured in the original G-BASE survey plotted against the new survey values. The R-squared values for all three metals are low: 0.11 for Pb, 0.30 for Zn and 0.44 for Cu. The sample with the most obvious difference in Figure 4.2 is highlighted and is an obvious outlier for Pb and Zn. When this point is removed the R-squared values increase to 0.68 for Pb, 0.37 for Zn and 0.54 for Cu. There also appears to be a systematic difference, with all best-fit lines lying below the 1:1 lines. This is likely to be due to the inefficient extraction of metals by the aqua regia digest for the new samples.

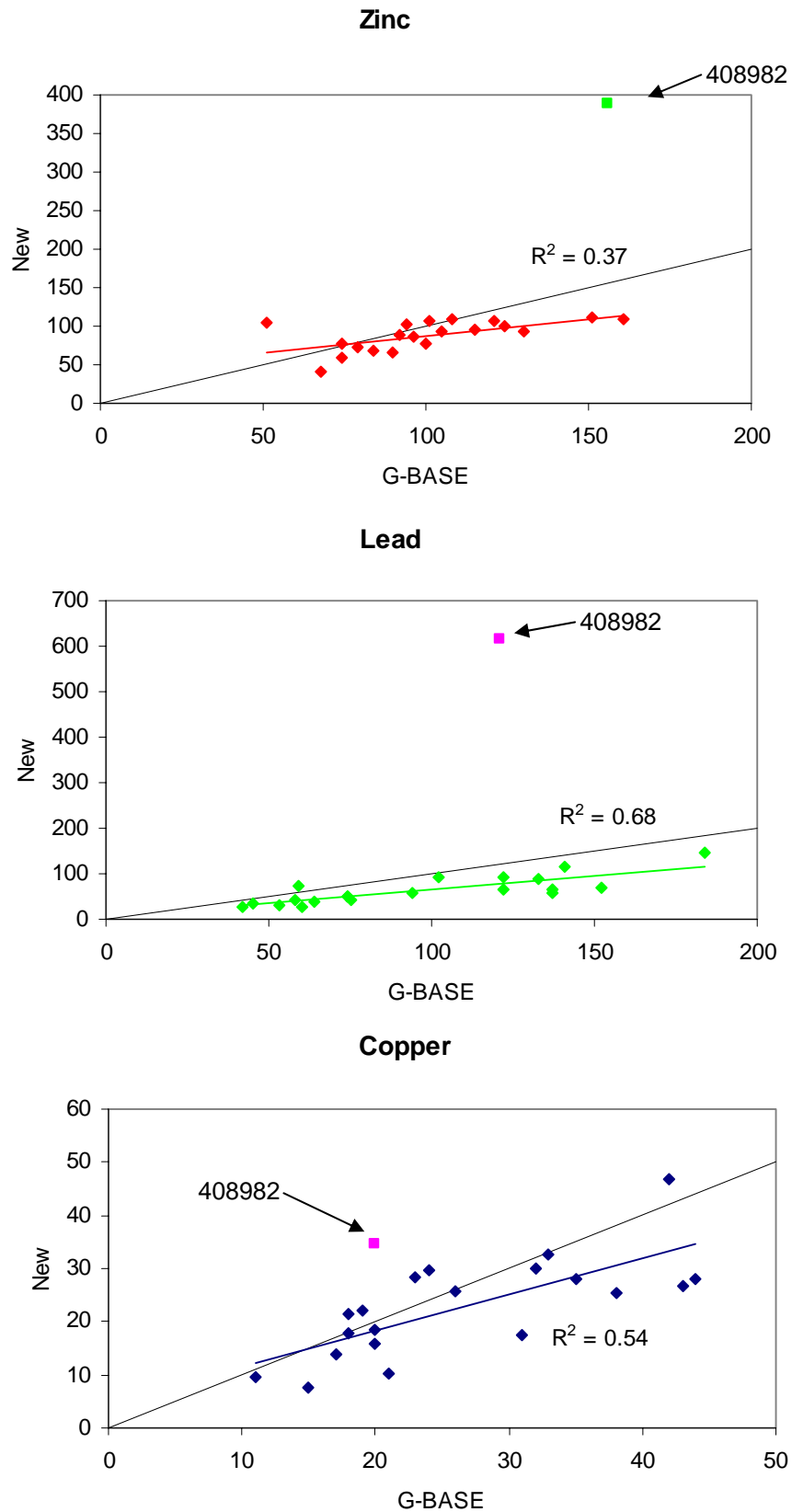


Figure 4.4: Scatter plots of soil metal concentrations ( $\text{mg kg}^{-1}$ ) from the original G-BASE survey against equivalent values obtained in the new survey.

#### 4.2.2.2 Prediction of zinc solubility

Owing to time constraints, only the solubility of Zn is studied here. Zinc is also the most interesting of the three metals as there are two methods of predicting solubility, using total or radio-labile Zn concentration.

The primary reason for re-sampling the G-BASE sites was to assess the metal solubility algorithm used in Chapter 3. Metal concentrations in the pore water were measured, and the speciation model WHAM was used to calculate the solubility of Zn (see §2.1.5.1). Thus measured results for  $-\log_{10}[M^{2+}]$  ( $p(M^{2+})$ ) can be compared to the results obtained from the algorithm (Equation 4.1 and Table 4.1).

$$pZn^{2+} = \frac{\log_{10}(Zn) + a + (b \times pH) + (c \times \log_{10}(I))}{n} \quad 4.1$$

where Zn is in mol kg<sup>-1</sup> C

<b>Model description</b>	<b>Parameters</b>			
	<b>n</b>	<b>a</b>	<b>b</b>	<b>c</b>
<b>Model<sub>Tot</sub></b>	0.969	-3.26	0.977	-1.16
<b>Model<sub>Lab</sub></b>	0.855	-2.20	0.757	-0.638

*Table 4.1: Parameters for the two versions of the model used to predict  $p(Zn^{2+})$  by Equation 4.1 using total (Model<sub>Tot</sub>) or radio-labile (Model<sub>Lab</sub>) Zn concentration. When using the labile model, the Zn concentration is multiplied by the percentage of Zn assumed to be labile.*



### Comparison of total and labile models

Figure 4.5 shows values of modelled  $p(\text{Zn}^{2+})$  against measured data. Two versions of the solubility model have been used for each sample point with either total Zn ( $\text{Model}_{\text{Tot}}$ ) concentration or radio-labile Zn ( $\text{Model}_{\text{Lab}}$ ) as a determinant of  $\text{Zn}^{2+}$  solubility. The two sets of parameters are shown in Table 4.1. A lability<sup>iii</sup> of 48.7% was assumed for  $\text{Model}_{\text{Lab}}$ . This value was obtained from the average measure of percentage radio-lability for all the samples used in the development of the model. If more time had been available the samples used in this study would have been measured for lability.  $\text{Model}_{\text{Lab}}$  gives a better match to the measured values, with an R-squared value of 0.44, as opposed to 0.39 for  $\text{Model}_{\text{Tot}}$ . The average difference between the modelled data and the measured data is 5% for  $\text{Model}_{\text{Lab}}$ , and 13% for  $\text{Model}_{\text{Tot}}$ . The average absolute difference in  $p(\text{Zn}^{2+})$  between modelled and measured data is 0.42 for  $\text{Model}_{\text{Lab}}$  and 0.88 for  $\text{Model}_{\text{Tot}}$ .

---

<sup>iii</sup> The term 'labile' is applied here to the chemically-reactive pool of metal in soil. This does not discriminate between electrostatically or chemically adsorbed metal ions, but is an operationally defined term which identifies the pool of metal in the solid phase able to respond to changes in solution activity of the metal ion within the time of measurement (Nakhone and Young, 1993).

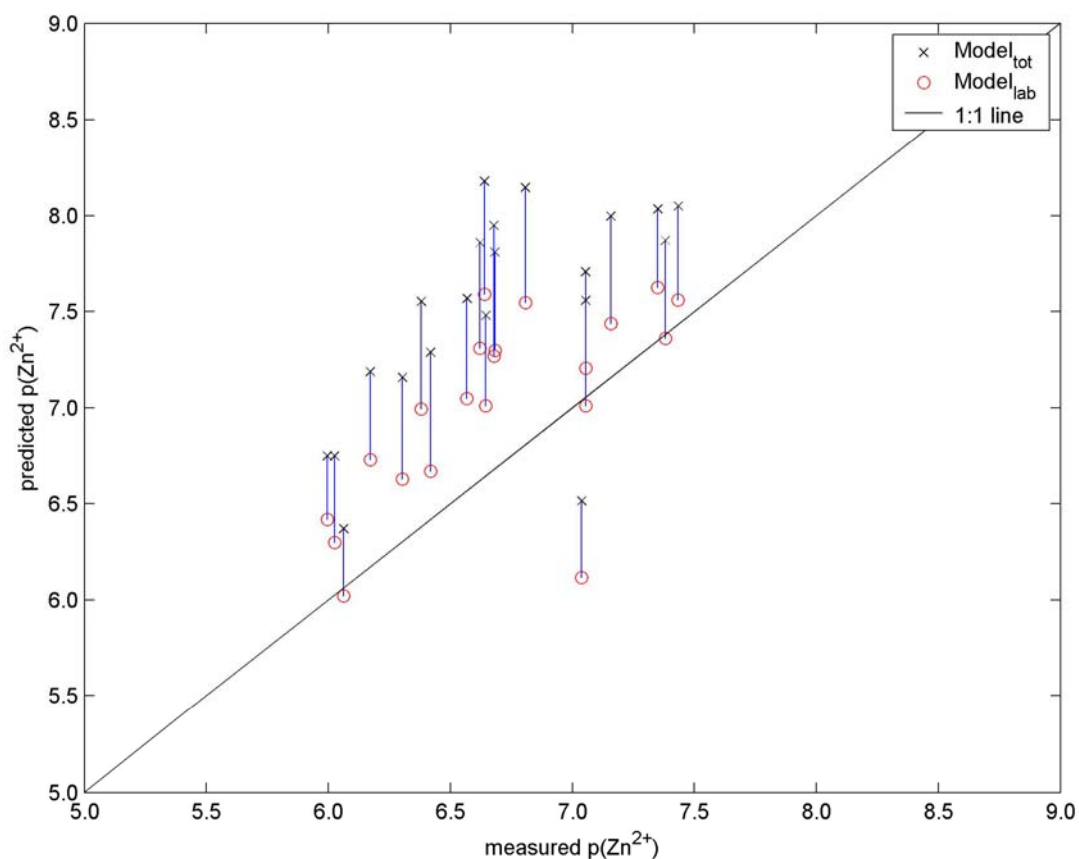


Figure 4.5: Modelled free ion activity for Zn ( $p\text{Zn}^{2+}$ ) against measured values (chemical analysis plus WHAM speciation). Two versions of the solubility model have been used with either total Zn concentration or radio-labile Zn (assuming a lability of 48.7%) as a determinant of  $\text{Zn}^{2+}$  solubility.

Figure 4.6 shows the results from the survey alongside the original data set used to parameterise the models using  $\text{Model}_{\text{Tot}}$  (Tye et al, 2003). Figure 4.7 shows the same information for  $p(\text{Zn}^{2+})$  modelled with  $\text{Model}_{\text{Lab}}$ , using the average percentage lability measured for the soils used for the original model parameterisation. It is difficult to predict where one would expect the current data set to lie in relation to the original solubility model in Figures 4.5 and 4.6. The model based on total Zn concentration ( $\text{Model}_{\text{Tot}}$ ) is likely to produce the greatest error in prediction because, unlike its ‘labile’ counterpart ( $\text{Model}_{\text{Lab}}$ ), it is more prone to variability arising from differences in the chemical form of Zn in soil (Figure 4.5). It is reasonable to expect that the model based on labile

Zn accounts for these differences to some extent. The original data set of Tye *et al* included a wide range of soil metal sources, including soils spiked with recently added metal salts and soils with a long history of exposure from relatively insoluble metal sources such as minespoil. Thus it is not surprising that  $\text{Model}_{\text{Tot}}$  shows the poorest fit, both to the original G-BASE data set and the new re-sample points.

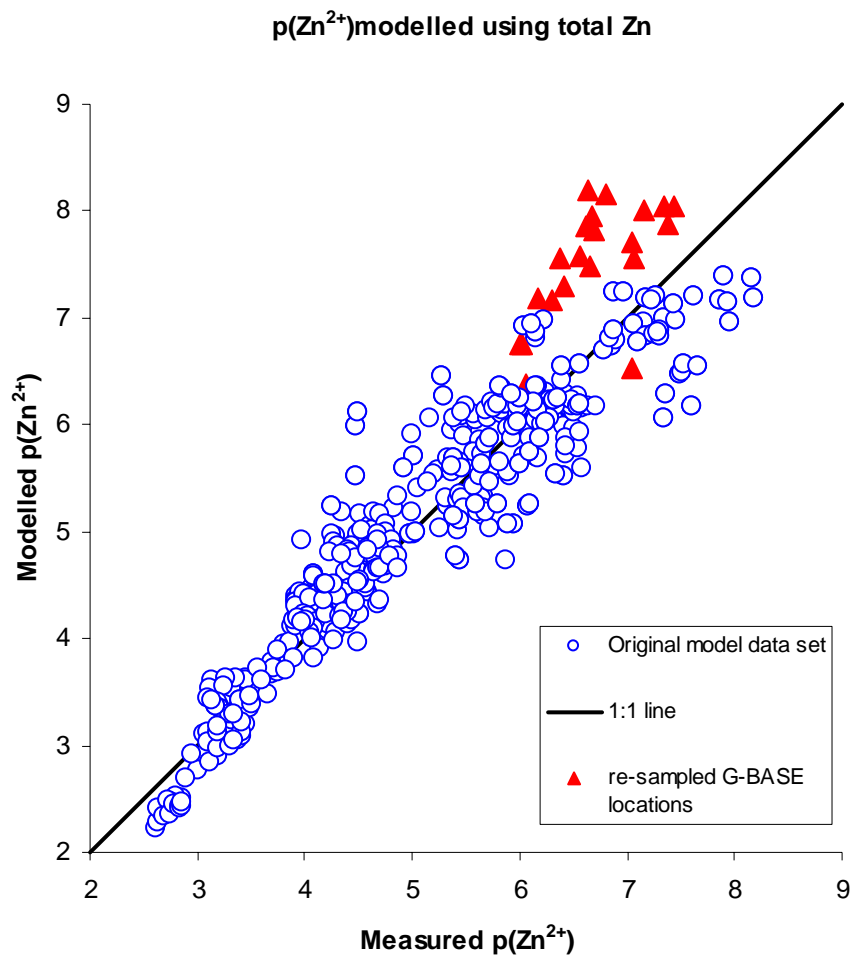


Figure 4.6: Original data set used for the parameterisation of  $\text{Model}_{\text{Tot}}$  with re-sampled G-BASE locations included.

### **Comparison of prediction using re-sampled data and original G-BASE data**

The new samples are among the smallest ( $\text{Zn}^{2+}$ ) values of the combined data set (largest  $p(\text{Zn}^{2+})$ ). This is to be expected given that they originate from uncontaminated agricultural soils – rather than the freshly spiked soils and contaminated sites which dominate the original model data set. On the other hand, it is interesting to note that the measured values of  $\text{Zn}^{2+}$  activity in the new samples are greater than would be predicted by the model;  $p(\text{Zn}^{2+})$  values are to the left of the 1:1 line in Figure 4.5. This may be because of the nature of the soils in the original data set which dominate the low end of the range of  $p(\text{Zn}^{2+})$  values and which therefore influenced the model parameterisation at low values of  $p(\text{Zn}^{2+})$ . These included calcareous clay soils in which Zn had become highly fixed, urban soils with a variety of Zn-rich artefacts (paint, metallic particles etc) and minespoil soils with residual Zn sulphide and carbonate deposits. In all cases these soils would produce a large apparent  $K_d$  value (i.e. relatively low solubility). By contrast, the Zn in the arable soils sampled in this study, although present at low concentrations and therefore likely to be adsorbed strongly, nevertheless appears to be more soluble.

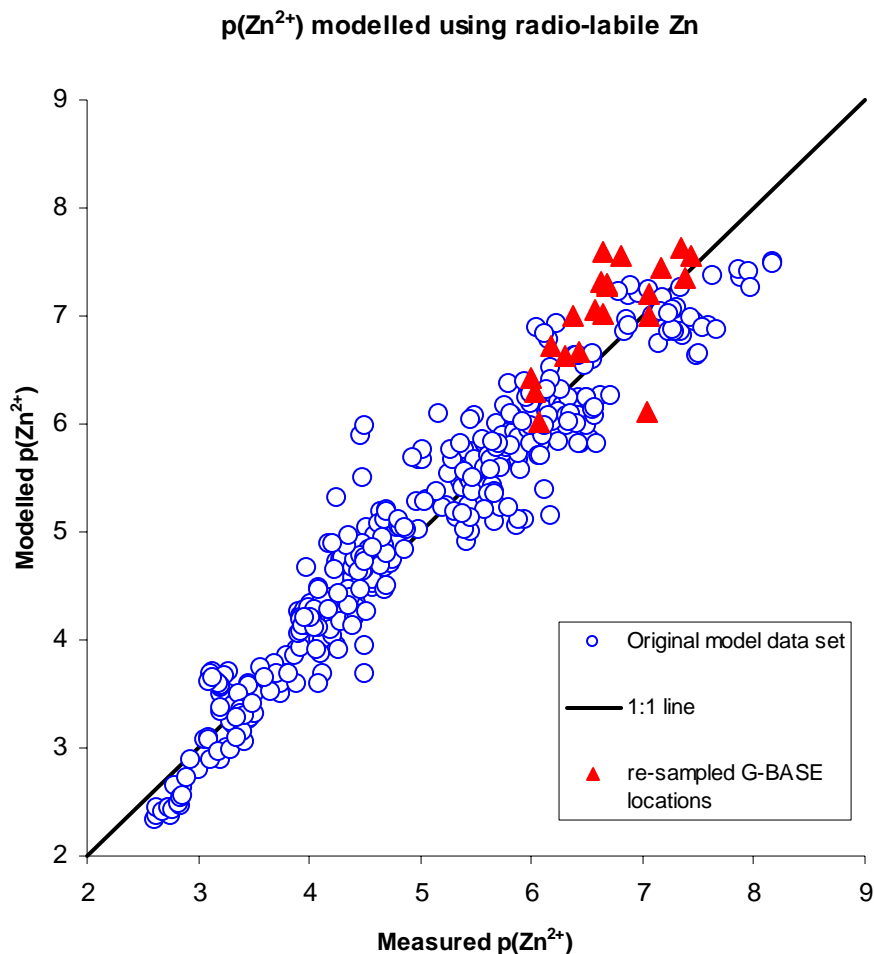


Figure 4.7: Original data set used for the parameterisation of *Model<sub>Lab</sub>* with re-sampled G-BASE locations included.

When *Model<sub>Lab</sub>* is used (Figure 4.7), the new samples lie closer to the 1:1 line than in Figure 4.6. They still lie mainly to the left of the line, showing that *Model<sub>Lab</sub>* also under-estimates Zn<sup>2+</sup> activity, although to a lesser extent than *Model<sub>Tot</sub>*. As with *Model<sub>Tot</sub>* this is likely to be owing to the different nature of the new samples to the soils used in the original data set. The under-estimation of both versions of the model could perhaps be improved by expanding the parameterisation data set to include arable soil samples. Using *Model<sub>Lab</sub>* brings the new samples closer to the 1:1 line than using *Model<sub>Tot</sub>*; it also brings the new samples closer to the original data set. The new samples move further using *Model<sub>Lab</sub>* than the original data set does. This has the effect of minimising the differences between the highly polluted soils in the original data set and the arable soils in the new samples.

The original aim of this thesis was to investigate whether metal solubility can be predicted from a data set such as G-BASE and subsequently mapped. Chapter 3 showed how the kriging process introduces unacceptable levels of uncertainty to the data. However, it might still be useful to use large data sets such as G-BASE to make point-predictions of solubility. In this chapter we have discussed the re-sampling of some G-BASE sites and measured the free ion activity of Zn ( $p\text{Zn}^{2+}$ ) in the soil solution using chemical analysis and WHAM speciation. The solubility model  $\text{Model}_{\text{Lab}}$  has been used to predict  $p(\text{Zn}^{2+})$  at the same locations using the pH and total soil Zn concentration measured by the re-sampling. The original values recorded in G-BASE are also available, and we can use  $\text{Model}_{\text{Lab}}$  to predict  $p(\text{Zn}^{2+})$  from this data as well. Figure 4.8 shows Figure 4.7 with the addition of  $p\text{Zn}^{2+}$  predicted from the original G-BASE data but compared to re-sampled measurements.

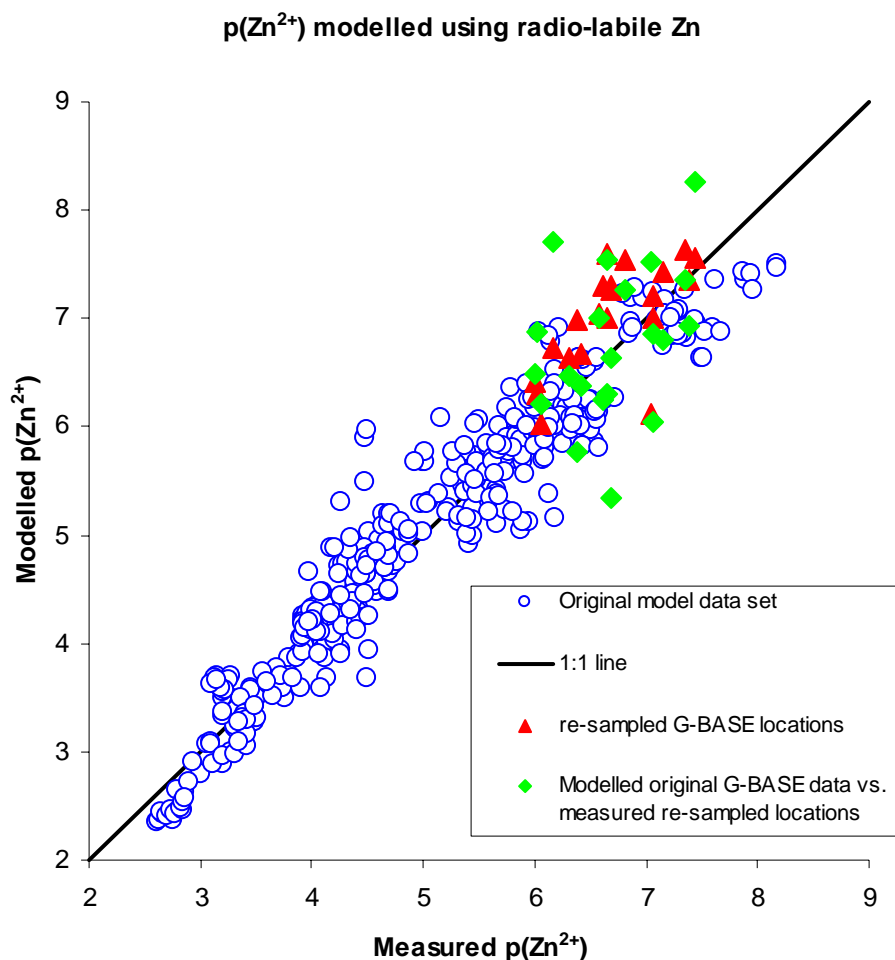


Figure 4.8: Original data set used for the parameterisation of  $\text{Model}_{\text{Lab}}$  with  $\text{Zn}^{2+}$  predictions at re-sampled and original G-BASE locations included.

The average difference between the modelled G-BASE data and measured Zn solubility at re-sampled G-BASE locations is 8%. The average difference between modelled and measured Zn solubility at re-sampled locations is 6%, which suggests that using G-BASE to predict metal solubility, even though the samples cannot be said to be at exactly the same location, gives a good prediction. Figure 4.9 compares the difference between G-BASE prediction and measurement of ‘new’ samples with the difference between the ‘new’ prediction and measurement. Where the model predicts lower zinc solubility than the measurement the difference is negative. The graph shows that the G-

BASE prediction was often lower than the measurement, whereas the “new” predictions are usually higher than the measurement.

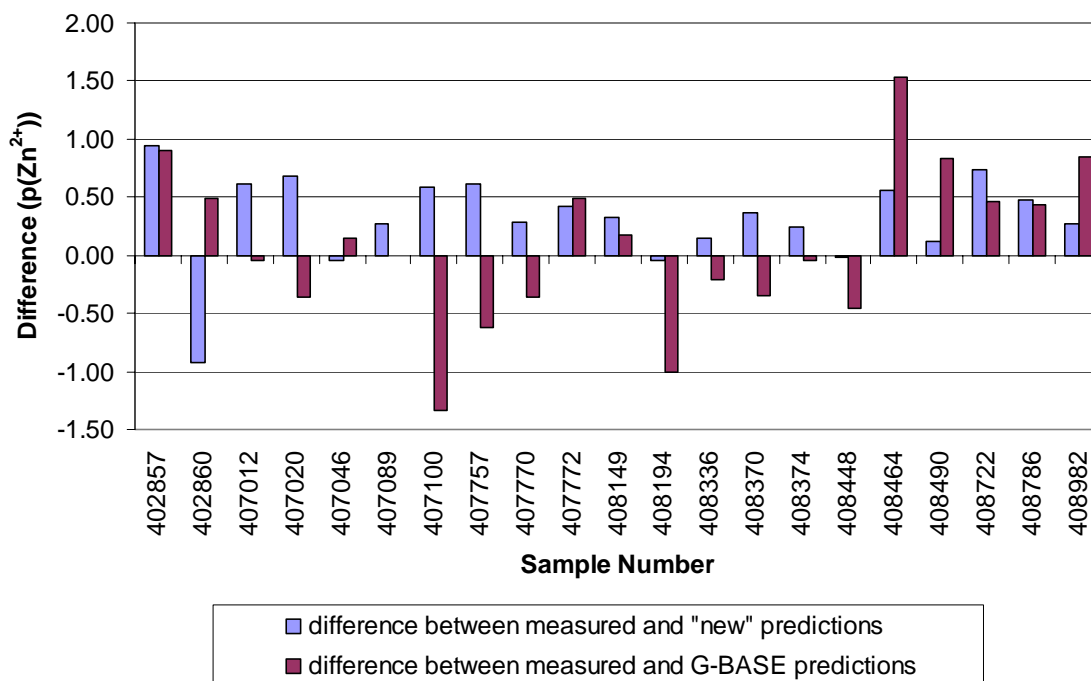


Figure 4.9: Difference between measured and predicted  $p(\text{Zn}^{2+})$  values using two sources of data for predictions.

### Analysis of how the algorithm depends on metal concentration and pH

Figure 4.10 is a surface plot of  $p(\text{Zn}^{2+})$  predicted by  $\text{Model}_{\text{Lab}}$  as pH and Zn concentration varies. Zn concentration goes up to  $1000 \text{ mg kg}^{-1}$ , going higher obscures changes at lower concentrations. The plot demonstrates how  $p(\text{Zn}^{2+})$  is affected by concentrations more commonly found in agricultural soils. It shows that at high concentrations  $p(\text{Zn}^{2+})$  is most influenced by pH, with small changes in concentration not influencing  $p(\text{Zn}^{2+})$  very much. However, at low concentrations, Zn seems to be much more important in predicting  $p(\text{Zn}^{2+})$ .



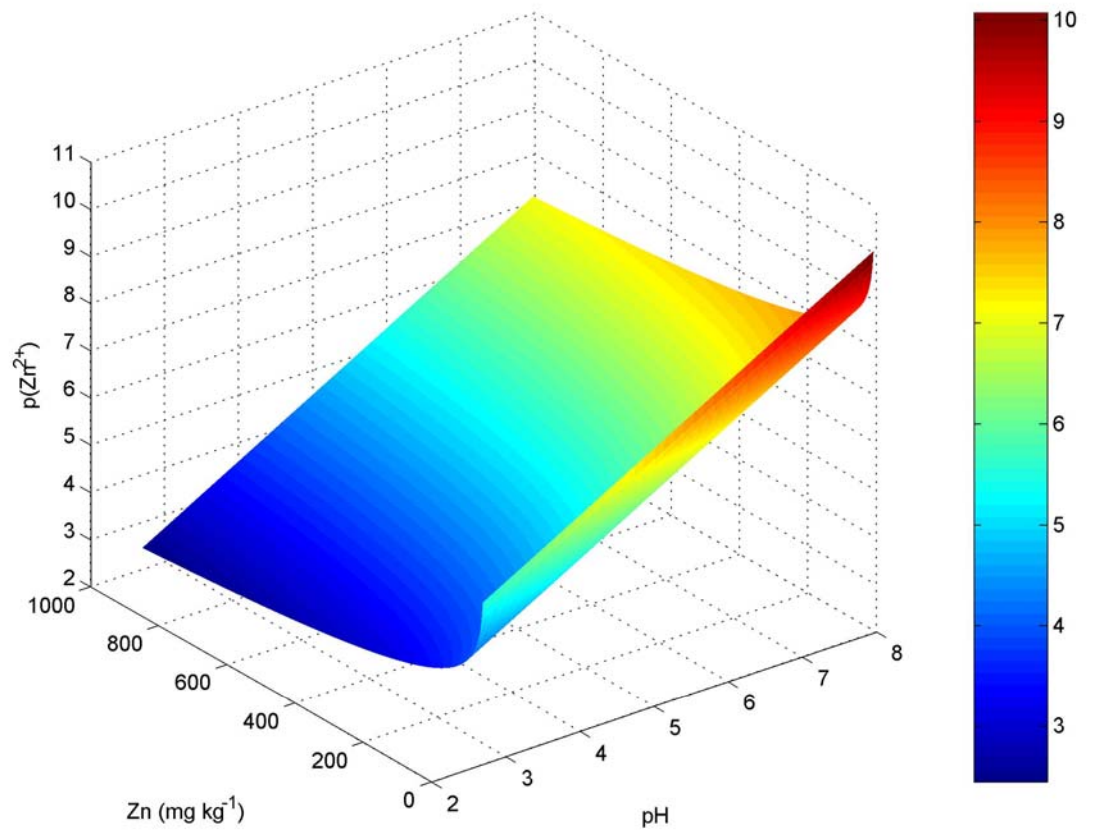


Figure 4.10: Surface plot of  $p(\text{Zn}^{2+})$  with increasing Zn concentration and pH.

### 4.3 CONCLUSIONS

The preliminary field work showed that there are considerable difficulties in re-locating sample sites. The effect of this on metal concentration was seen again in the final field work, with Pb showing the largest average difference in concentration between original G-BASE and new samples (see Figure 4.3).

In predicting  $\text{Zn}^{2+}$ ,  $\text{Model}_{\text{Lab}}$  gives better predictions than  $\text{Model}_{\text{Tot}}$ , with the average difference between modelled and measured data 5% for  $\text{Model}_{\text{Lab}}$  and 13% for  $\text{Model}_{\text{Tot}}$ .

When plotted with the original model parameterisation data set, the new samples are at the lowest  $\text{Zn}^{2+}$  (highest  $p(\text{Zn}^{2+})$ ) end due to the nature of the

original data set being based on contaminated soils. The under-estimation of both  $\text{Model}_{\text{Lab}}$  and  $\text{Model}_{\text{Tot}}$  is probably owing to the model being strongly influenced by the parameterisation at the opposite end of the scale of  $p(\text{Zn}^{2+})$ .

Despite the re-sampled soils being essentially separate locations to the original G-BASE samples, the difference between new measured  $\text{Zn}^{2+}$  and predictions made using G-BASE is only 2% greater than when predictions are made using new samples (8% difference between measured and G-BASE predictions and 6% difference between measured and new predictions). This suggests that they can be considered to be the same location for the purposes of predicting  $\text{Zn}^{2+}$  despite re-location difficulties.

## **5. SHORT-SCALE pH INVESTIGATION**

### **5.1 INTRODUCTION**

This chapter investigates the short-scale spatial variability of pH. This investigation was triggered by the results of the investigation of the G-BASE data in Chapters 3 and 4 which showed pH contributed most to the uncertainty of the solubility algorithm and also varies on a smaller spatial scale than the metal data.

The objectives of the chapter are to present a review of the spatial variability of soil pH, which is in §5.1.2, and the influence of pH on metal solubility, §5.1.3. Section 5.2 presents the results of the pH variability investigation, including the variogram and pH map of the field. An inter-laboratory trial was conducted to investigate the variability in pH due to other operators, locations and methodologies. Section 5.3 uses the idea of ‘sampling uncertainty’ (Ramsey 1998) to improve the variogram by taking into account other information about the data. Section 5.4 presents the results of other field-scale studies of pH for comparison, and section 5.5 uses the data to simulate G-BASE sampling and wheat uptake of metals. The laboratory methods used are fully described in §2.1.

#### **5.1.1 Background**

Soil pH is relevant to this study for a number of reasons. Metal solubility shows considerable dependence upon pH (Tye et al 2003). Consequently, uncertainty in the measurement of pH is transferred to the prediction of metal solubility, although the concentration of metal ions in soil pore water also depends upon other factors, such as the quantity of metal in the soil. The geostatistical analysis of the G-BASE data in Chapter 3 suggests that pH is more spatially variable than the total soil metal concentrations of Cu, Zn and Pb. The large nugget variance of the pH variogram (accounting for 60% of the sill variance) in comparison with the metal variograms (50% of the sill

variance for Pb and Cu; 30% for Zn) indicates that a large part of the pH variability may be missed by sampling at the resolution adopted by the G-BASE project (one sample approximately every 2.5 km<sup>2</sup> of land area).

The spatial variability of soil pH is affected by many factors; management practices alone may cause pH to change by over one unit between individual fields (Scott Young, *Personal Communication*). The proportion of arable soils in England and Wales with pH less than 6.0 decreased from 10% in 1969-73 to 4% in 1990-93, reflecting the better targeting of lime inputs in recent years (Webb et al., 2001). Although liming has become more accurate, underlying variations in soil characteristics within a field will still lead to pH variation across a field unit.

### **5.1.2 Causes of spatial variability of pH**

The factors that affect soil pH may operate over a wide range of spatial scales. For example, at the smallest scale plant roots take up NH<sub>4</sub><sup>+</sup> ions and release H<sup>+</sup> ions, resulting in a lower pH in the rhizosphere than in the bulk soil a few millimetres away. At intermediate distances there are many influences on soil pH. Mineral and organic matter application such as fertiliser addition or uneven atmospheric deposition can lead to significant changes in pH over distances of several metres. Differences in biomass production, deposition of animal urine patches, changes in soil texture and drainage patterns can also cause variation in pH over similar distances. Over larger distances (> 1 km) changes in topography, parent material (Rawlins et al., 2003) and land use are likely to be the greatest influence on soil pH.

Some of the processes likely to operate within a single land management unit (i.e. a field) are discussed below.

#### *5.1.2.1 Urine Patches*

On grazing land urine patches can represent a locally high input of nitrogen (300 – 500 kg ha<sup>-1</sup>), most of which is urea (Shand et al., 2002). Rapid

hydrolysis of urea results in an increase in soil solution pH. Shand et al. (2002) found that synthetic sheep urine applied to a natural field soil caused an increase of 1 pH unit within 7 days of application. After this time the pH slowly returned to its original level over 28 days as nitrification and plant uptake of  $\text{NH}_4^+$  reversed the increase in pH caused by urea hydrolysis. In the experiment the synthetic urine was applied over an area of 4 metres by 1 metre, roughly reflecting the scale of urine patches that might be found in the field.

#### 5.1.2.2 Ammonium fertiliser application

On arable land, the application of fertiliser may be the most important influence on soil pH. The likely change in soil pH following the application of an ammonium fertiliser can be estimated from consideration of the nitrification reaction and soil pH buffer power (Table 5.1; Rowell, 1994).

Equation 5.1 estimates the change in soil pH ( $\Delta\text{pH}$ ) resulting from an application of  $\text{NH}_4\text{-N}$  fertiliser ( $a$ ,  $\text{kg N ha}^{-1}$ ) to a soil with a buffer capacity ( $b$ ,  $\text{t CaCO}_3 \text{ ha}^{-1} \text{ yr}^{-1}$ ). The N application ( $a$ ) is converted to an input of acid ( $\text{mol H}^+ \text{ ha}^{-1}$ ), assuming 2  $\text{H}^+$  ions released per molecule of ammonium nitrified. The buffer capacity ( $b$ ) is converted to an equivalent value expressed in  $\text{mol H}^+ \text{ ha}^{-1} \text{ pH}^{-1}$  (note: molecular weight of  $\text{CaCO}_3 = 100$ ).

Soil Texture	Buffer Capacity ( $\text{t CaCO}_3 \text{ ha}^{-1} \text{ pH}^{-1}$ )
Light	6
Medium	7
Heavy	8
Organic	10
Peat	16

Table 5.1: Buffer capacities for different soil textures (Rowell, 1994)

$$\Delta pH = \frac{\left( \frac{a \times 1000}{14} \right) \times 2}{\left( \frac{b \times 10^6}{100} \right) \times 2} \quad 5.1$$

For reference, the average nitrogen application on tillage crops in 2000 was 149 kg ha<sup>-1</sup> (DEFRA, 2001), although in practice at least half of this would be as nitrate. The use of nitrogen fertiliser has changed dramatically over the years, doubling between 1969 and 1983, and then half of this increase had been lost by 1993 (Skinner et al., 1998).

Using Equation 5.1 and the average nitrogen fertiliser application in 2000, the variation in soil pH can be estimated (Figure 5.1). If an application of 150 kg ha<sup>-1</sup> is heterogeneously applied such that at a small scale some areas receive no N, whereas others receive 300 kg N ha<sup>-1</sup>, the maximum difference in pH that could be expected would be 0.35 pH units on a light soil.

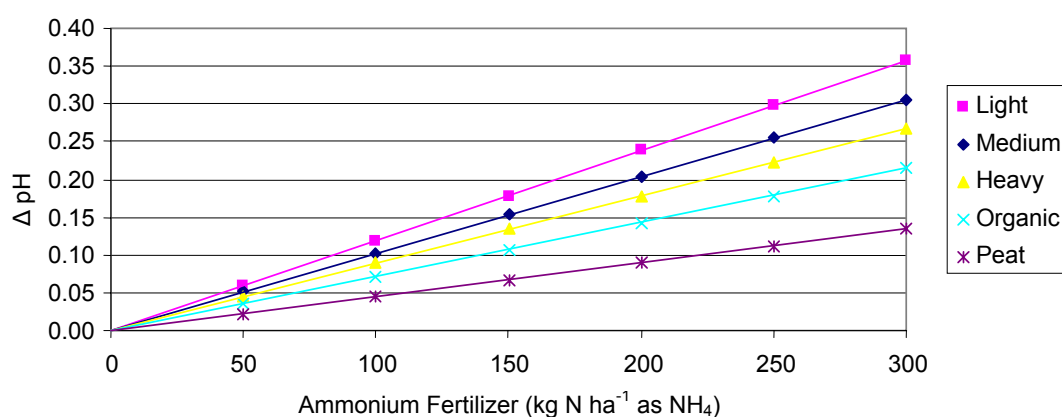
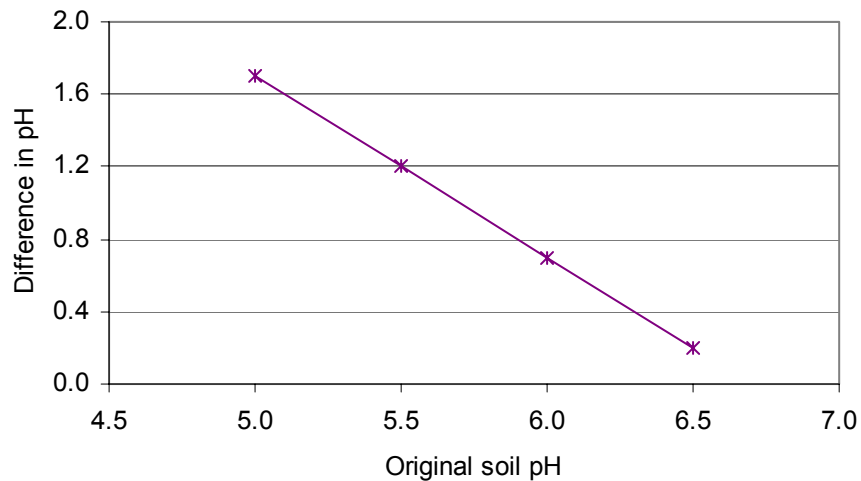


Figure 5.1: Expected shift in soil pH from different applications of ammonium fertiliser on five soil textures, calculated using equation 5.1. Typical application of nitrogen fertiliser in 2000 was 149 kg ha<sup>-1</sup> (DEFRA, 2001).

### 5.1.2.3 Liming

The application of lime to arable land is a management strategy that is intended to have an influence on soil pH. Lime is normally applied in order to increase soil pH to 6.5 – the optimum pH for most crops. Fields are usually managed as complete units, with (nominally) uniform application rates of fertiliser or lime across the whole field. Any natural underlying variation will therefore remain, albeit at an adjusted average pH level. However, the method of application may not be uniform, creating further variation. As with nitrogen fertiliser use, agricultural lime consumption has changed over time. Lime use peaked after the Second World War in the period 1956 to 1963 with approximately 6.5 million tonnes annually. Consumption has declined since, with 4.2 million tonnes applied in 1969 and 2.9 million tonnes in 1993 (Skinner et al., 1998). The proportion of arable soils with pH <6.0 decreased from 10% in 1969-73 to 4% in 1990-93, reflecting the better targeting of lime inputs (Webb et al., 2001).

The largest pH variation across a field would occur where the land has been both limed and fertilised. If the applications are patchy, one area could have received just lime, raising the pH, while an adjacent patch receiving only fertiliser would have a lower pH. Figure 5.2 illustrates the resulting difference in local pH for a medium textured soil and different initial soil pH values. The difference could be very large for soils of initially low pH. The lime treatment is intended to achieve pH 6.5 and the acidifying effect of nitrification is calculated from Equation 5.1. Calculations assume a 200 kg N ha<sup>-1</sup>.



*Figure 5.2: Difference in pH between a limed patch and a fertilised patch ((NH<sub>4</sub>)<sub>2</sub>SO<sub>4</sub>) on a medium textured soil for different initial soil pH values.*

#### 5.1.2.4 Time

Soil pH can change over time, depending on land use and management practice. Agricultural soils used for crops are artificially managed to maintain an optimal pH level. Applications of lime are typically at intervals of a few years and therefore soil pH levels will fluctuate between applications. Applications of fertiliser usually occur annually. The Representative Soil Sampling Scheme (RSSS) was carried out by the Ministry of Agriculture, Fisheries and Food (MAFF) and the Agricultural Development and Advisory Service (ADAS) between 1969 and 1993. During this time the pH of permanent grassland has declined in a linear manner from just over 5.7 to 5.4 (Skinner et al., 1998). Under arable and ley-arable cropping there have been no significant changes in this period (Skinner and Todd, 1998), probably due to management practices.

Over the longer term changes in soil pH can occur even without additions of lime or fertiliser. The extent to which pH will change depends on the land use and on previous treatments. Rothamsted Research (Harpenden, U.K.) has conducted long term studies on soil pH (Blake et al., 1999). Two plots are on



very old (> 300 years) permanent grassland cut for hay, which is the landuse most similar to the arable field studied in this thesis. One (3a) has been unfertilised and limed, and the other (3d) has been unfertilised and unlimed. The pH of 3a has increased from the estimated value in 1856, but has fluctuated in response to the applications of lime as would be expected. The pH of 3d has fallen by 1 pH unit over the duration of the experiment indicating that natural processes can also influence soil pH, but might be masked by management.

#### 5.1.2.5 Drainage

Soil pH is greatly influenced by the drainage conditions of the soil. When an aerobic soil is submerged, its pH decreases during the first few days, reaches a minimum and then increases asymptotically to a fairly stable value of 6.7 to 7.2 in a few weeks (Ponnamperuma, 1972). This results in the pH of waterlogged soils with a higher aerobic pH (> 7) falling due to the build-up of carbonic acid. By contrast, the pH of soils with a lower aerobic pH will rise due to reduction reactions which consume  $H^+$  ions (Ponnamperuma, 1972). For example the reduction half-reaction of  $Fe(OH)_3$ :

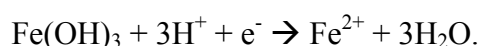


Figure 5.3 shows schematically how the pH of a soil changes over time once waterlogged. The principle applies to all submerged soils, although the pH range of the equilibrium point can change slightly. Marsh soils have a larger range than most, from 5.0 to 7.0 (Ponnamperuma, 1972). The overall effect is that saturated soils have a smaller range of pH values than their aerobic counterparts. Patchy anaerobism would cause patchiness in pH across a field; pH would vary due to distance from field drains for example. In trying to measure this effect, the influence of sample processing should also be considered, as soil is usually dried before testing.

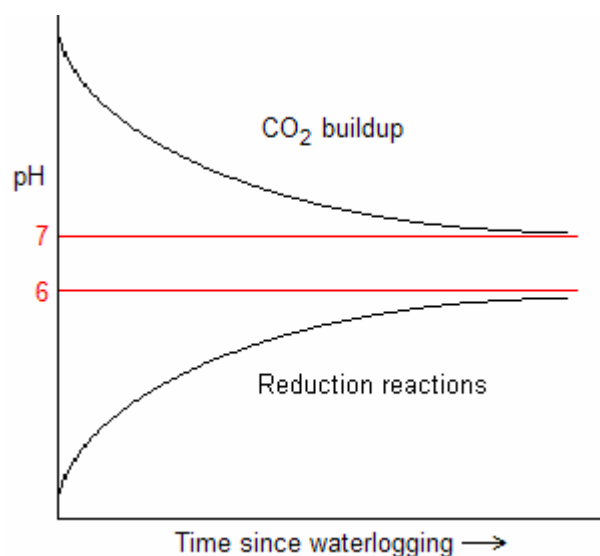


Figure 5.3: Schematic change in soil pH over time when waterlogged, pH on the y-axis and time on the x-axis. Red lines show the typical equilibrium range.

### 5.1.3 Influence of pH on metal solubility

Factors which affect the spatial variability of pH are also likely to influence variation in metal solubility. The amount of metal that is in a mobile and possibly bioavailable form can be described using a simple distribution coefficient ( $K_d$ ) as discussed in §1.2. This approach is used in a large number of environmental fate models. However, it is widely recognised that single  $K_d$  coefficients are not appropriate to represent metal solubility because they vary with factors such as pH, organic matter content and total metal. The metal solubility algorithm used in this study is a simple ‘semi-empirical’ equation. However, it effectively (i) identifies soil humus as the principal adsorption surface for the free ion ( $M^{2+}$ ), (ii) allows for progressive weakening in sorption strength with increased site occupancy through a power term on ( $M^{2+}$ ), and (iii) aggregates the various effects of pH (changes in surface potential and  $H^+$  competition). Such models represent a significant improvement over the use of fixed  $K_d$  values, taking into account many more factors than  $K_d$ . As was found in chapter 3, most of the observed variability in solubility prediction depends primarily on soil pH, followed by total soil metal content.

Sauvé et al (1998) give an example of the influence of pH. They found that the pH-dependent solubility of Pb varied from  $3.6 \mu\text{g Pb L}^{-1}$  at neutral pH to  $10400 \mu\text{g Pb L}^{-1}$  under strongly acidic conditions. In order to estimate the influence of pH on metal solubility in this thesis, the algorithms used in this study and the average soil metal contents from the field work described in chapter 4 were used. Increasing the pH from 5 to 7.5 decreases free ion activity of  $\text{Pb}^{2+}$ ,  $\text{Zn}^{2+}$  and  $\text{Cu}^{2+}$  to less than 1% of their respective values at pH 5 when calculated using the algorithm from this study and an average total metal concentration.

Using average metal concentrations from field work in chapter 4 and the metal solubility algorithms used in this study we can estimate the change in metal solubility. An example 'in-field' pH variance of one unit (see Figure 5.2) from 5.5 to 6.5 pH units provides a change that could be expected in the study region. The increase in solubility from pH 6.5 to pH 5.5 amounted to 94.4% for Cu, 87.8% for Zn and 97.1% for Pb.

The objective of the field work in this chapter was to quantify the different sources of variation which arise when an operator takes a soil sample from a location and measures pH in order to predict metal solubility - and hence metal uptake by plants - in that region. The expected sources of variation can be divided into natural spatial variation (as outlined above), experimental artefacts caused by primary sampling and those introduced by the laboratory methods. A secondary, and more subjective, aim was to investigate at what resolution pH data is needed in order to produce metal solubility predictions that are useful for the end-user. It is clear from chapter 3 that the G-BASE sampling scale misses much of the spatial variability of pH, and therefore variability of metal solubility. However, the benefits of sampling pH at a smaller scale may be difficult to quantify. Sampling at a smaller scale is more expensive, both in terms of time and resources. When undertaking a survey it is important to clearly define the aims of the survey in terms of the accuracy of predictions in order to decide on the right scale of sampling. The ideal would be to balance the needs of the survey with the increasing cost of sampling at greater intensity to find the optimum sampling frequency.

### 5.1.5 Location of field study

The study of local (in-field) variability of pH was carried out in an arable field under 'organic' management, on the University Farm at Bunny, near Keyworth, Nottinghamshire (Figure 2.6).

A 200 m × 100 m grid was established with samples taken at 10 m intervals. During sampling the soil was extremely wet and it was noticeable that drainage conditions varied across the field, with some areas waterlogged. Sampling methods are described in §2.3.3. The soil was clay and samples were taken from 15 cm deep.

## 5.2 RESULTS AND DISCUSSION

### 5.2.1 pH electrode selection

An experiment was undertaken to select the best electrode for the study (see § 2.1.1.4). There were two aims to the experiment:

- to determine whether the suspension effect is significant when using a standard method for determining the pH of soil aqueous slurries.
- to select the most appropriate electrode in order to minimise uncertainty in the soil pH measurements for the field survey.

Figures 5.4 and 5.5 show the change in recorded pH with time for two soils: Q (Pwelliperian) and U (Evesham) from archived control soils used in a previous study (Tye et al. 2003, see § 2.1.1.4). Each graph shows the variation in pH for the supernatant and the suspended slurry for each soil sample. Most readings were stable after 10 to 12 minutes, except for the medium-flow electrode in the case of soil Q, which required over 20 minutes to reach an apparent equilibrium. The same electrode reached an apparent equilibrium within ten minutes for soil U.

In both soils the 'slow-flow' electrode was quicker to respond to the pH of the soil after insertion into the slurry or supernatant. The 'slow-flow' electrode also

gave the least difference in pH between the supernatant and the slurry. This is most clearly illustrated by the results for soil U. The difference between the slurry and supernatant was up to 0.2 pH units with the 'fast-flow' electrode, and 0.05 with the 'medium-flow' electrode, but the 'slow-flow' electrode produced almost identical readings for the slurry and supernatant. Thus the 'slow-flow' electrode was selected for the pH measurements as it showed a minimal difference between suspended slurry and supernatant readings and also achieved pH equilibrium most rapidly.

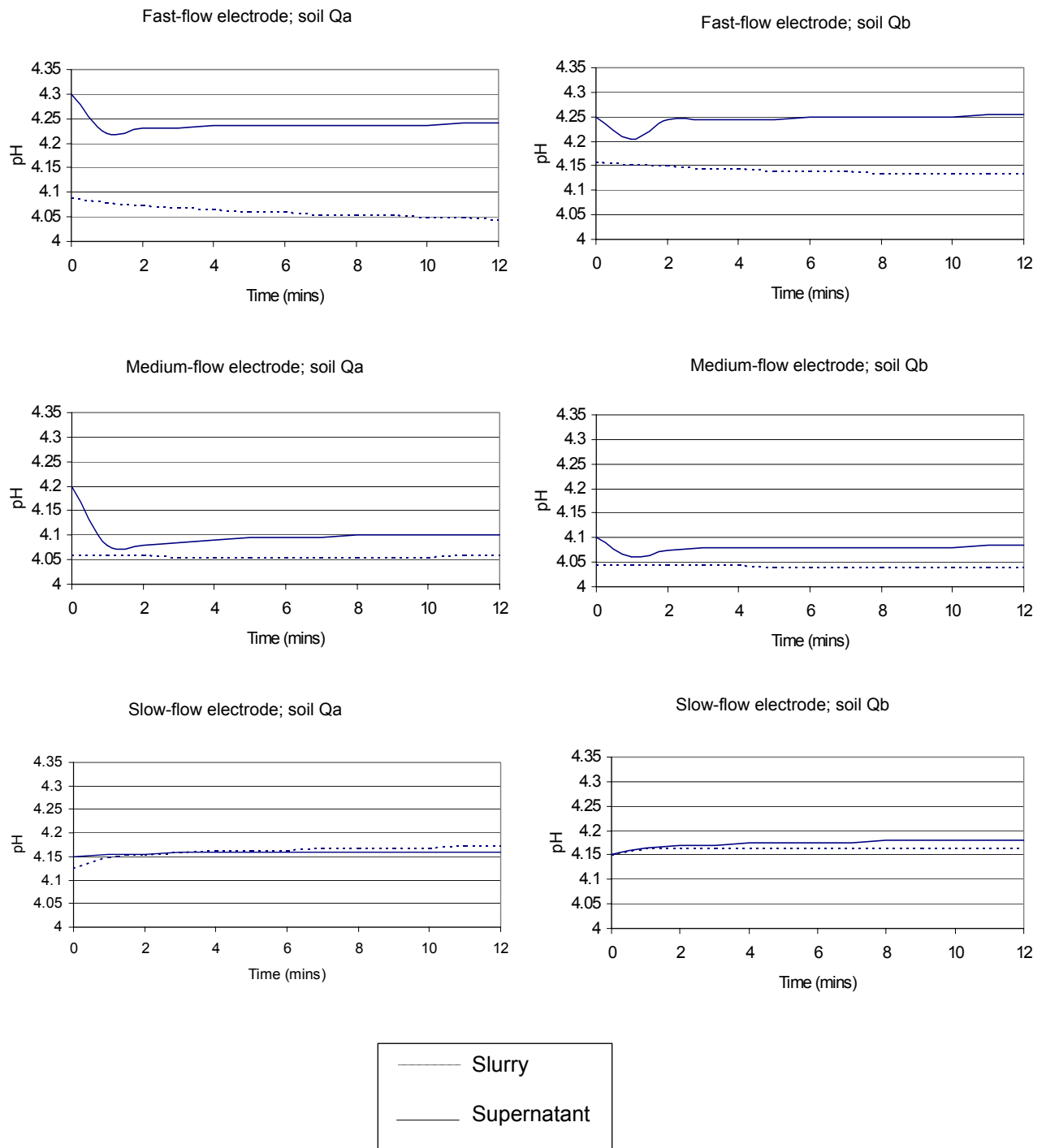


*Figure 5.4: Chart reader results for soil Q. Each electrode ('slow-flow', 'medium-flow' and 'fast-flow') was tested twice, with the sub-samples labelled as 'a' and 'b'. Each of the above graphs shows the supernatant measurement and slurry measurement on a single sub-sample of soil (see §2.1.1.4).*

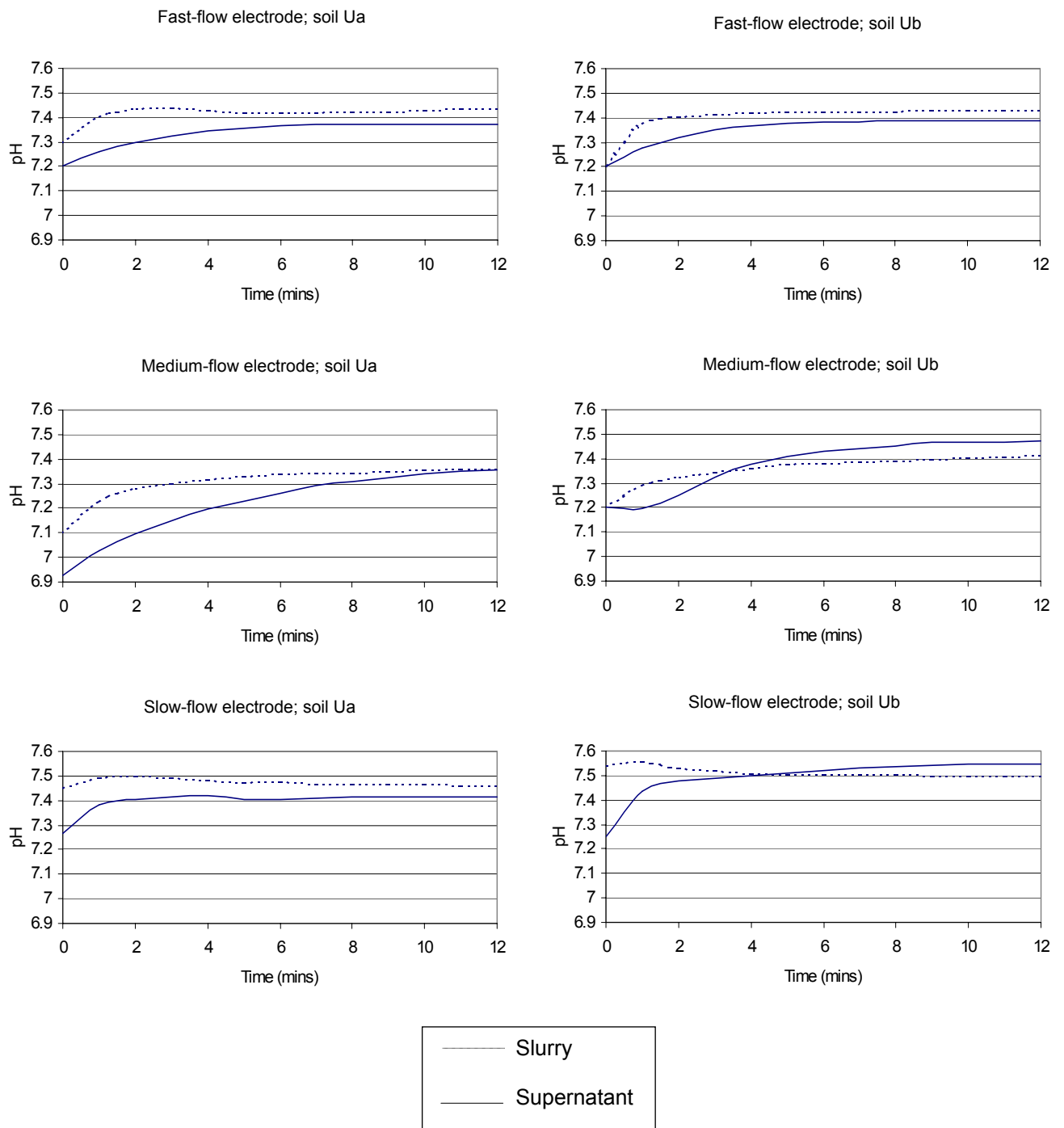


Figure 5.5: Chart-reader graphs for soil U. Each electrode ('slow-flow', 'medium-flow' and 'fast-flow') was tested twice, with the sub-samples labelled as 'a' and 'b'. Each of the above graphs shows the supernatant measurement and slurry measurement on a single sub-sample of soil (see §2.1.1.4).

### 5.2.2 Results of field sampling

The soil survey at Bunny resulted in a total of 289 top soil pH values, presented as a histogram in Figure 5.6. The distribution appears to be approximately normal. The mean value was 7.07 with a standard deviation of 0.303. The standard error of the 20 duplicate samples was 0.03, which is the same order of magnitude as the resolution of the pH meter's display (0.01). The central two thirds of the results fell within a range of 0.6 pH units, which is both two times the standard deviation and comparable with the variation across a field that would be expected from influences such as management variation.

Figure 5.7 is a box-and-whisker comparison of the results from the whole data set compared to the results from the quality control sample (see §2.3.3.2), which was tested 29 times. On these schematic plots, the whiskers extend only to the most extreme values within the inner “fences”, which are at a distance of 1.5 times the interquartile range beyond the quartiles. Outliers are plotted with green crosses. “Far” outliers (red crosses) lie beyond the outer fences, which are at a distance of three times the interquartile range beyond the quartiles. The diagram shows one clear outlier, which was removed before statistical analysis.

The mean pH of the control values was 6.90, with a standard error of 0.0105 and a standard deviation of 0.0558, which is equal to the resolution of the recording device (0.01).



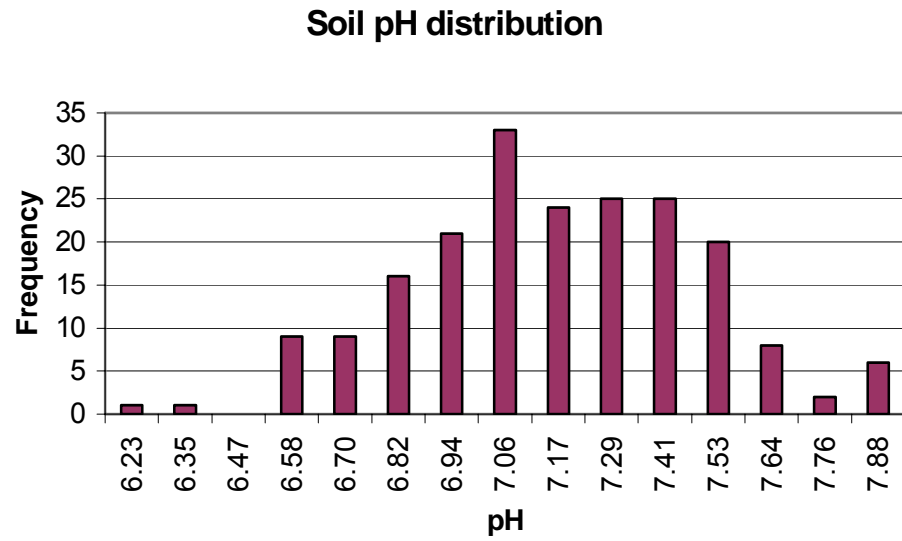


Figure 5.6: Histogram of 289 soil pH values at Bunny

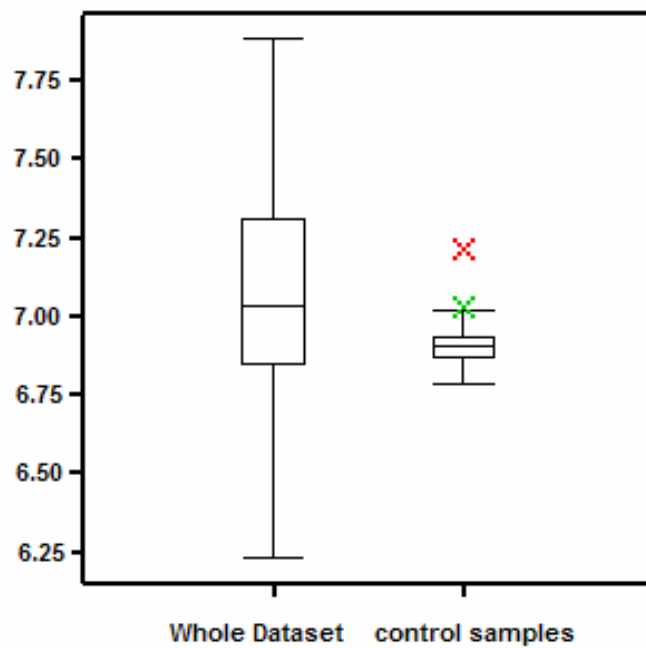
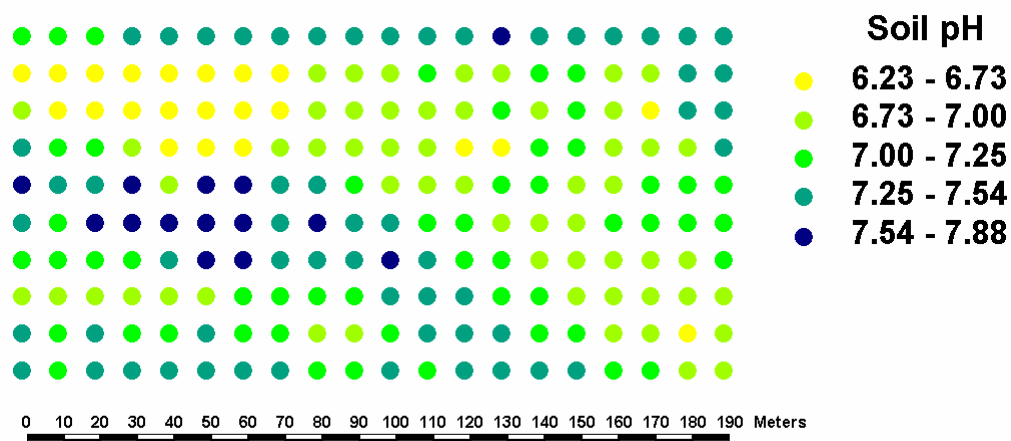


Figure 5.7: Box-and-whisker diagram showing the variation in recorded pH for the whole data set and for the control soil from the Bunny study site.

Figure 5.8 shows the distribution of the pH values spatially over the area sampled within the field. There appear to be some patches of similar pH levels in one area, but no real trend.



*Figure 5.8: Spatial distribution of soil pH values across the study field at Bunny.*

In order to analyse the spatial variation in more detail a variogram of the field was modelled. This was done using Genstat®, in a similar way to the variograms of the G-BASE data in chapter 3. A regression analysis involving fitting linear and quadratic functions to the data showed that the percentage of variance accounted for by these functions was 11.4%. This supports the visual observation that there was no obvious trend in the distribution of values.

### 5.3 SAMPLING UNCERTAINTY AND IMPROVING THE VARIOGRAM

#### 5.3.1 Measurement Uncertainty

Measurement uncertainty is an important concept in science and includes not only uncertainty arising from chemical analysis but from the sampling procedure as well. In the case of environmental and geochemical investigations, primary sampling is often the greatest source of uncertainty (Ramsey, 1998). Consideration of lab-based procedures alone will potentially result in an underestimation of the uncertainty involved. Thus, during the

survey at Bunny, additional samples were taken at randomly selected sites across the field in order to estimate the sampling uncertainty. The method is based on Ramsey (1998) and described in §2.3.3.1.

The terminology used when discussing uncertainty is important. Measurement uncertainty has been defined informally as ‘the interval around the result of a measurement that contains the true value with a high probability’. This is different from the error, which is ‘the result of a measurement minus the true value of the measurand’ and contains both a random and systematic component. Bias is ‘the difference between the expectation of the test result and an accepted reference value’ (Ramsey, 1998).

As discussed in §2.2.3.1 the approach used to determine sampling uncertainty requires a single sampler applying a single protocol. This is the most straightforward method for estimation of sampling uncertainty; a different approach is needed where different protocols or workers are used. In this case we had a small team of samplers but under the direction of a single person who was present at every sampling event. Duplicate chemical analyses were made on both sample duplicates in a balanced design (see Figure 5.9).

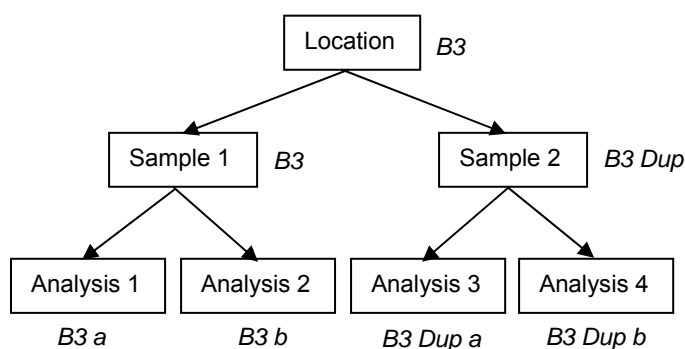


*Figure 5.9: Balanced design for duplicate sampling, including example sample labels.*

An important aspect in estimating the sampling uncertainty concerns the sampling protocol for the duplicate samples. In this case the grid was carefully measured out so the duplicate samples were taken by rotating the quadrat through 45° while still centred on the same spot, as shown in Figure 5.10.

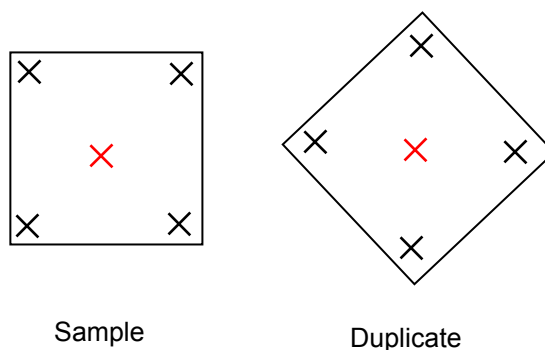


*Figure 5.10: Orientation of sample and duplicate sample for sampling uncertainty analysis. The X marks are the locations of the 5 sub-samples taken within the 1 m square sampling support and aggregated to form a single sample.*

### 5.3.2 Results of the Uncertainty Analysis

The principle behind measurement uncertainty is described in more detail in §2.3.3.1. The three components of the variability (sampling, analysis and geochemical) can be separated using classical analysis of variance. However, classical ANOVA is strongly affected by outliers, and Ramsey (1998) has described a programme to carry out a robust analysis of variance (ROBCOOP4, which is available from the JAAS website: <http://www.rsc.org/jaas>). The program also calculates the classical ANOVA as a comparison. The results are shown in Table 5.2.

<b>Classical ANOVA</b>		Mean = 7.01	
	Geochemical	Sampling	analysis
Sums of Squares	6.73	0.113	0.0759
Sigma Values	0.295	0.043	0.044
Percent Variance	95.8	2.07	2.09
Sigma total	0.301		

<b>Robust ANOVA</b>		Mean = 7.01	
	Geochemical	Sampling	analysis
Sigma Values	0.335	0.045	0.042
Percent Variance	96.8	1.71	1.52
Sigma total	0.341		

*Table 5.2: Output of ROBCOOP4 programme showing classical and robust ANOVA results.*

For the data from Bunny, the results of the classical and robust ANOVAs are very similar. The data do not have any obvious outliers, possibly due to samples being collected over a relatively small area and the fact that the field has uniform management and may have been homogenised due to ploughing. The data is also not excessively skewed (with a skewness of 0.23). It was decided, therefore, to use the classical ANOVA results.

Sampling variance ( $s_{\text{samp}}^2$ ) and analytical variance ( $s_{\text{anal}}^2$ ) can be classed as measurement uncertainty. The third component is geochemical variance ( $s_{\text{geochem}}^2$ ) and is the between-location variance due to real variation of the analyte across the target. The three components can be summed to give the total variance, which is the same as the standard deviation of all the measurements.

The measurement uncertainty ( $u$ ) can be estimated from the combination of the sampling and analytical variance:

$$u = s_{\text{meas}} = \sqrt{(s_{\text{samp}}^2 + s_{\text{anal}}^2)}$$

For this data, the total variance of the survey was 0.301 pH units, of which 96% (0.295 pH units) was due to geochemical uncertainty, 2% (0.043 pH units) is due to sampling uncertainty and 2% (0.044 pH units) due to analytical uncertainty. The measurement uncertainty was 0.295 pH units.

Ramsey (1998) suggests a fitness-for-purpose criterion to help decide whether or not a method can be improved. First the sampling variance should not contribute more than 4% to the total variance (2% in this case). Secondly, the analytical variance should not exceed 20% of the measurement uncertainty, if the measurement component is not to be limited by the analytical component (50% in this case). Finally the measurement variance should contribute less than 20% to the total variance if the measurements are to give a clear representation of the true variation of the analyte across the sampling target. In this case the measurement variance contributed 4.16% to the total, which is well below the recommended threshold.

The only aspect of the above analysis that would benefit from any improvement is the analytical variation. The method used was intended to minimise variation as much as possible. It appears that the analytical variance is therefore close to the point at which significantly more effort would be required to reduce the variance.

### 5.3.3 The Variogram

The variogram is modelled in the same way as those in Chapter 3, but in this situation we have extra information from the uncertainty analysis that can be included to refine the variogram. The nugget variance represents the unresolved error due to analytical error and natural variation at spatial scales less than the smallest sampling interval. This equates to the analytical variance, which is calculated by squaring the analysis sigma value from the ANOVA (0.044). This gives a nugget value of  $1.94 \times 10^{-3}$ . The duplicate variance can be calculated from the sampling sigma value squared plus the analysis sigma value squared ( $0.043^2 + 0.044^2$ ) which equals  $3.87 \times 10^{-3}$ . This has a spatial component – the distance that the duplicate sample was from the original

location. In this case we have plotted it on the variogram at 1 m as this is the maximum separation distance between the duplicate samples (see Figure 5.15).

GenStat® does not have the facility to input a chosen nugget value, but by setting the data up in Excel, and using the optimisation tool ‘Solver’ to find the optimum sill and range, the variogram in Figure 5.11 was created.

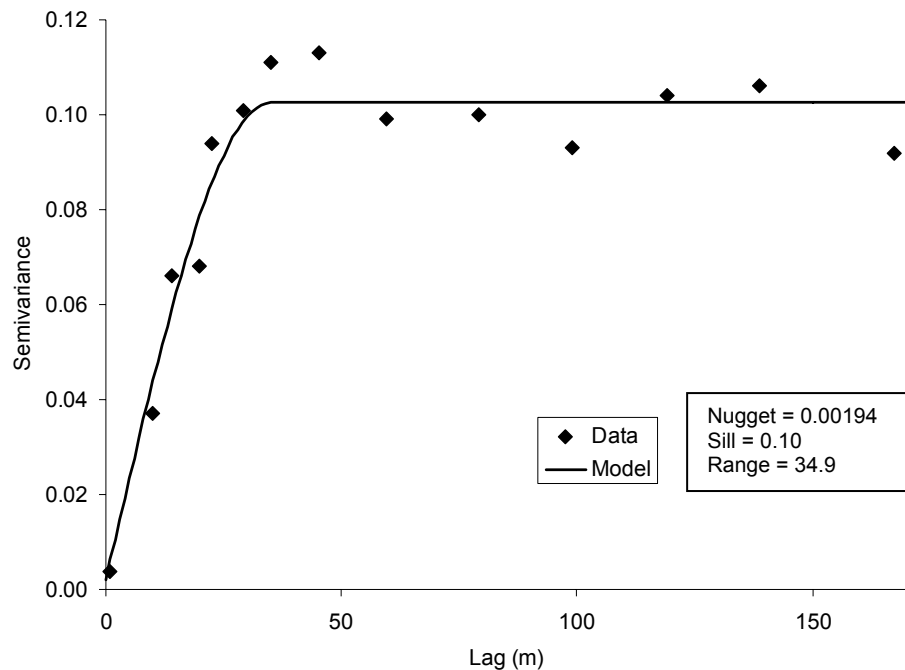


*Figure 5.11: Improved variogram of pH at Bunny. Spherical model, with a fitted nugget and the semivariance at 1m added.*

## 5.4 INTER-LABORATORY TRIAL

In order to further examine the errors introduced at the laboratory stage of a sampling campaign, samples of the quality control sample (5H) were sent to 11 laboratories within the U.K. to be measured using their own standard procedures. The only stipulation was that the same ratio of soil to deionised water be used (1:2.5) to suspend the soil for pH assay. The reason for this approach was that the solid:solution ratio and the suspending solution employed are usually the only pieces of information offered in ‘Materials and

methods' sections of scientific papers. The methods used by individual laboratories, and their results, are shown in Table 5.3 and Figure 5.12.

Laboratory	result	shake time	stand time	electrode position	stabilising time	standards?
A	6.86	15 mins	2 and 24 hrs*	settling suspension	until stable	no
B	6.90	mix	20 mins	settling suspension	5 mins	no
C	6.76	mix	?	Slurry	until stable	4
D	6.48	1 mix	14 mins	Slurry	until stable	1
E	7.08	1 min	15 mins	Slurry	until stable	2
F	6.80	5 min	2 hrs	Slurry	until stable	no
G	6.80	mix	30 mins	Slurry	until stable	no
H	6.61	15 mins	0	Slurry	60s	no
I	6.92	stirred	0	Supernatant	until stable	buffer check
J	6.75	mix (X2)	60 mins	Slurry	30s	no
K	7.02	30 mins	30 mins	Slurry	until stable	no - many repeat tests
L	6.90	1 hr	0	settling suspension	6mins	no - many repeat tests

*Table 5.3: pH value of soil 5H determined in the inter-laboratory trial with differences in methodology shown. The 12 participating institutions (in alphabetical order) were: BGS (British Geological Survey) 'U-block', BGS 'E-block', CEH (Centre of Hydrology and Hydrology), The University of Edinburgh, The University of Glasgow, IGER (Institute of Grassland and Environmental Research), Lancaster University, The University of Newcastle, Rothamsted Research Station, NSRI (National Soil Resources Institute), The University of Reading and The University of Nottingham (the results from the 'control' soil).*

*\*The result for this soil was obtained by averaging two measurements taken from the same suspension 22 hours apart.*



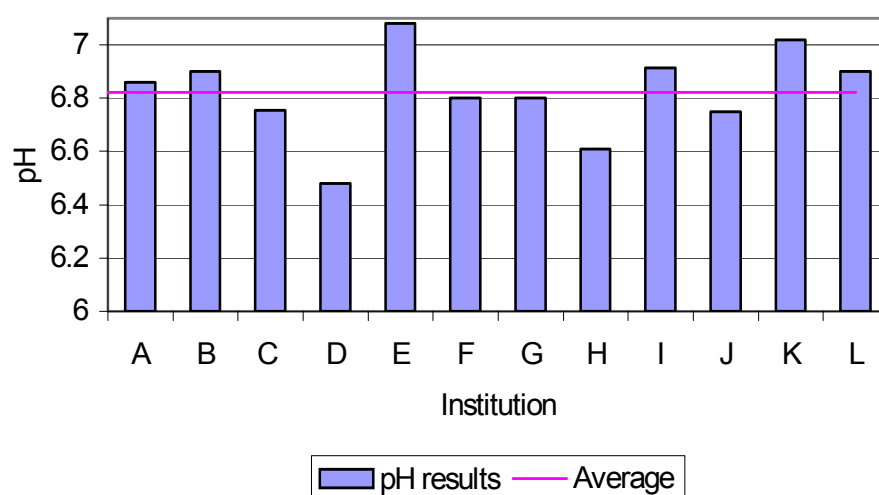


*Figure 5.12: pH value of soil 5H determined in the inter-laboratory trial including the mean result.*

The institutions are labelled with letters for confidentiality, but the result from our measurement of the control soil is labelled ‘L’. In our laboratory, 29 measurements were made, with one outlier removed, leaving the average of 28 measurements as pH 6.90. Table 5.4 compares the statistics of the inter- and intra-lab data. The average of the inter-lab data was slightly lower than the intra-lab results, and the range, standard error, and standard deviation were higher. The intra-lab mean was within 1.6 standard errors of the mean of the inter-lab trial results suggesting that the method used for the Bunny survey (§ 2.1.1.5) was successful in achieving a reliable pH measurement.

Data	Mean	Standard Error	Standard Deviation	Range
Inter-lab	6.82	0.05	0.17	0.60
Intra-lab	6.90	0.01	0.06	0.25

*Table 5.4: Comparison of statistics for the inter- and intra-lab data.*

Figure 5.13 is a histogram of the results of the inter and intra-lab data together and illustrates the greater variation in the inter-lab data suggested by the larger range and standard deviation. It seems reasonable to expect results from a number of laboratories to be more variable than results from a single institution. The intra-lab results were produced by just two operators, and

although the results were measured over a period of a few weeks, they were carried out on the same equipment in the same location. Differences in method, temperature, or CO<sub>2</sub> pressure at different locations could give rise to systematic errors, contributing to the higher variation in the inter-lab results. There was no obvious link between the results and any of the operational variables listed in Table 5.3. In particular there was no link between the values obtained and equilibration time. The most likely cause of variation is the different electrodes used by different institutions. The results in §5.2.1 show a variation in results from using different electrodes from the same manufacturer. The comparison suggests that the method used at Nottingham minimised as much variation as possible.

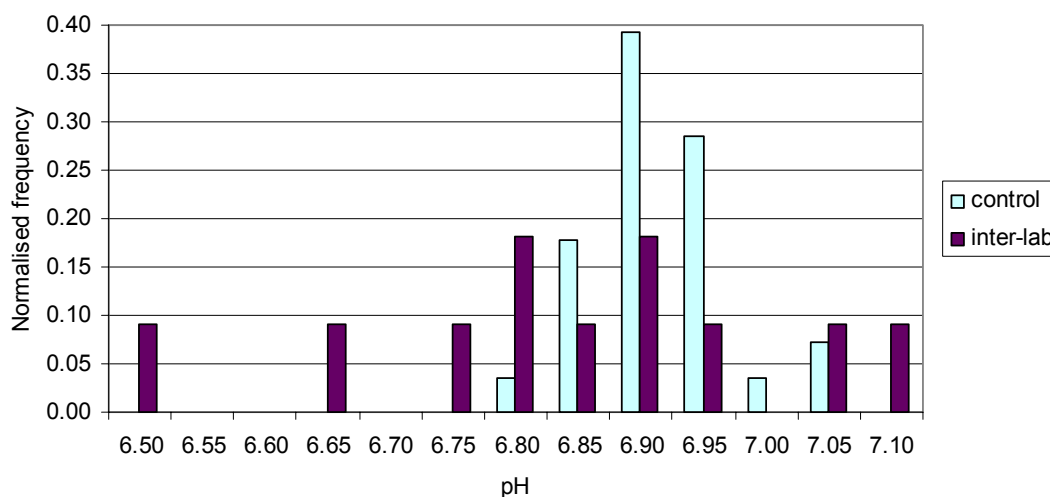


Figure 5.13: Histograms of data from the inter- and intra- laboratory trials.

## 5.5 COMPARISON WITH OTHER FIELD STUDIES

Two other field studies of pH, carried out on a similar sample grid were found in the literature. Silva *et al* (2003) studied a field in Portugal, and Vieira and Gonzalez (2003) studied a field in São Paulo State, Brazil. The majority of other soil pH studies appear to have been carried out on a larger scale. Vieira and Gonzalez used the same 10 m grid as the Bunny study, but collected only 81 samples. Silva *et al* used a 6 m grid and collected 192 samples. All three

studies found the spherical model to be the best fit for the variogram. The parameters for the fitted models are shown in Table 5.5, and the three variograms are compared in Figure 5.14.

Variogram	Range	Sill	Nugget	Interval
Vieira	41.9 m	0.1	0.08	10 m
Silva	18.6 m	0.018	0.002	6 m
Bunny	34.9 m	0.10	0.002	10 m

Table 5.5: Model parameters of the three variograms – all using the spherical model.

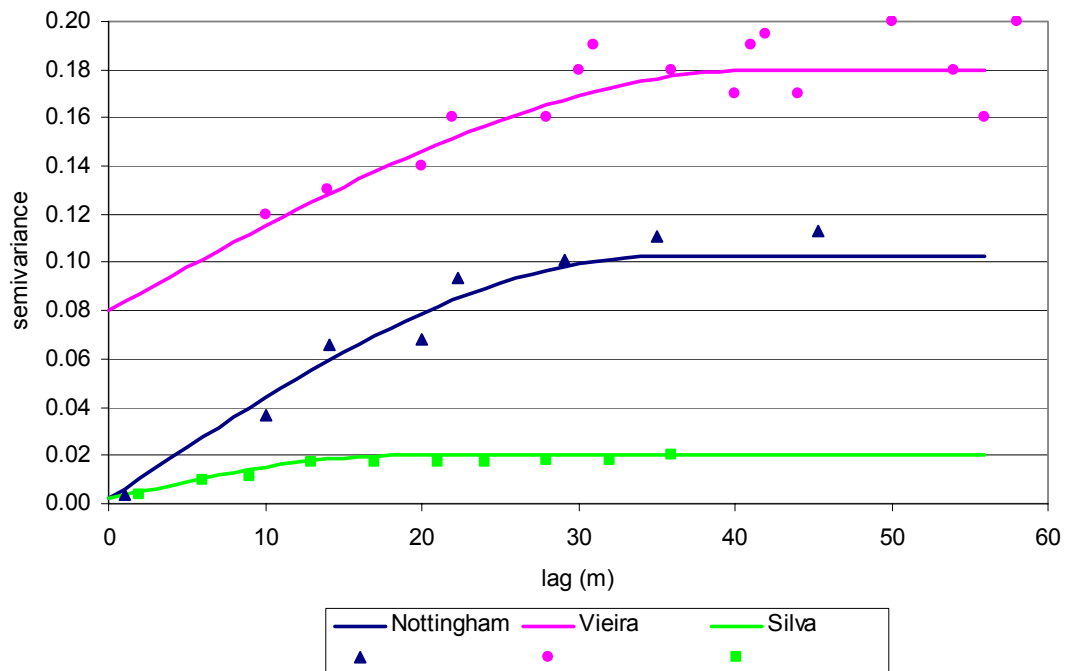


Figure 5.14: pH variograms for Bunny (this study), Portugal (Silva) and Brazil (Vieira). All variograms use the spherical model.

It is very difficult to compare the properties of soils of different types in different locations because of the heterogeneous nature of soil. The different variances are related not only to different natural properties, but also differing land management practices. However, it is quite interesting to note that the

parameters are reasonably similar. The larger nugget in the Vieira case indicates a greater amount of unresolved error, showing that samples at a smaller lag distance as in the Silva case and at Bunny resolve more of the variance at short ( $<10$  m) spatial scales.

Another field study of pH was reported by Webster and Oliver (2001), where a field survey of pH was carried out at Broom's Barn Farm. Samples were taken on a 1 m grid; the variogram is shown in Figure 5.15. The range was 272 m, the sill 0.382 and the nugget was zero.

The Broom's Barn data has been plotted on a separate graph to the other examples as the range is much larger in this case. Broom's Barn shows how different soil type, land management and sample interval can have a dramatic effect on the resulting variogram. The three variograms in Figure 5.15 are reasonably similar given their different geographical locations, whereas the Broom's Barn variogram has a much larger range.

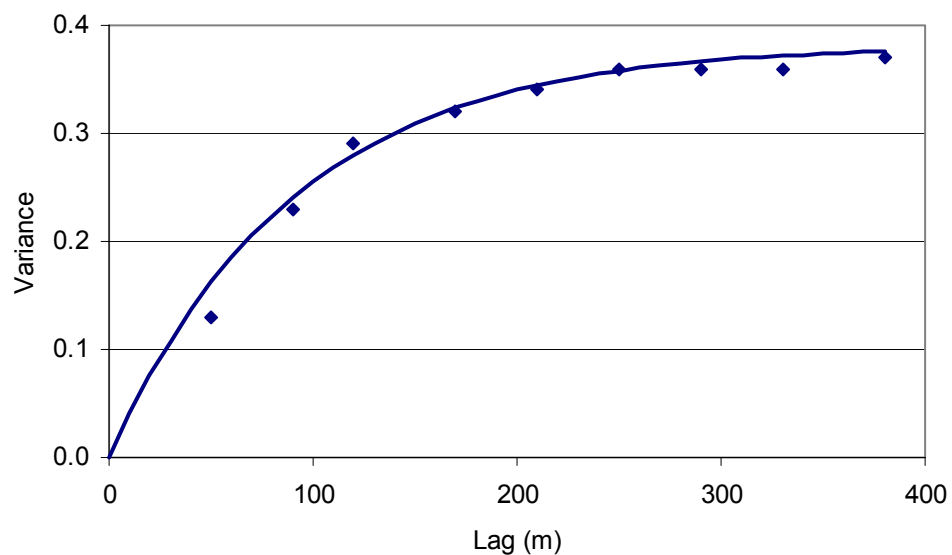


*Figure 5.15: Variogram of pH at Broom's Barn Farm. The points are the experimental semivariances, and the solid line is the best fitting exponential model; the parameters of which are shown in Table 5.6 (Webster and Oliver 2001).*

## 5.6 SIMULATION EXPERIMENTS

### 5.6.1 Simulation of G-BASE sampling protocol

The survey at Bunny was conducted on a sample support of 1 m at 10 m intervals across the field. The G-BASE sample support is 20 m, at a resolution of one sample every 1-2 kilometre squared of land surface, so a maximum of one sample in a field is obtained. The aim of sampling using the G-BASE protocol (based on five bulked samples – the outcome being that the variance is reduced) is to obtain an average value for the area, averaging out any “hot spots” of anomalously high or low values. Using the 10 m grid of the Bunny survey, it is easy to simulate taking a G-BASE sample in the field at Bunny, using the standard 20 m sampling support. Multiple alternative G-BASE values were simulated by repeatedly averaging the pH value from the four corners and the centre of a 20 m square superimposed on the 10 m Bunny data (see Figure 5.16).

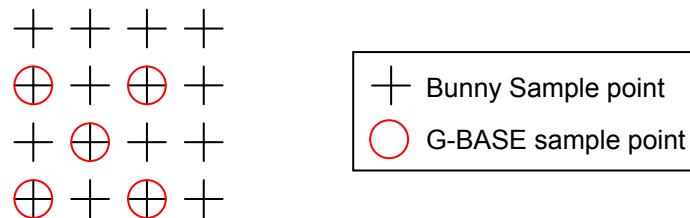


*Figure 5.16: diagram showing a simulated G-BASE sample using the Bunny survey. The red circles of the G-BASE samples together constitute the sample support used under G-BASE and give a single aggregated sample.*

The template for the G-BASE simulation can then be moved across the entire field, and in this way all possible G-BASE sampling simulations are calculated. Figure 5.17 shows a histogram of the Bunny data and the G-BASE simulation data for the field. Table 5.6 shows the statistical analysis of this exercise.

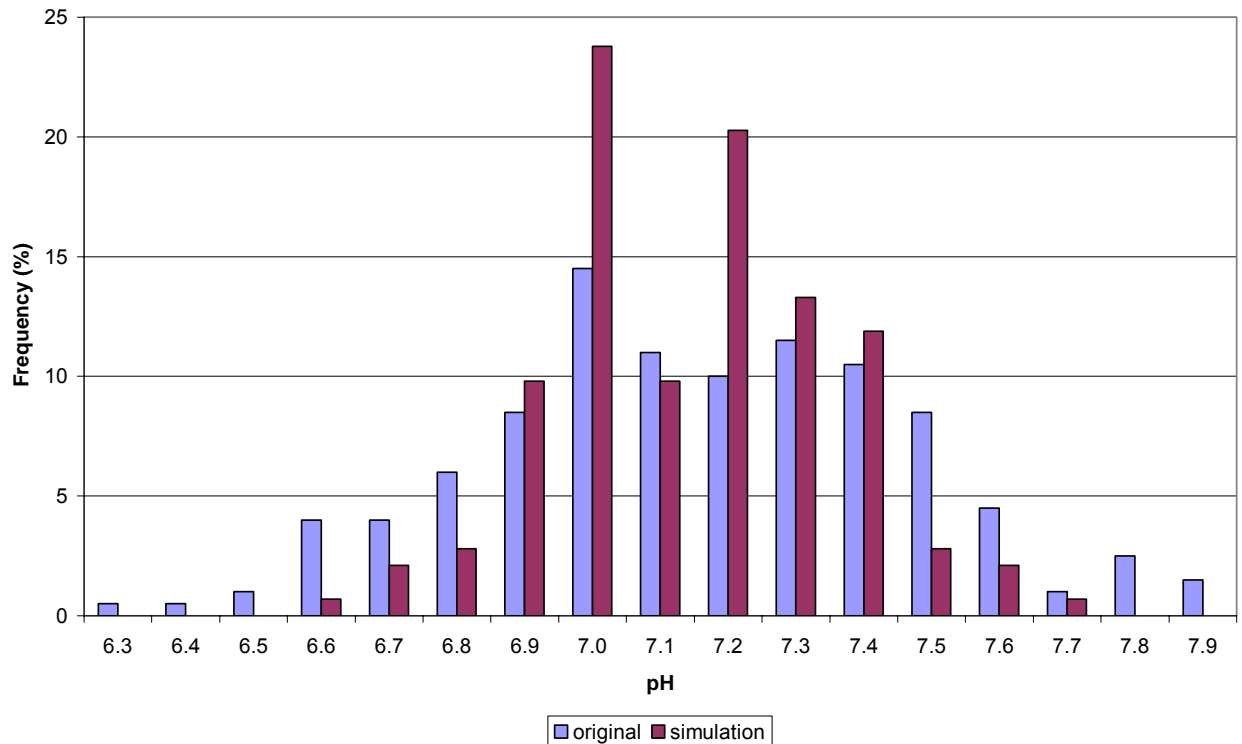


Figure 5.17: Histogram of pH values for Bunny data and repeatedly simulated G-BASE sampling.

	Bunny data	G-BASE simulation
Mean	7.11	7.09
Standard Error	0.02	0.02
Standard Deviation	0.31	0.21
Range	1.65	1.03

Table 5.6: Summary statistics for the Bunny data and simulated G-BASE data.

The averaging process imposed by the G-BASE sampling protocol results in the high and low values being lost. The range is reduced from 1.65 to 1.03 pH units. The mean value is also reduced slightly, indicating that some outliers may exist in the original data. This experiment shows that the G-BASE sampling protocol serves its purpose in achieving a representative sample of the area by bulking samples from a large (20 m) support, as the distributions are very similar. However, it also shows that for situations where the pH is an important factor, the G-BASE protocol will miss much of the short scale

spatial variation and the high and low values are removed by bulking the samples. Ninety per cent of the G-BASE simulated values fall within the mean  $\pm 1$  standard deviation of the mean of field values. The mean of the absolute difference between each G-BASE simulation and the mean value of the measurements for the whole field was 0.169 pH units. This means that, on average, a G-BASE simulation picked at random will be within 0.2 pH units of the “real” field mean.

### 5.6.2 Simulation of wheat uptake of zinc and cadmium

The amount of Zn and Cd that could be taken up into wheat can be predicted using a similar algorithm to the solubility algorithm. The approach used here is a development of that used by Hough *et al* (2003) and applied to a large wheat grain data set by Morales Scott *et al* as part of ongoing research in the School of Biosciences at the University of Nottingham. Cd is used because wheat uptake algorithms for Pb and Cu had not yet been obtained. The wheat uptake of Cd and Zn was simulated using Equation 5.2 and measured pH values, estimated organic carbon content and the maximum permissible concentrations of Cd and Zn in soil after application of sewage sludge to agricultural land (MAFF, 1998). The sludge limits were used because increasing amounts of sewage sludge is being disposed of by application to arable land (see §1.1). The appropriate parameters are shown in Table 5.7. Figures 5.18 and 5.19 show histograms for simulated Cd and Zn uptake by wheat for the site at Bunny, and Table 5.8 shows the summary statistics.

$$\text{Log}(M_{\text{grain}}) = a - b(\text{pH}) + c\text{Log}\left(\frac{M_{\text{soil}} \times 100}{\% \text{OrgC}}\right) \quad 5.2$$

	<i>a</i>	<i>b</i>	<i>c</i>	<i>M<sub>soil</sub></i>
<b>Zn</b>	1.168	0.121	0.343	200 mg/kg
<b>Cd</b>	0.284	0.341	0.532	3 mg/kg

Table 5.7: Parameters for the wheat uptake algorithm (Equation 5.2). *a*, *b* and *c* are constants.

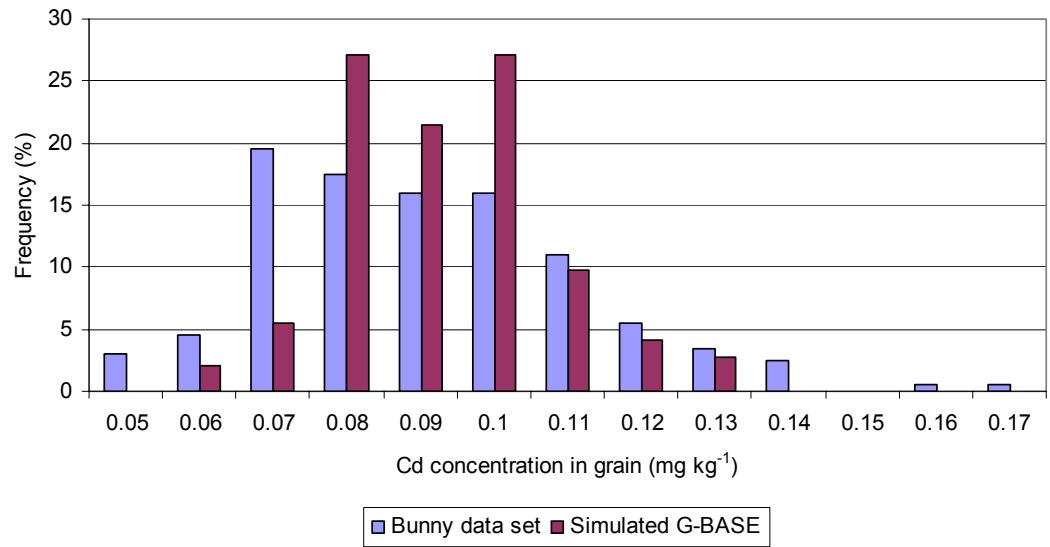


Figure 5.18: Histogram of wheat grain Cd content at Bunny using the sludge soil application limit for Cd. Values calculated for the Bunny data set and for the simulated G-BASE samples are shown.



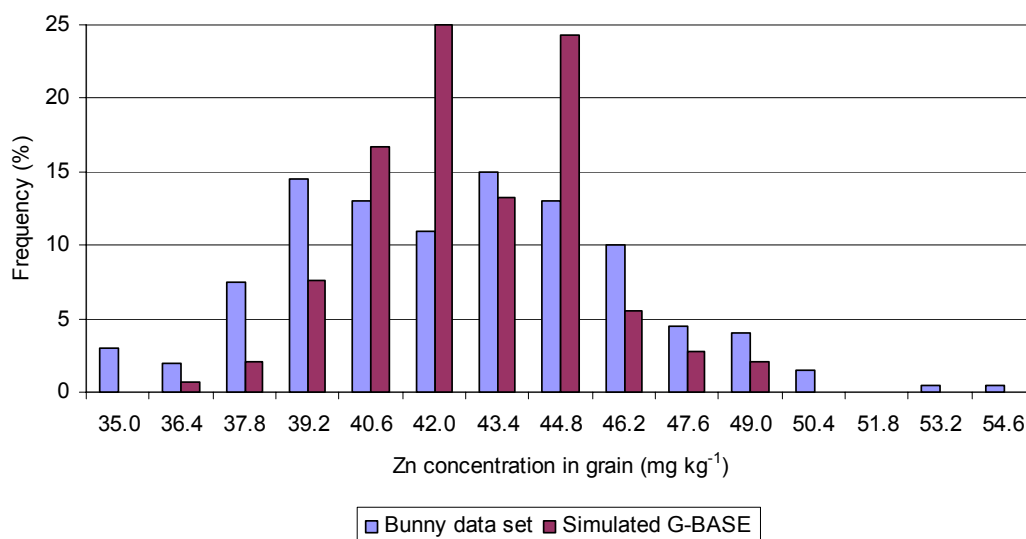


Figure 5.19: Histogram of wheat grain Zn content at Bunny using the sludge soil application limit for Zn. Values calculated for the Bunny data set and for the simulated G-BASE samples are shown.

	Cd concentration in wheat grain (mg kg <sup>-1</sup> ) from Bunny data set	Cd concentration in wheat grain (mg kg <sup>-1</sup> ) from G- BASE data set	Zn concentration in wheat grain (mg kg <sup>-1</sup> ) from Bunny data set	Zn concentration in wheat grain (mg kg <sup>-1</sup> ) from G- BASE data set
Mean	0.086	0.087	41.84	42.07
Standard Error	0.002	0.001	0.26	0.20
Standard Deviation	0.022	0.014	3.67	2.39
Range	0.121	0.069	19.63	11.94
Minimum	0.046	0.056	36.18	33.67
Maximum	0.167	0.125	48.12	52.29

Table 5.8: Summary statistics for modelled Cd and Zn uptake by wheat.

There are no specific regulations on the maximum concentrations of Zn permitted in food. However, in 1953 the Food Standards Committee set a guideline for the UK of 50 mg kg<sup>-1</sup> in foods (Expert group on Vitamins and Minerals, 2002). Only two of the 200 sample points create a value above 50 mg kg<sup>-1</sup> in this situation, and the mean Zn concentration in the wheat grains was 42 mg kg<sup>-1</sup>, which is below the guideline.

The Food Standards Agency set a maximum of 0.24 mg kg<sup>-1</sup> of Cd in wheat (dry weight basis). All of the sample points yield lower values than this, with

the average across the field being  $0.086 \text{ mg kg}^{-1}$ . The distribution is skewed towards the lower values of Cd in grain. This suggests that if the field at Bunny was used for sludge disposal, any wheat grown there would be fit for consumption.

The mean simulated uptake for the field could be calculated in two ways. First is to calculate the uptake at each sample point across the field and calculate the mean. Second is to use the mean pH for the field and calculate a single uptake value. The difference in these approaches is insignificant, with the second approach producing a lower value for Zn and Cd uptake, being 97% of the first approach for Cd and 99.6% for Zn.

As with pH, wheat uptake based on G-BASE simulations produced a smaller range for both Zn and Cd than wheat uptake from the full Bunny data set.

### **5.6.3 Simulated metal solubility at Bunny**

The metal solubility algorithms (§3.1.2) were used with estimated metal concentrations to simulate the variation in metal solubility across the field site at Bunny. Concentrations used were  $200 \text{ mg Zn kg}^{-1}$  (maximum permissible concentration in soil after application of sewage sludge, MAFF, 1998),  $112 \text{ mg Pb kg}^{-1}$  and  $34 \text{ mg Cu kg}^{-1}$  (typical values from Westphalian sub-set of G-BASE). Figures 5.20, 5.21 and 5.22 show the distribution of metal solubility values for the entire data set and for the simulated G-BASE samples described in §5.6.1. Table 5.9 shows the statistics for each metal.

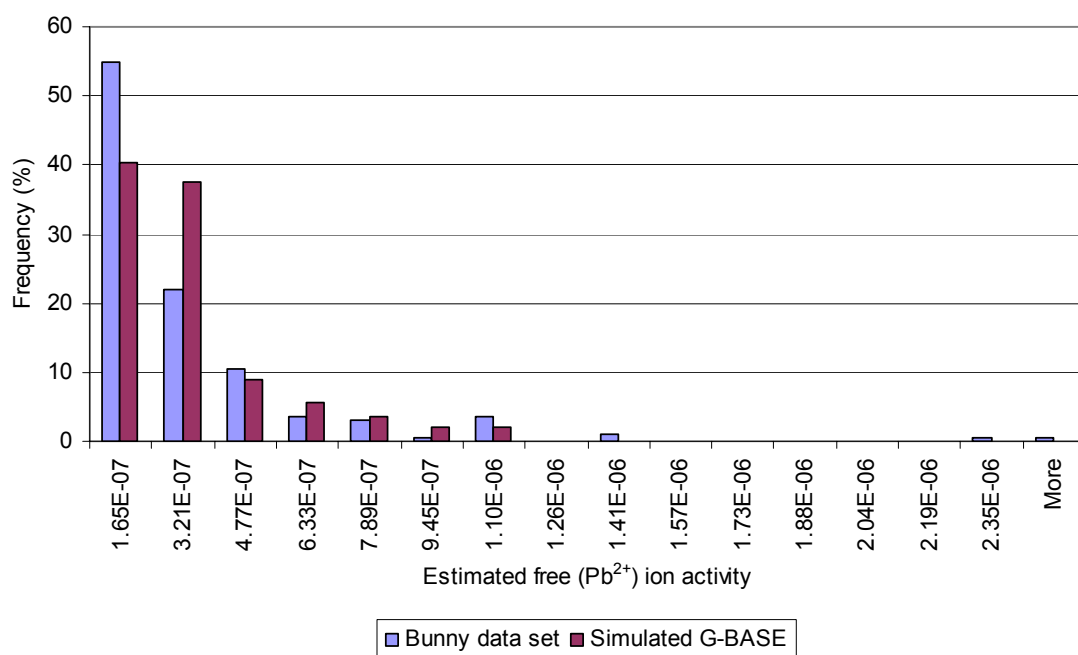


Figure 5.20: Estimated free ( $Pb^{2+}$ ) ion activity at the Bunny field site derived from the full topsoil pH data set and simulated G-BASE sample values.

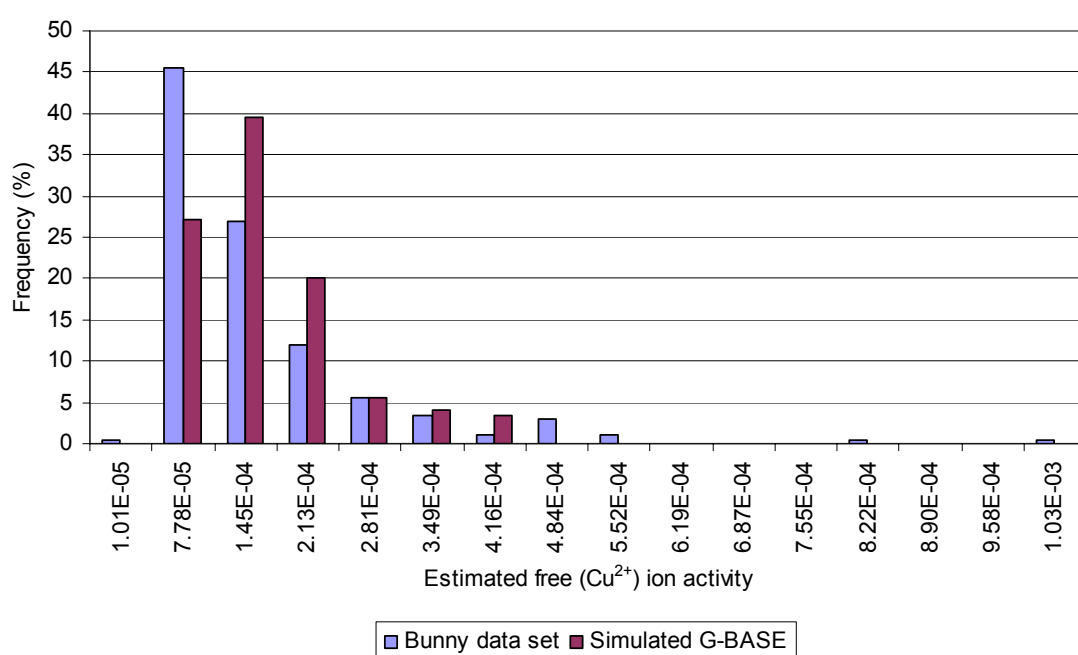


Figure 5.21: Estimated free ( $Cu^{2+}$ ) ion activity at the Bunny field site derived from the full topsoil pH data set and simulated G-BASE sample values.

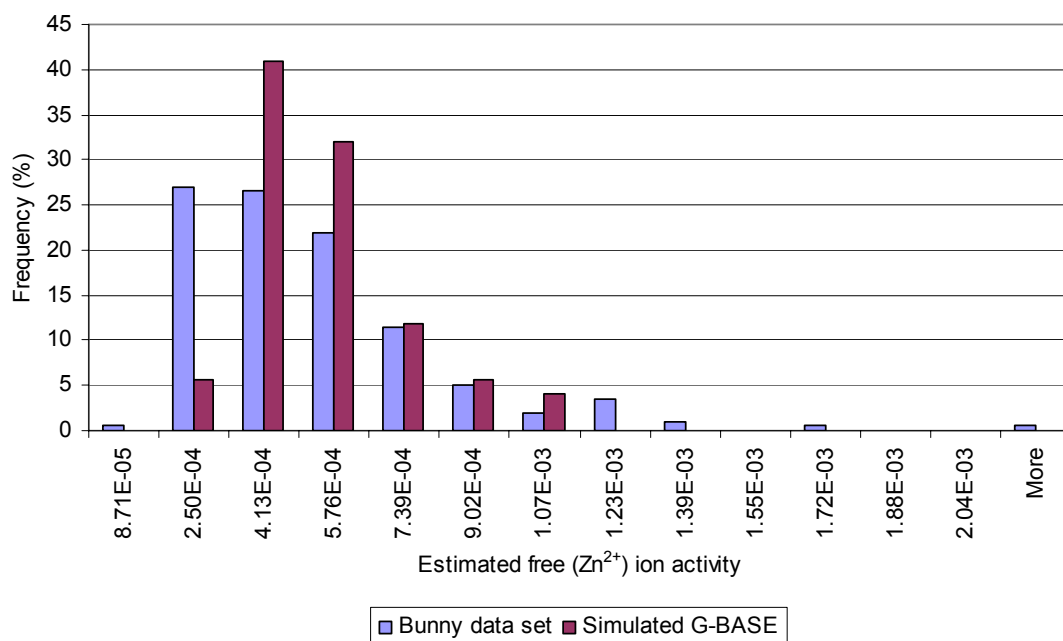


Figure 5.22: Estimated free (Zn<sup>2+</sup>) ion activity at the Bunny field site derived from the full topsoil pH data set and simulated G-BASE sample values.

<b>Pb</b>	Field	Simulated G-BASE	Using mean pH
Mean	$2.51 \times 10^{-7}$	$2.63 \times 10^{-7}$	$1.37 \times 10^{-7}$
Standard Deviation	$3.53 \times 10^{-7}$	$2.12 \times 10^{-7}$	
Skew	4.28	1.87	
Range	$3.12 \times 10^{-6}$	$1.04 \times 10^{-6}$	

<b>Cu</b>	Field	Simulated G-BASE	Using mean pH
Mean	0.00013	0.00013	$8.64 \times 10^{-5}$
Standard Deviation	0.00013	$8.06 \times 10^{-5}$	
Skew	3.08	1.47	
Range	0.0010	0.00038	

<b>Zn</b>	Field	Simulated G-BASE	Using mean pH
Mean	0.00045	0.00047	0.00038
Standard Deviation	0.00029	0.00019	
Skew	1.87	0.99	
Range	0.00196	0.0009	

Table 5.9: Pb, Cu and Zn free metal ion activity using an estimated metal concentration across the field for the full Bunny data set (Field) and at simulated G-BASE points. The value obtained by using the mean pH value is also shown.

As with the simulated G-BASE pH values, the G-BASE solubility values have a smaller range, smaller skewness but similar mean value. Interestingly, using the mean pH value across the field gives a lower mean free metal ion activity for all three metals.

## 5.7 CHAPTER SUMMARY

The survey at Bunny was carried out because variograms of the Westphalian region based on G-BASE data suggests that the scale of the G-BASE project ‘misses’ much of the spatial variability. Analysis of the solubility algorithm also shows that pH contributes the greatest amount of uncertainty to predictions.

The literature shows that spatial variation of pH is caused by many factors over a range of scales. At a field-scale the most important processes that might be causing variation are urine patches, fertiliser, lime application and drainage. All these factors also lead to variation in free metal ion activity in the pore water.

220 soil samples were collected, resulting in 289 pH values. Variation in measurements across the field was comparable with variation that could be expected from management practices. Quality control measurements showed a standard deviation equal to the resolution of the recording device, indicating accurate, consistent measurements. Spatial distribution of pH across the field showed no real trend.

Measurement uncertainty analysis was used to assess the field and laboratory methods. The only area outside the parameters recommended by Ramsey (1998) was analytical variance. This was an area which I worked hard to minimise, testing the electrodes and the technique before-hand and being as consistent with the method as possible. The inter-laboratory trial supports the view that variation was indeed minimised as much as possible. The intra-laboratory mean was within 1.6 standard errors of mean of the inter-laboratory trial.

Results from the analysis of measurement uncertainty were incorporated into the variogram, using the analytical variance as the nugget and the duplicate variance at a 1 m lag interval (being the maximum distance of separation between samples and their duplicates).

Three other field studies of pH were compared. Two were sampled on a similar grid to Bunny (10 m) with one on a 10 m grid and one on a 6 m grid. A third was taken on a 1 m grid. The two on similar grids were surprisingly similar to the variogram at Bunny, considering the variations in soil types, land use and management that potentially exist. The study on a 1 m grid showed a very different range – 272 m, compared to 18 to 42 m for the Bunny site and the other published variograms.

Previous work in the thesis was conducted on G-BASE data, and G-BASE samples can be simulated from the 10 m × 10 m Bunny sampling grid. All potential G-BASE simulations were calculated across the field and showed that the mean and range of values were reduced – indicating that outliers are ‘smoothed’ by using the G-BASE protocol. On average the absolute difference between each G-BASE simulation and the mean original value was 0.169 pH units showing that, on average, a random G-BASE simulation picked to represent the field will be similar to the mean for the entire field. This illustrates that the G-BASE procedure gives an accurate estimation of the mean for a given field even though the scale of the G-BASE survey might miss the small-scale variation within fields.

Wheat uptake of Zn and Cd were estimated for both the original full Bunny data set and simulated G-BASE values. Results suggest that if the field was used for sludge disposal, wheat grown would be safe for consumption at topsoil metal concentrations equivalent to the sludge regulations limits. As with pH, the wheat uptake estimations from simulated G-BASE values had a smaller range than the original values. The mean of the G-BASE simulations are slightly higher than the mean of all the samples, see Table 5.10. Metal solubility for Pb, Cu and Zn showed the same patterns as wheat uptake and pH.

	Cd	Zn
Full Bunny Data set	0.086	41.8
G-BASE simulation mean	0.087	42.1

*Table 5.10 Mean wheat grain concentrations of Cd and Zn from the full Bunny data set and the simulated G-BASE samples.*

## **6. CONCLUSIONS**

### **6.1 THESIS SUMMARY**

The preliminary investigation of the G-BASE data in the Humber-Trent region found that variograms of total soil metal concentrations (Pb, Zn, Cu) based over distinct soil parent materials had different properties in terms of the range of autocorrelation and sill variance. This is similar to the findings of Webster (2000) who showed that variograms for different classes of soil on the Jurassic outcrops of central England differed substantially. This suggests that more accurate estimates of soil properties can be obtained from geostatistical analysis on samples from a single parent material. Hence a subset of the soil data from the Humber-Trent region over a single parent material was chosen and for this study the raw data (pH and Pb, Cu and Zn concentration) was kriged. The particular area chosen was selected because it was predicted that metal concentrations in the soil solution would be detectable in the region. The uncertainty on the kriged results for Pb, Cu and Zn was reasonable (mean values were 29% for Pb, 11% for Cu, 20% for Zn), as was the uncertainty on pH estimates (mean of 15%). The kriging and mapping of Pb revealed a strong spatial trend in Pb concentration with high values in the west and lower values in the east. This is possibly owing to historical lead mining and smelting in the Peak District which is to the west of the area studied. When the metal solubility algorithm was applied to the G-BASE data and kriged, the uncertainty on the metal solubility predictions were extremely high (mean values were 188% for Pb, 417% for Cu and 153% for Zn). A Monte Carlo analysis showed that pH contributes the greatest amount of uncertainty in the algorithm, and it is also the parameter with the highest nugget value in the variogram indicating that the sampling resolution might not have captured a large part of the short-scale spatial variation.

Given the high uncertainty on the kriged solubility predictions, G-BASE sample sites were re-sampled in order to test the solubility algorithm on in situ soil solutions. The metal concentration results showed that it is extremely



difficult to re-sample points that were located using triangulation. In future this should become less of a problem owing to the increased use of GPS which increases the accuracy of the recorded location in soil geochemical surveys. The prediction of Zn solubility at the re-sampled G-BASE site was investigated. A lability of 48% was assumed (the average lability of the original model data-set). Zinc solubility was measured at the sample sites and also predicted using the model. The algorithm predictions match well with the measured solubility, with an average difference of 6%. Although the new and original G-BASE locations are essentially separate sites owing to the uncertainty of relocation, using G-BASE data to predict  $p(\text{Zn}^{2+})$  only increases the average difference between prediction and measurement to 8%. These values are accurate and show that for point data the algorithm provides effective predictions of metal solubility. It is the spatial interpolation of the data that causes uncertainty rather than the model or the raw data set..

It is interesting to note that the difference in solubility predictions using the new sample sites and G-BASE data are very similar despite essentially being separate sites. This suggests that using a single solubility value for an area might be more feasible than the spatial variability of pH would suggest.

The field-scale study of the spatial variability of soil pH showed that pH is the most spatially variable parameter of the solubility algorithm and is potentially influenced by many factors (urine patches, ammonium fertiliser application, liming, time and drainage – see §5.1.2). The variogram of soil pH across a single field showed that there is spatial variability even at a small scale (metres). This suggests that more information on the pH spatial distribution might be helpful when mapping metal solubility. An uncertainty analysis showed that even under the well controlled conditions of the sampling programme, the analytical variance of pH accounted for 50% of the measurement uncertainty. Ramsey (1997) suggests that for a method to be fit-for-purpose this should be less than 20%. This shows that the analysis of soil pH is a major factor in solubility prediction uncertainty. An inter-laboratory trial was also conducted and showed greater variation than the results recorded at Nottingham, which is to be expected. The Nottingham results were very

close to the average of the inter-laboratory trial, suggesting that the results from the Nottingham laboratory were reliable.

Chapter 3 showed that the main influence on metal solubility is pH. Chapter 5 showed that pH is the most spatially variable parameter in the prediction of metal solubility. It therefore seems reasonable to assume that solubility would vary as pH varies across an area and that it would therefore be spatially variable. However, the findings from chapter 4 seem to indicate that solubility might not be as spatially variable as chapter 3 would suggest. In summary,  $\text{Zn}^{2+}$  was measured in soil by returning to selected G-BASE locations.  $\text{Zn}^{2+}$  was then predicted both from the resampled G-BASE sites and the historical G-BASE samples. The new sample cannot be said to be at the same location owing to difficulties in relocation. The difference between measured values and new predictions is 6%, and the difference between measured values and the historical G-BASE site predictions is 8%, suggesting that a single prediction of solubility for a field might be more appropriate than previously thought.

The field study also showed that the G-BASE sampling protocol achieves its aim of collecting a representative sample of the field. There is little difference between using average values for a field to predict the amount taken up by wheat and predicting wheat uptake at points before averaging. As grain is bulked at harvest this means either approach would be valid. However, for discrete crops such as cabbage or carrots, uptake at points will be more important as hotspots will not be diluted by mixing.

## 6.2 THESIS CONCLUSIONS

Although the solubility algorithm is fairly accurate, kriging the data to predict solubility at a smaller scale introduces large errors (mean values were 188% for Pb, 417% for Cu and 153% for Zn). This thesis has established that this uncertainty arises from a number of sources. Firstly the algorithm itself introduces uncertainty, with the parameter for pH introducing the most (percentage contribution to the variance for pH was 75% for Pb, 54% for Zn

and 49% for Cu, see §3.4.2.2). Secondly uncertainty is introduced in the ‘sampling error’ owing to small scale geochemical variation and the uncertainty of returning to the location specified (Ramsey et al., 1997). A third source is ‘measurement error’ in the laboratory, specifically methods used to measure pH and metal concentration. The pH field study showed that for pH this was 50%, when the suggested maximum for fitness-for-purpose is 20%. This is despite tight control over sampling and analysis. The final source of error arises from kriging the data to estimate values at locations between existing data points to give values at shorter intervals of separation.

The pH field study demonstrated that for the purposes of estimating the amount of metal that could be taken up by food crops, a single solubility value for the field would be appropriate for grain crops as these are bulked at harvest so any hot spots would be averaged out. A different approach might be needed for discrete crops. From this research, solubility prediction at points is good, but interpolation of that data introduces high errors of between 153 and 417%. This level of uncertainty means it is difficult to have confidence in the predictions, which limits their usefulness. In ideal circumstances the points in a geochemical survey will be located in the fields where a prediction of solubility is required, and the algorithm can be applied. Where points are not ideally located further sampling might be required.

### **6.3 SUGGESTIONS FOR FURTHER WORK**

It would be interesting to investigate the uncertainties on solubility predictions made by kriging the raw data to a finer grid before applying the algorithm (as opposed to applying the algorithm at G-BASE points and then kriging the solubility predictions). The decision was made to krig after predicting solubility as it was assumed that kriging once would introduce less uncertainty than kriging twice. However, owing to the high uncertainties created using this method it would be worthwhile to investigate an alternative way of predicting solubility at a finer scale.

The trend in the lead concentration could be investigated to determine the origins. It is an interesting finding as no other metals exhibit the same regional trend. Lead isotope analyses of the soil samples could be used to determine if the lead was derived from the mining industry in the peak district.

A field study measuring both  $\text{Zn}^{2+}$  in soil solution and pH in more detail across an area would provide more insight into the ideal level at which predictions of solubility should be made and the correlation between pH and solubility. A compromise between resolution and uncertainty will have to be made.

Measurement of Zn lability in the soil samples taken for the large-scale field work would allow a more accurate prediction of Zn solubility. The algorithm and WHAM could also be applied to Pb and Cu to examine whether these metals show the same tendencies as Zn.

## BIBLIOGRAPHY

ANDERSON, P. DAVIDSON, C.M. LITTLEJOHN, D. URE, A.M. GARDEN, L.M and MARSHALL, J. (1998) Comparison of techniques for the analysis of industrial soils by atomic spectrometry. *International Journal of Environmental Analytical Chemistry* 71 (1), 19-40

ATTEIA, O. DUBOIS, J.P. WEBSTER, R. (1994) Geostatistical Analysis of Soil Contamination in the Swiss Jura. *Environmental Pollution* 86(3), 315-327.

BELLIS, D. COX, A.J. STATON, I. McLEOD, C.W. and SATAKE, K. (2001). Mapping airborne lead contamination near a metals smelter in Derbyshire, UK: spatial variation of Pb concentration and 'enrichment factor' for tree bark. *Journal of Environmental Monitoring* 3(5), 512-514.

BLAKE, L. GOULDING, K.W.T. MOTT, C.J.B. and JOHNSTON, A.E. (1999). Changes in soil chemistry accompanying acidification over more than 100 years under woodland and grass at Rothamsted Experimental Station, UK. *European Journal of Soil Science* 50(3), 401-412.

BLAKE, L. GOULDING, K.W.T. MOTT, C.J.B. and POULTON, P.R. (2000). Temporal changes in chemical properties of air-dried stored soils and their interpretation for long-term experiments. *European Journal of Soil Science* 51(2), 345-353.

BLOOM, P.J (2000) Soil pH and pH Buffering in *Handbook of Soil Science* (ed M E Sumner). Florida, CRC Press

Di BONITO, M (2004) *Trace elements in soil pore water: a comparison of sampling methods* University of Nottingham PhD Thesis.

BRITISH GEOLOGICAL SURVEY (2000) *Regional geochemistry of Wales and part of west-central England - stream sediment and soil*. British Geological Survey, Keyworth.

BURROUGH, P.A. AND McDONNELL R.A. (2000). *Principals of Geographical Information Systems*, Oxford University Press.

CANCÈS, B. PONTHEIU, M. CASTREC-ROUELLE, M. AUBRY, E. and BENEDETTI, M.F. (2003) Metal ions speciation in a soil and its solution: experimental data and model results. *Geoderma* 113, 341-355

CLARK, I. and HARPER W.V. (2000). *Practical Geostatistics 2000*. Scotland, Geostokos (Ecosse) Limited.

CRESSIE, N. (1993). *Statistics for Spatial Data*. New York, John Wiley and Sons.

DAVIS, B.M. (1987). Uses and Abuses of Cross-Validation in Geostatistics. *Mathematical Geology* 19(3), 241-248.

DEFRA (2001) The British Survey of Fertiliser Practice. Fertiliser use on farm crops for crop year 2000.

DEFRA (2003) Final project report on Sampling strategies and soil monitoring, DEFRA

ENVIRONMENT AGENCY. 1999. UK Sewage Sludge Survey - National Presentation. Environment Agency, Report P2/065/1.

EXPERT GROUP ON VITAMINS AND MINERALS (2002) Revised review of Zinc

FULLER, R.M. GROOM, G.B. and JONES, A.R. (1994) The Land Cover Map of Great Britain: an automated classification of Landsat Thematic Mapper data. *Photogrammetric Engineering and Remote Sensing* 60, 553-562

GARDINER, D.T. MILLER, R.W. BADAMCHIAN, B. AZZARI, A.S. SISSON, D.R. (1995) Effects of repeated sewage sludge applications on plant accumulation of heavy metals. *Agriculture, Ecosystems and Environment* 55 1-6

GASCHO, G.J. PARKER, M.B. GAINES, T.P. (1996). Re-evaluation of suspension solutions for soil pH. *Communications in Soil Science and Plant Analysis* 27(3-4), 773-782.

GOOVAERTS, P. (2001). Geostatistical modelling of uncertainty in soil science. *Geoderma* 103(1-2), 3-26.

GOVINDARAJU, K. (1994). Compilation of Working Values and Sample Description for 383 Geostandards. *Geostandards Newsletter* 18, 1-158.

HOUGH, R.L., YOUNG, S.D. and CROUT, N.M.J. (2003). Modelling of Cd, Cu, Ni, Pb and Zn uptake, by winter wheat and forage maize, from a sewage disposal farm. *Soil Use and Management* 19, 19-27

INSTITUTE OF GEOLOGICAL SCIENCES (1977). Quaternary Map of the United Kingdom. *Ordnance Survey (for Institute of Geological Sciences)*, Southampton

INSTITUTE OF GEOLOGICAL SCIENCES (1979). Geological Map of the United Kingdom (south). *Ordnance Survey (for Institute of Geological Sciences)*, Southampton

JOPONY, M. and YOUNG, S.D. (1994) The solid  $\leftrightarrow$  solution equilibria of lead and cadmium in polluted soils. *European Journal of Soil Science* 45, 59-70

LASLETT, G.M. and MCBRATNEY, A.B. (1990). Further Comparison of Spatial Methods for Predicting Soil-Ph. *Soil Science Society of America Journal* 54(6), 1553-1558.

LINNET, N. (1970). *pH Measurements in Theory and Practice*. Copenhagen, Radiometer A/S.

MAFF (1998). *The soil code: Code of good agricultural practice for the protection of soil*.

MATHERON G. (1963), Principles of Geostatistics *Economic Geology* 58 1246-1266

McBRIDE, M. SAUVÉ, S. and HENDERSHOT, W (1997) Solubility control of Cu, Zn, Cd and Pb in contaminated soils. *European Journal of Soil Science* 48, 337-346

MILITINO, A.F. AND UGARTE, M.D. (2001). Assessing the covariance function in geostatistics. *Statistics & Probability Letters* 52(2). 199-206.

NAKHONE, L.N AND YOUNG, S.D. (1993) The significance of (radio-) labile cadmium pools in soil. *Environmental Pollution* 82, 73-77

OLIVER, M.A. AND WEBSTER, R. (1991). How Geostatistics Can Help You. *Soil Use and Management* 7(4), 206-217.

PLONER, A. (1999). The use of the variogram cloud in geostatistical modelling. *Environmetrics* 10(4), 413-437.

PONNAMPERUMA, F.N. (1972). The chemistry of submerged soils. *Advances in Agronomy* 24, 29-96

RAMSEY, M.H. (1997). Measurement uncertainty arising from sampling: Implications for the objectives of geoanalysis. *Analyst* 122(11), 1255-1260.

RAMSEY, M.H. (1998). Sampling as a source of measurement uncertainty: techniques for quantification and comparison with analytical sources. *Journal of Analytical Atomic Spectrometry* 13(2), 97-104.

RAWLINS, B.G. LISTER, T.R. and MACKENZIE, A.C. (2002) Trace-metal pollution of soils in northern England. *Environmental Geology* 42, 612-620

RAWLINS, B.G. WEBSTER, R. and LISTER, T.R. (2003). The influence of parent material on topsoil geochemistry in Eastern England. *Earth surface processes and landforms* 28, 1389-1409.

ROWELL, D.L. (1994). *Soil Science Methods and Applications*, Longman

SALDANA, A. STEIN, A. ZINCK, J.A. (1998) Spatial variability of soil properties at different scales within three terraces of the Henares River (Spain). *Catena* 33(3-4), 139-153.

SAUVÉ, S. McBRIDE, M.B. NORVELL, W.A. and HENDERSHOT, W.H. (1997) Copper solubility and speciation of in situ contaminated soils: Effects of copper level, pH and organic matter. *Water, Air and Soil Pollution* 100, 133-149

SAUVÉ, S. McBRIDE, M. and HENDERSHOT, W. (1998). Soil Solution Speciation of Lead(II): Effects of Organic Matter and pH. *Soil Science Society of America Journal* 62, 618-621

SAUVÉ, S. HENDERSHOT, W. ALLEN, H.E. (2000) Solid-solution partitioning of metals in contaminated soils: Dependence on pH, total metal burden, and organic matter. *Environmental Science & Technology* 34(7), 1125-1131.

SHAND, C.A. WILLIAMS, B.L. DAWSON, L.A. SMITH, S. and YOUNG, M.E. (2002). Sheep urine affects soil solution nutrient composition and roots: differences between field and sward box soils and the effects of synthetic and natural sheep urine. *Soil Biology and Biochemistry* 34, 163-171.

SILVA, V.R. REICHERT, J.M. STORCK, L. and FEIJÓ, S. (2003) Spatial variability of chemical soil properties and corn yield on a sandy loam soil. *Revista Brasileira de Ciência do Solo* 27, 1013-1020

SKINNER, R.J. and TODD, A.D. (1998). Twenty-five years of monitoring pH and nutrient status of soils in England and Wales. *Soil Use and Management* 14, 162-169.

von STEIGER, B. WEBSTER, R. SCHULIN, R. and LEHMANN, R. (1996) Mapping heavy metals in polluted soil by disjunctive kriging. *Environmental Pollution* 94(2), 205-215

SUMNER, M.E. (1994). Measurement of Soil-pH - Problems and Solutions. *Communications in Soil Science and Plant Analysis* 25(7-8), 859-879.



TIPPING, E. RIEUWERTS, J. PAN, G. ASHMORE, M.R. LOFTS, S. HILL, M.T.R. FARAGO, M.E. and THORNTON, I.(2003). The solid-solution partitioning of heavy metals (Cu, Zn, Cd, Pb) in upland soils of England and Wales. *Environmental Pollution* 125(2): 213-225.

TYE, A.M. YOUNG, S.D. CROUT, N.M.J. ZHANG, H. PRESTON, S. BARBOSA-JEFFERSON, V.L. DAVISON, W. McGRATH, S.P. PATON, G.I. KILHAM, K. and RESENDE, L. (2003). Predicting the activity of  $\text{Cd}^{2+}$  and  $\text{Zn}^{2+}$  in soil pore water from the radio-labile metal fraction. *Geochimica et Cosmochimica Acta* 67(3), 375-385.

VIERIA, S.R. and GONZALEZ, A.P. (2003) Analysis of the spatial variability of crops, yield and soil properties in small agricultural plots. *Bragantia Campinas* 62(1), 127-138

WEBB, J. LOVELAND, P.J. CHAMBERS, B.J. MITCHELL R and GARWOOD, T. (2001). The impact of modern farming practices on soil fertility and quality in England and Wales. *Journal of Agricultural Science* 137, 127-138

WEBSTER, R. (2000). Is soil variation random? *Geoderma* 97(3-4), 149-163.

WEBSTER, R. AND OLIVER, M.A. (2001). *Geostatistics for Environmental Scientists*. Chichester, John Wiley & Sons Ltd.

WENG, L. TEMMINGHOFF, E.J.M. LOFTS, S. TIPPING, E. and VAN RIEMSDIJK, W.H. (2002) Complexation with dissolved organic matter and solubility control of heavy metals in a sandy soil. *Environmental Science and Technology*. 36, 4804-4810

WILD, E and EASTWOOD, I (1992), Soil Contamination and smelting sites. *Historical Metallurgy Society: Boles and Smeltermills Seminar*.

ZANG, R and WIENHOLD, B.J (2002), The effect of soil moisture on mineral nitrogen, soil electrical conductivity, and pH. *Nutrient Cycling in Agroecosystems* 63, 251-254

## APPENDIX I

### Example program for creation of a variogram using GenStat®

```

job 'Analysis of Zn data'

variate xx, yy, zn

" Open file of data "
" All data are assumed to be in this file "
open 'WEST_zn.txt'; channel=2

" Now read the numeric data "
read [channel=2; setnvalues=y; skip=*] \
    xx, yy, k

" Descriptive statistics "
describe [select=nval,mean,median,skew,var,sd] k

" This section carries out a trend surface analysis"
calc xmin=min(xx)
calc ymin=min(yy)

calc x=xx-xmin
calc y=yy-ymin

calc xy=x*y
calc x2=x*x
calc y2=y*y
model k;\
residuals=r; fittedvalues=f
terms x,y,x2,xy,y2,k
fit x,y,x2,y2,xy

"Use this section to remove trend if necessary"
"calc k=k-f
describe [select=nval,mean,median,skew,var,sd] k"

dgraph y=r;x=x
dgraph y=r;x=y

scalar zbar, zsd, zvar

VARIATE [VALUES=0] Angles
& [VALUES=180] Segments

calc zz=k
calc zbar = mean(zz)
calc zvar = var(zz)
calc zsd = sqrt(zvar)
print zbar, zvar, zsd

" This section forms the experimental variogram. Step and Xmax can be
altered to improve fit"

FVARIOGRAM [PRINT=statistics; Y=yy; X=xx; STEP=1800;
XMAX=18000; \
DIRECTIONS=Angles; SEGMENTS=Segments] \
zz; VARIOGRAM=zzk; COUNTS=zcounts; DISTANCES=Midpoints

```

```

variate Vgram [#Angles],Lag [#Angles}, Count [#Angles}
Calculate Vgram [ ] = zzk$ [*, 1]
&          Lag [ ] = Midpoints$ [*, 1]
&          Count [ ] = zcounts$ [*,1]
print Lag [0], Vgram[0], Count [0]

calc bot=0.0
axes 1; ylower=bot; xlower=0
pen 1...4; colour=1; symbol=1...4
device 1
graph [nrows=15;ncolumns=40;ylower=bot] Vgram[ ]; Lag[ ]
dgraph Vgram [ ]; Lag [ ]; Pen=1

"the for-loop fits models to the data and produces a measure of fit for each"

FOR Mod='SPHERICAL' , 'EXPONENTIAL' , 'DOUBLESFERICAL'
  MVARIOGRAM [MODEL=#Mod; PRINT=model,summary,estimates; \
    WEIGHTING=cbyvar; WINDOW=1; TITLE=Mod; XUPPER=25000] \
    zzk; COUNTS=zcounts; DISTANCES=Midpoints
ENDFOR

stop

```

## APPENDIX II

### GenStat® output from file shown in Appendix I

```

13  job 'Analysis of Zn data'
14
15  variate  xx, yy, zn
16
17  " Open file of data "
18  " All data are assumed to be in this file "
19  open 'WEST_zn.txt'; channel=2
20
21  " Now read the numeric data "
22  read [channel=2; setnvalues=y; skip=*] \
23      xx, yy, k

      Identifier   Minimum   Mean   Maximum   Values   Missing
          xx      423810   440542   453180     405         0
          yy      345210   376136   400350     405         0
          k         10.00    111.5    289.0     405         0

24
25  " Descriptive statistics "
26  describe [select=nval,mean,median,skew,var,sd] k

Summary statistics for k

      Number of values = 405
              Mean = 111.5
              Median = 106.0
Standard deviation = 40.1
              Variance = 1607.7
              Skewness = 1.0

27
28  " This section carries out a trend surface analysis"
29  calc xmin=min(xx)
30  calc ymin=min(yy)
31
32  calc x=xx-xmin
33  calc y=yy-ymin
34
35  calc xy=x*y
36  calc x2=x*x
37  calc y2=y*y
38  model k;\
39  residuals=r; fittedvalues=f
40  terms x,y,x2,xy,y2,k
41  fit x,y,x2,y2,xy

41.....

***** Regression Analysis *****

Response variate: k
Fitted terms: Constant, x, y, x2, y2, xy

```

## \*\*\* Summary of analysis \*\*\*

	d.f.	s.s.	m.s.	v.r.
Regression	5	48877.	9775.	6.49
Residual	399	600628.	1505.	
Total	404	649505.	1608.	

Percentage variance accounted for 6.4

Standard error of observations is estimated to be 38.8

\* MESSAGE: The following units have large standardized residuals:

Unit	Response	Residual
1	289.0	4.70
2	257.0	3.55
3	255.0	3.47
4	253.0	3.45
5	246.0	3.70
6	230.0	4.00
7	229.0	3.74

\* MESSAGE: The error variance does not appear to be constant:  
large responses are less variable than small

responses

\* MESSAGE: The following units have high leverage:

Unit	Response	Leverage
6	230.0	0.056
24	187.0	0.065
184	109.0	0.049
194	107.0	0.046
251	99.0	0.046
287	93.0	0.162
374	68.0	0.051
402	18.0	0.062
405	10.0	0.046

## \*\*\* Estimates of parameters \*\*\*

	estimate	s.e.	t(399)
Constant	3.8	24.5	0.15
x	0.01069	0.00203	5.26
y	0.001025	0.000766	1.34
x2	-2.32E-07	5.38E-08	-4.31
y2	5.18E-09	8.58E-09	0.60
xy	-7.17E-08	2.50E-08	-2.87

42

43 "Use this section to remove trend if necessary"

44 "calc k=k-f

-45 describe [select=nval,mean,median,skew,var,sd] k"

46

47 dgraph y=r;x=x

48 dgraph y=r;x=y

49

50 scalar zbar, zsd, zvar

51

52 VARIATE [VALUES=0] Angles

53 & [VALUES=180] Segments

54

55 calc zz=k

56 calc zbar = mean(zz)

57 calc zvar = var(zz)

```

58      calc zsd = sqrt(zvar)
59      print zbar, zvar, zsd

          zbar          zvar          zsd
        111.5         1608         40.10

60
61  " This section forms the experimental variogram. Step and
62  can be altered to improve fit"
63      FVARIOGRAM [PRINT=statistics; Y=yy; X=xx; STEP=1800;
64  XMAX=18000; \
65  DIRECTIONS=Angles; SEGMENTS=Segments] \
66  zz; VARIOGRAM=zzk; COUNTS=zcounts;
67  DISTANCES=Midpoints

Variogram of                                zz

General mean                                111.484
General variance                            1607.6860

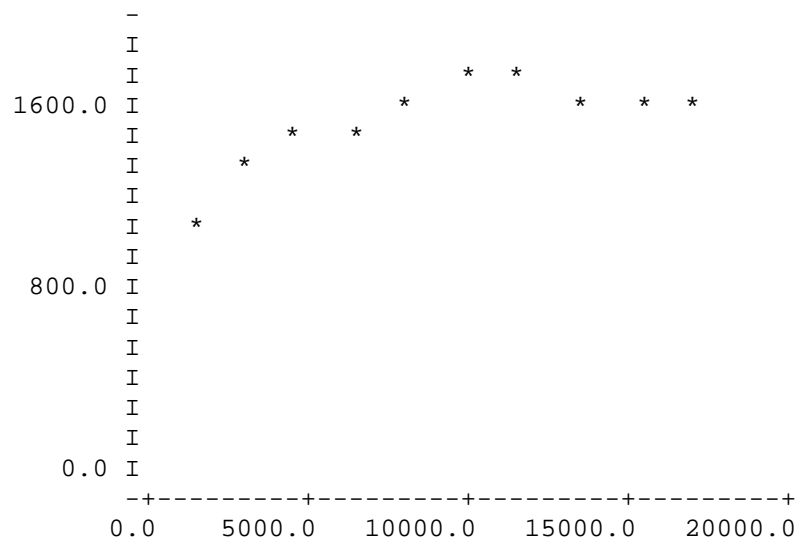
Based on 405 observations
Maximum lag 18000 and step length 1800.00

66
67      variate Vgram [#Angles],Lag [#Angles}, Count [#Angles}
68      Calculate Vgram [ ] = zzk$ [*; 1]
69      &                               Lag [ ] = Midpoints$ [*; 1]
70      &                               Count [ ] = zcounts$ [*;1]
71      print Lag [0], Vgram[0], Count [0]

          Lag[0]          Vgram[0]          Count[0]
          1359          1002           682
          2792          1335          2192
          4540          1469          3229
          6317          1486          4164
          8119          1614          4633
          9916          1668          4816
          11699         1681          4904
          13490         1652          4880
          15306         1648          4747
          17099         1641          4497

72
73      calc bot=0.0
74      axes 1; ylower=bot; xlower=0
75      pen 1...4; colour=1; symbol=1...4
76      device 1
77      graph [nrows=15;ncolumns=40;ylower=bot] Vgram[ ]; Lag[ ]

```



Vgram[0] v. Lag[0] using symbol \*

```

78 dgraph Vgram [ ]; Lag [ ]; Pen=1
79
80 "the for-loop fits models to the data and produces a
measure of fit for each"
81
82 FOR Mod='SPHERICAL' , 'EXPONENTIAL', 'DOUBLESFERICAL'
83     MVARIOGRAM [MODEL=#Mod; PRINT=model,summary,estimates; \
84         WEIGHTING=cbyvar; WINDOW=1; TITLE=Mod; XUPPER=25000]
\
85         zzk; COUNTS=zcounts; DISTANCES=Midpoints
86 ENDFOR

```

\*\*\*\*\* Variogram model: spherical \*\*\*\*\*

```

y = c0 + c*(1.5*x/a-0.5*(x/a)**3) for x.lt.a
y = c0 + c                        for x.ge.a

```

\*\*\*\*\* Nonlinear regression analysis \*\*\*\*\*

```

Response variate: y
Weight variate: rwt
Nonlinear parameters: a
Model calculations: spherical

```

\*\*\* Summary of analysis \*\*\*

	d.f.	s.s.	m.s.	v.r.
Regression	2	435615.	217808.	42.06
Residual	7	36246.	5178.	
Total	9	471861.	52429.	

Percentage variance accounted for 90.1  
Standard error of observations is estimated to be 72.0

\*\*\* Estimates of parameters \*\*\*

	estimate	s.e.
a	10197.	1195.
* Linear		
c	638.5	84.2
Constant	1017.6	84.6

\*\*\*\*\* Variogram model: exponential \*\*\*\*\*

$y = c0 + c*(1-EXP(-x/a))$

\*\*\*\*\* Nonlinear regression analysis \*\*\*\*\*

Response variate: y  
 Weight variate: rwt  
 Nonlinear parameters: a  
 Model calculations: negex1

\*\*\* Summary of analysis \*\*\*

	d.f.	s.s.	m.s.	v.r.
Regression	2	445124.	222562.	58.27
Residual	7	26737.	3820.	
Total	9	471861.	52429.	

Percentage variance accounted for 92.7  
 Standard error of observations is estimated to be 61.8

\*\*\* Estimates of parameters \*\*\*

	estimate	s.e.
a	2881.	534.
* Linear		
c	993.	158.
Constant	672.	167.

\*\*\*\*\* Variogram model: double spherical \*\*\*\*\*

$y = c0 + c1*(1.5*x/a1-0.5*(x/a1)**3)$   
 $+ c2*(1.5*x/a2-0.5*(x/a2)**3)$  for  $x.le.a1$   
 $y = c0 + c1 + c2*(1.5*x/a2-0.5*(x/a2)**3)$  for  $a1<x<a2$   
 $y = c0 + c1 + c2$  for  $x.ge.a2$

\*\*\*\*\* Nonlinear regression analysis \*\*\*\*\*

Response variate: y  
 Weight variate: rwt  
 Nonlinear parameters: a1, a2  
 Model calculations: doubospherical[1], doubospherical[2]

\*\*\* Summary of analysis \*\*\*

	d.f.	s.s.	m.s.	v.r.
Regression	4	459933.	114983.	48.20



Residual	5	11928.	2386.
Total	9	471861.	52429.

Percentage variance accounted for 95.4  
Standard error of observations is estimated to be 48.8

\*\*\* Estimates of parameters \*\*\*

	estimate	s.e.
a1	3014.	1669.
a2	11516.	1513.
* Linear		
c1	676.	415.
c2	495.	114.
Constant	488.	484.

87

88 stop

\*\*\*\*\* End of Analysis of Zn data. Current data space: 1  
block, peak usage 33%  
at line 86.

GenStat Release 6.1 (PC/Windows 98) 03 September  
2004 16:21:24  
Copyright 2002, Lawes Agricultural Trust (Rothamsted  
Experimental Station)

---

GenStat Sixth Edition  
GenStat Procedure Library Release PL14

---